

**Dynamics of water and nutrients in transpiration stream  
and stem tissues of *Phaseolus vulgaris* and the  
regulation of axial nutrient fluxes:**  
Development and application of a tracer technique combining  
stable isotopes and cryo-secondary ion mass spectrometry  
(cryo-SIMS)

Kumulative Dissertation

zur Erlangung des Doktorgrades  
der Mathematisch-Naturwissenschaftlichen Fakultät  
der Heinrich-Heine-Universität Düsseldorf

vorgelegt von

**Ralf Metzner**

aus Hanau

Oktober 2009



aus dem Institut für Chemie und Dynamik der Geosphäre 3:  
Phytosphäre (ICG-3)  
und der Zentralabteilung für chemische Analysen (ZCH)  
Forschungszentrum Jülich GmbH

Gedruckt mit Genehmigung der  
Mathematisch-Naturwissenschaftlichen Fakultät der  
Heinrich-Heine-Universität Düsseldorf

Referent: Prof. Dr. Ulrich Schurr  
Koreferent: Prof. Dr. Andreas Weber

Tag der mündlichen Prüfung: 02.02.2010



## **Selbstständigkeitserklärung**

Hiermit erkläre ich, dass ich die vorliegende Dissertation eigenständig und ohne fremde Hilfe angefertigt habe. Arbeiten Dritter wurden entsprechend zitiert. Diese Dissertation wurde bisher in dieser oder ähnlicher Form noch bei keiner anderen Institution eingereicht. Ich habe bisher keine erfolglosen Promotionsversuche unternommen.

Jülich, den

---

Ralf Metzner

## **Statement of authorship**

I hereby certify that this dissertation is the result of my own work. No other person's work has been used without due acknowledgement. This dissertation has not been submitted in the same or similar form to other institutions. I have not previously failed a doctoral examination procedure.

To my father and my sister

---

## Zusammenfassung

Die Mechanismen und Regulation der Nährstoffnutzung in Pflanzen zu verstehen ist eine wichtige Aufgabe für die Pflanzenwissenschaften. In der Grundlagenforschung würde dies den wissenschaftlichen Fortschritt auf den Gebieten der Aufnahme, des Transports und der bedarfsspezifischer Verteilung von Nährstoffen vorantreiben und es zudem ermöglichen, Pflanzen mit optimierter Nährstoffnutzungseffizienz zu züchten. Durch die Wurzel aufgenommene Nährstoffe werden mit dem Transpirationsstrom in den Spross transportiert. Da Wasser- und Nährstoffbedarf sich oft voneinander unterscheiden, ist es von großer Bedeutung, aufzuklären, wie Pflanzen den Transport und die bedarfsspezifische Akquisition beider Ressourcen regulieren. Da die Xylemgefäße, welche Wasser und Nährstoffe leiten, inert sind, kann eine Regulation der Wasser- und Nährstoffflüsse nur unter Beteiligung der benachbarten lebenden Gewebe stattfinden. Um die Regulation dieser Flüsse zu untersuchen, ist es daher notwendig, den Austausch zwischen dem Transpirationsstrom und den umgebenden Geweben zu untersuchen.

Isotopentracer sind gut geeignet um Austauschprozesse in Geweben zu untersuchen, da sie mit den zu verfolgenden Spezies chemisch identisch sind. Für die meisten Nährstoffe und für Wasser sind angereicherte stabile Isotope verfügbar und können mit abbildenden massenspektrometrischen Techniken, wie etwa Sekundärionenmassenspektrometrie (SIMS), mit subzellulärer lateraler Auflösung detektiert werden, vorausgesetzt, dass die Tracerverteilung bis zum Ende der Analyse bewahrt werden kann. Kryogenische Probenpräparation erlaubt die Erhaltung der Tracerverteilungen selbst bei hochdiffusionsfähigen Ionen, wie etwa  $K^+$ . Daher war die Entwicklung eines Analyseprotokolls, welches eine kryogenische Probenpräparation mit der Analyse durch SIMS an hydratisiert gefrorenen Proben (Cryo-SIMS) verbindet, eines der Ziele der vorliegenden Dissertation. Routinemäßige rasterelektronenmikroskopische Aufnahmen der gefrorenen Proben (cryo-SEM) wurden zum Zweck der Qualitätskontrolle und der Gewebeidentifikation in das Protokoll integriert. Probenserien mit mehreren unterschiedlich langen Tracerapplikationsperioden erlaubten die Untersuchung der dynamischen Aspekte der Regulation, trotz der statischen Natur der Methode.

Eine detaillierte Charakterisierung der Austauschdynamiken von Wasser und drei Makronährelementen (Mg, K und Ca) zwischen den Xylemgefäßen und den Stängelgeweben einer Rankbohne (*Phaseolus vulgaris* cv. Fardenlosa Shiny) wurde durch

das neue Protokoll ermöglicht. Dies gab einen Hinweis auf Austauschwege und –Hot Spots, deren Regulationspotential und die Regulation von axialen Nährstoffflüssen in den Xylemgefäßen. Für Wasser wurde hierbei ein ungehinderter Austausch zwischen Xylemgefäßen und Stängelgeweben festgestellt, während im Gegensatz dazu der Austausch von Magnesium, Kalium und Calcium stärkeren Beschränkungen unterlag. Diese Studie lieferte Hinweise, dass eine rein apoplastischer Austausch zwischen dem Transpirationsstrom und den Stängelgeweben möglich ist, was nahe legt, dass die Zusammensetzung der Nährstoffe im Apoplast der Gewebe ähnlich der in den Xylemgefäßen ist. Daher kann eine Kontrolle der Nährstoffflüsse in den Xylemgefäßen durch Aufnahme und Abgabe von Nährstoffe durch die Zellen der verschiedenen Stängelgewebe erfolgen. Große Unterschiede im Austausch mit den Xylemgefäßen weisen auf die Existenz von zwei verschiedenen funktionellen Domänen im Stängel hin. Erstens legen die Austauschcharakteristiken des Xylemparenchyms und des Markgewebes für das Xylemparenchym nahe, dass das Xylemparenchym als schneller Puffer und Regulator des axialen Flusses und das Mark als lokales Speichergewebe vor allem für Calcium fungiert. Zweitens weist der erheblich langsamere Austausch der peripheren Gewebe (Kambium und Phloem) auf eine untergeordnete Rolle in der Regulation der axialen Flüsse hin, mit der Möglichkeit einer Separation dieser Gewebe von den Xylemgefäßen durch eine apoplastische Barriere gegen Nährstoffbewegungen. Auf eine Kaliumhomöostase im Xylem des Stängels weist außerdem die Höherregulierung der Kaliumkonzentration in einer anfänglich verdünnten Lösung während der Durchströmung des Stängels hin.

Die Ergebnisse dieser Dissertation betonen die Bedeutung der Gewebe der Sprossachse für den Transport und die bedarfsspezifische Verteilung von Nährstoffen in der Pflanze und illustrieren die Möglichkeiten der neuentwickelten Technik. Dieser Beitrag zu unserem Verständnis der pflanzlichen Nährstoffnutzung könnte in der Zukunft dabei helfen Züchtungsstrategien für Pflanzen mit einer höheren Nährstoffnutzungseffizienz zu entwickeln für eine nachhaltigere und zugleich produktive Landwirtschaft.



## Summary

Understanding the mechanisms and regulation of nutrient utilization within plants is an important task for plant sciences. For basic research this would advance scientific progress for example in nutrient uptake, transport and demand-specific distribution, but it would also facilitate breeding of plants with optimized nutrient use efficiency. Nutrients taken up by the roots are transported to the shoot with the transpiration stream. Because the demand for water and nutrients often diverges, it is important to clarify how plants regulate the demand-specific acquisition and transport of both resources. The xylem vessels conducting water and nutrient flow are inert, therefore any regulation needs to involve activity of the neighbouring living tissues. So, for investigating the regulation of nutrient and water fluxes, it is a prerequisite to characterize the exchange between transpiration stream and surrounding tissues.

Isotope tracer techniques are well suited for investigating exchange processes within tissues because the tracers are chemically identical to the traced species. For most nutrients and for water, enriched stable isotopes are available and can be detected with imaging mass spectrometric techniques such as secondary ion mass spectrometry (SIMS) at subcellular spatial resolution, provided the distribution of tracers in the sample can be preserved until the analysis is complete. Cryogenic sample preparation allows preservation of authentic tracer distribution, even of highly diffusible ions, such as  $K^+$ . Therefore, development of an analytical protocol combining cryogenic sample preparation and SIMS analysis of frozen-hydrated samples (cryo-SIMS) was one of the goals of this thesis. Routine imaging of the frozen-hydrated samples with scanning electron microscopy (cryo-SEM) was included in the protocol for quality control and tissue identification. Sample series with several tracer application periods allowed investigation of dynamic aspects of the exchange, despite the static nature of the technique.

Detailed characterization of exchange dynamics for water and three macronutrients (Mg, K and Ca) between xylem vessels and stem tissues in stems of climbing bean (*Phaseolus vulgaris* cv. Fardenlosa Shiny) was enabled by the new protocol, and revealed hot spots and pathways of exchange, their regulation potential and axial flux regulation of nutrients in the xylem vessels. For water, uninhibited exchange between xylem vessels and stem tissues was found, but in contrast the exchange of magnesium, potassium and calcium was more restricted. This study provided evidence that purely apoplastic exchange between the

transpiration stream and stem tissues is possible, suggesting that the nutrient composition of the tissue apoplast is similar to that of the xylem vessels. Therefore control of nutrient flux in the xylem vessels may occur by sequestration and release of nutrients by the cells of individual stem tissues. Strong inter-tissue differences in the exchange with the xylem vessels indicated two functional domains in the stem. First, exchange characteristics of the xylem parenchyma and pith, suggests that the xylem parenchyma functions as a fast buffer and regulator of the axial flow, and the pith as a local storage tissue (i.e. for calcium). Second, much slower exchange of the more peripheral tissues (i.e. cambium and phloem) indicates a minor role in axial flow regulation, with possible separation of these tissues from the vessels via an apoplastic barrier to nutrient movement. Potassium homeostasis in the stem xylem was also suggested by an up-regulation of potassium concentration of an initially dilute solution while it was passing through the stem.

The findings in this thesis emphasize the importance of stem tissues for nutrient transport and demand-specific distribution within the plant and illustrate the power of the newly developed technique. This contribution to our understanding of plant nutrient utilization may in the future help to develop plant breeding strategies towards plants with a higher nutrient use efficiency for a more sustainable and productive agriculture.

---

## Table of contents

Zusammenfassung .....	1
Summary.....	3
1 Introduction.....	7
1.1 Motivation.....	7
1.2 Water and nutrient transport in plants.....	7
1.3 Investigating xylem vessel-tissue interactions.....	9
1.3.1 Isotopic tracer detection by secondary ion mass spectrometry (SIMS).....	10
1.3.2 Performance characteristics of the cryo-SIMS on plant samples .....	12
1.3.3 Physiological information from cryo-SIMS studies .....	14
1.4 Interactions between xylem vessels and stem tissues.....	15
1.4.1 Water and nutrient radial pathways .....	16
1.4.2 Nature of radial movement .....	19
1.4.3 Interaction of xylem with different surrounding tissues.....	21
1.4.4 Nutrient exchange and water status .....	28
1.4.5 Axial flux regulation by stem tissues.....	29
2 Synopsis.....	32
3 Publications used for this dissertation .....	33
4 References.....	34
5 Publications of the dissertation.....	41
5.1 First publication: Imaging of nutrients in plant tissues using cryo-SIMS .....	41
5.2 Second publication: Radial movement of cationic nutrients in stems .....	56
5.3 Third publication: Dynamics of water and nutrients in stems .....	104
6 Acknowledgements.....	147

## Citations of publications in this dissertation

The publications belonging to this cumulative dissertation are cited in the following way. Submitted manuscripts are labelled as “sub” followed by the year of submission. See section 3 for complete references.

#	Citation	Journal	Status
1	Metzner et al., 2008	Plant Physiology	published
2	Metzner et al., sub 2009a	Plant Physiology	submitted
3	Metzner et al., sub 2009b	Plant, Cell & Environment	submitted

# **1 Introduction**

The mechanisms and regulation of plant nutrient utilization are of high importance for plant biology and agricultural science. This doctoral dissertation is concerned with the role of the stem in regulation of water and mineral nutrient flow in the plant, which required development of an analytical protocol to investigate interactions between stem tissues and the transpiration stream. This protocol allowed a characterization of the exchange of different stem tissues with the transpiration stream and of the impact of this exchange on axial flow of water and nutrients.

## **1.1 Motivation**

Resource use efficiency is a crucial aspect for the performance, growth and development of any organism. Plants, as sessile organisms, are especially dependent on local resources. Therefore the local availability of water and mineral nutrients like nitrogen, phosphate and potassium is often growth limiting. For understanding how efficient plants use such resources, understanding the mechanisms and regulation of nutrient utilization within the plant is highly important. Therefore transport and demand-specific distribution in the plant is an important field in both plant physiology and plant nutrition, with growing interest in the dynamics of these processes, facing an ever faster changing dynamic environment. With respect to more applied sciences, the understanding of nutrient utilization is the basis for breeding strategies to produce plants that use available resources more efficiently for production of food and other plant-based resources like fibres or pharmaceutical raw material. Furthermore knowledge about nutrient utilization in plants will enable demand-specific fertilization for a more sustainable and efficient agriculture.

## **1.2 Water and nutrient transport in plants**

The stem of higher plants and its tissues have a key role in distribution of nutrients and water within the plant. During the evolution of higher plants the development of specialized long-distance transport tissues enabled growth into the highly water-vapour deficient atmosphere. This growth meant also spatial separation of roots as water and nutrients acquiring organs and the leaves as photosynthetic organs connected by the stem.

Therefore one of the major functions of the stem in plant resource utilization is the transport of water and mineral nutrients taken up by the roots and the distribution among the aboveground organs.

The demand of water and nutrients in the organs changes dramatically with their individual development, e.g. when a leaf reaches maturity nutrient demand for growth decreases but transpirational water flow increases due to intensified gas exchange. In contrast to these slow changes in demand, water delivery by the transpiration stream is highly variable, depending on environmental conditions. Therefore, without strong regulation of nutrient flux, excess nutrient could accumulate in organs with high transpiration, (i.e. mature leaves), and be deficient in plant parts with low transpiration (e.g. fruit, shoot apex). Excess of nutrients may cause toxicity and require energy consuming inclusion, excretion or recirculation to prevent damage, while deficiency hinders growth, development and functioning of the organ. Since the xylem transport pathways are made up of inert xylem vessels, which have limited buffering capacity due to adsorbed ions, regulation of nutrient flux in these vessels must involve activity of the living tissues surrounding the vessels via retrieval, storage and release of nutrients or even transfer to and from the phloem.

Most research concerning the regulation of nutrient distribution via the xylem has focussed on each end of the transpiration stream, namely on xylem loading in roots (Steudle and Peterson, 1998; de Boer and Volkov, 2003; Köhler and Raschke, 2007), on leaf unloading (Leigh and Storey, 1993; Canny, 1995; Fricke, 2004) and on re-circulation via the phloem (Marschner et al., 1997; Jeschke and Hartung, 2000). Nevertheless, stem tissues are likely to participate in the regulation of nutrient flux in the shoot e.g. by xylem–phloem (McNeil, 1980; Dasilva and Shelp, 1990; van Bel, 1990) or xylem–xylem transfers (Atkins, 1999) for supply of low-transpiring organs with sufficient amounts of mineral nutrients for growth and development. Furthermore stems have gained some attention because of their role in water storage, especially in trees (Gartner, 1995; Meinzer et al., 2006).

While those investigations showed that regulation in the stem may take place, for a mechanistic understanding of water and nutrient distribution within the plant, addressing the interaction between transpiration stream and stem tissues with cellular detail is necessary.

### 1.3 Investigating xylem vessel-tissue interactions

For the experimental approach, the study of the small-scale interactions between xylem vessels of a transpiring plant and the surrounding stem tissues poses a big challenge.

Regulatory interactions of the xylem vessels with the surrounding tissues consist basically of the exchange of water and nutrients. While nutrients can be taken up, stored and released by active processes in the tissues, water moves along hydrostatic or osmotic gradients, which may also be influenced directly or indirectly by tissue activity. Whole plant budgets of nutrient partitioning (e.g. Jeschke and Hartung, 2000) and perfusion experiments of stems (e.g. Gilmer and Schurr, 2007) showed this exchange, but could not localize it among the tissues and their apoplastic, symplastic and vacuolar compartments. Nevertheless these details are critical for understanding the role of the exchange processes for whole-plant physiology. Ideally such processes would be investigated non-invasively with online-monitoring of the flows of water and nutrients, but even MRI, which is capable of flow imaging of water in xylem and phloem (Windt et al., 2006) does not have the spatial resolution necessary to investigate tissue-level interactions nor the capability of imaging nutrient fluxes at this scale.

The introduction of isotopic tracers into the system is a classical approach in plant science to visualize exchange of both nutrients and water (e.g. Marschner, 1995) between different compartments. Such tracers are isotopes of the element under investigation that show identical chemical properties as the natural element but can be discriminated from it by a certain characteristic. For radioactive isotopes this characteristic is the emission of radiation, while for enriched stable isotopes it is the change in the isotopic abundance of the sample that can be detected by mass spectrometric techniques. Some investigators have also used elements with similar chemical characteristics as those of the target element (e.g. Sr for Ca; Storey and Leigh, 2004), so called elementtracers, but these may not mimic the target element completely (Marschner and Schimansky, 1968; Jeschke, 1970), especially when moving across membranes (Hedrich and Schroeder, 1989; Reintanz et al., 2002).

For the detection of exchange between the xylem vessels and stem tissues a very high spatial resolution is needed. Movement of radiotracer may be traced noninvasively in the living plant (Thorpe et al., 2007) with extraordinary sensitivity, but the spatial resolution does not allow for detecting tissue-level interactions, even with such sophisticated techniques as positron emission tomography (Jahnke et al., 2009). Microautoradiographics of sectioned material can offer the spatial resolution required for some elements (e.g.

Dickson et al., 1985; Thellier et al., 2001) but due to long exposure time the samples need to be fixed, typically by drying or embedding in resin, techniques that do not reliably immobilize diffusible analytes (Zierold, 1992; Goldstein et al., 1994).

Stable isotope tracers are detected by the change in isotopic abundance in the plant caused by the isotopically enriched tracer, and the spatial resolution is determined by the technique for measuring the local isotopic abundance. The spatial resolution for modern mass spectrometric techniques like secondary ion mass spectrometry (SIMS) is more than sufficient for tracer imaging in cellular and subcellular compartments. This high spatial resolution is preferable, as apoplast, symplast and vacuoles differ considerably in their permeability and regulatory possibilities for water and nutrient exchange (Steudle and Peterson, 1998). Nevertheless the detection of stable isotope tracers is far more complex compared with radiotracers and the detection sensitivity is inferior, as a significant change in isotopic abundance is necessary to detect their presence.

It should be noted that the necessary application of tracers to the experimental system is in itself a critical step for any tracer technique. While in some cases the application may be done minimal invasively (e.g. labelled CO<sub>2</sub> applied to photosynthetically active leaves) it is often destructive to the plant and may severely disturb the transport system. Therefore the impact of application procedures on the water and nutrient movement should be carefully evaluated.

In conclusion, xylem vessel-stem tissue interaction can be monitored by stable isotope tracer techniques, if the spatial resolution of the detection technique is adequate.

### **1.3.1 Isotopic tracer detection by secondary ion mass spectrometry (SIMS)**

Detection of (stable) isotope tracers by SIMS offers high detection sensitivity with spatial resolutions in the nanometre range. While the technique is frequently used in the material sciences and semiconductor industry the technique has occasionally been used for biological samples such as biomaterial surfaces (Belu et al., 2003), cultured cells and mammalian tissues (Chandra et al., 2000) and vacuoles of plant tissue (Derue et al., 2006).

The principles of SIMS and its application to plant tissues have been described in Metzner et al. (2008). In this study a SIMS instrument with time-of-flight mass analyzer (ToF-SIMS) was used, therefore in the following the technical details for this type of instrument will be given. SIMS instruments with magnetic sector field mass analyzers have also been used for isotope tracer studies with biological specimen (Lechene et al., 2007), with their



own advantages and disadvantages compared to the ToF-SIMS, but a detailed comparison of the differences is beyond the scope of this thesis. Nevertheless, the lower beam damage to the sample of the ToF-SIMS, the possibility for massive parallel detection of different tracers and other analytes together with commercially available equipment for the preparation and analysis of biological specimen make ToF-SIMS instruments more favourable for applications in the biomedical field. For simplicity of speech the ToF-SIMS will be termed short as SIMS in the following text. In brief, SIMS employs a focussed, pulsed primary ion beam that is rastered across the sample surface to sputter and ionize material. These so called secondary ions are then analyzed by a mass spectrometer. In a SIMS instrument equipped with a time-of-flight mass spectrometer, a complete mass spectrum is recorded for each pixel in the raster. Therefore maps for different isotopes or molecules can be extracted from the same measurement and multi tracer experiments are straightforward. SIMS is highly surface sensitive and only minimally destructive to the sample, enabling further analysis e.g. with scanning electron microscopy at cryogenic temperatures (cryo-SEM). The spatial resolution for SIMS can be better than 150 nm (Vickerman and Briggs, 2001), determined by the focus of the primary ion beam, and is therefore well suited for probing even small tissue cells with diameters of less than 10  $\mu\text{m}$ . A large maximal field of view with 500 x 500  $\mu\text{m}$  enables overview images of entire quadrants of cross sections of stems in thin plants, which is a clear advantage over single cell based detection methods like ion selective electrodes (Leigh, 2001). Furthermore the detection needs no modification of the sample, such as the application of a matrix in MALDI (Heeren et al., 2006), that might interfere with the detection of mineral nutrients. In frozen hydrated plant tissue samples, such as used in this study, mapping of macronutrients like magnesium, potassium and calcium at physiological concentrations was demonstrated with secondary ion mass spectrometry with magnetic sector field-detection (Derue et al., 2006) and with ToF-SIMS (Metzner et al., 2008). With the more widespread electron microprobe (e.g. electron dispersive x-ray analysis; EDXA), in most cases this is not possible due to lower detection sensitivity (Metzner et al., 2008). A general limitation of the SIMS-technique is the inability to quantify concentrations of nutrients in the plant samples due to a dependency of the signal generation (i.e. ionisation) on the immediate atomic vicinity of the analyte (matrix) which is very inhomogeneous in biological samples (Metzner et al., sub 2009b). For the detection of stable isotope tracers this is not critical, since all isotopes of an element are affected identically, and the matrix effect cancels out during calculation of isotopic abundances. A relative quantification of

the nutrients originating from the tracer in the plant can be done based on the fractions originating from the introduced tracer in contrast to those present beforehand in the plant (Metzner et al., sub 2009a).

Sample preparation is a critical step for the authenticity of the data concerning mobile nutrients and water. For SIMS analysis the samples must withstand an ultra-high vacuum environment for a measurement time in the range of hours, so the distribution of diffusible analytes needs to be preserved until the analysis is complete. The best method to preserve the *in planta* distribution of analytes and make it stable under vacuum conditions is shock-freezing and analysis of frozen-hydrated samples (Echlin, 1992; Zierold, 1992; McCully et al., 2009). Techniques like chemical fixation or freeze-drying and resin embedding of the samples cannot prevent loss or redistribution of analytes during sample preparation (Zierold, 1992). Therefore all samples analyzed during this study were shock frozen and analyzed frozen-hydrated by SIMS (cryo-SIMS). While for shock-freezing of samples with diameters of 2 to 3 mm, such as used in this study, vitrification is generally not possible, cryo-SEM applied routinely to the samples revealed no damage of the tissue structure due to ice crystal growth (Metzner et al., 2008). On the other hand for much larger samples the speed of freezing would likely not have been fast enough to prevent growth of large ice crystals, which might damage the tissue structure during freezing and lead to redistribution artefacts.

A limitation for the widespread use of the cryo-SIMS technique is that it is at the moment very labour intensive and time consuming. Preparation and analysis of a single sample during this study usually took three days. Therefore large numbers of replicates for good statistics are usually not possible. Instrument time may also be a problem, since SIMS instruments are still quite expensive. On the other hand they are often available in physics and material sciences departments and may be adapted for part-time biological research.

In conclusion, SIMS offers the spatial resolution and sensitivity to detect stable isotope tracers of nutrients and water and frozen-hydrated sample preparation offers preservation of authentic distribution of diffusible tracers during are analysis.

### **1.3.2 Performance characteristics of the cryo-SIMS on plant samples**

Application of cryo-SIMS to study water, magnesium, potassium and calcium in the transpiration stream and stem tissues of climbing bean showed its suitability for investigating interactions between transpiration stream and stem tissues. Stable isotope

tracers were continuously supplied to the transpiration stream of cut transpiring shoots, until sections were removed from the stem, that were immediately shock frozen and analyzed still frozen hydrated (for full detail see Metzner et al., 2008). Using this technique, this study allowed for the first time parallel detection of isotopically labelled water ( $\text{H}_2^{18}\text{O}$  and  $\text{D}_2\text{O}$ ) and stable isotopes of the macronutrients magnesium ( $^{26}\text{Mg}$ ), potassium ( $^{41}\text{K}$ ) and calcium ( $^{44}\text{Ca}$ ; Metzner et al., sub 2009a and b). With parallel detection a comparison between the spreading of all tracers among cells and tissues was easily possible and revealed unexpected differences in the movement of the various nutrients and between solvent and solutes (Metzner et al., sub 2009b). Comparison of the water tracers showed that they can both be applied equally as tracers in plants (Metzner et al., sub 2009b), which enables the cryo-SIMS technique to be combined with magnetic resonance imaging (MRI) where  $\text{D}_2\text{O}$  serves as a contrast agents (e.g. Link and Seelig, 1990) but also with non-imaging mass spectrometric techniques where  $\text{H}_2^{18}\text{O}$  is more widely used (Barbour, 2007). Supplementary sodium and rubidium, the latter often used as an element tracer for potassium, could also be imaged with high detail (Metzner et al., 2008). While quantification of sodium was not possible, due to the lack of a suitable stable isotope tracer, its detailed mapping is nevertheless of high interest to complement single cell and whole plant studies concerning salinity (e.g. Munns and Tester, 2008).

The spatial resolution of the cryo-SIMS technique allowed imaging of stable isotope tracer distributions in tissue areas as large as  $500 \times 500 \mu\text{m}$  with a spatial resolution of 7 to  $10 \mu\text{m}$ . This enabled the identification of all tissues participating in exchange with the xylem vessels by their labelling. At this spatial resolution symplastic, apoplastic and vacuolar labelling could not be separated easily, but the examination of the tissue structure of each sample after cryo-SIMS analysis (see Fig. 2b in Metzner et al., 2008) confirmed that in most cells the vacuoles took up by far the largest part of the cell lumina, so data for these tissues will largely represent vacuolar labelling. This is similar to the limitations of single cell sampling and analysis (Leigh, 2001) where also mainly the vacuoles are sampled, but as they dominate intracellular volume and are the main storage site their composition provides a meaningful estimate of cell composition (Leigh and Storey, 1993), at least if the plant is not starved in nutrients (Leigh, 2001). Exceptions from this rule are the axial contact cells of the xylem parenchyma, surrounding the xylem vessels and the sieve and companion cells of the phloem, where all or a major part of the cell lumen is taken up by cytoplasm.

Smaller areas, not larger than 150 x 150  $\mu\text{m}$  could be imaged with spatial resolutions better than 1  $\mu\text{m}$  in the high lateral resolution mode (Figure 6 in Metzner et al., 2008), but only potassium and water tracer could be mapped with acceptable uncertainties in signal identification (Metzner et al., sub 2009b). Due to limitations of measurement time only the proto-/ metaxylem area, including xylem parenchyma and inner cells of the pith could be imaged in all samples. This spatial resolution allowed a distinct separation of tracer in symplast, vacuoles and apoplast of these tissues (Metzner et al., 2008; Metzner et al., sub 2009b).

In conclusion, in frozen-hydrated plant samples the cryo-SIMS protocol can be used to image tracers for water and nutrients with spatial resolution sufficient for detecting diffusible stable isotope tracers down to the subcellular level.

### **1.3.3 Physiological information from cryo-SIMS studies**

Interactions between transpiration stream and stem tissues can be revealed by characterization of exchange between cellular and subcellular compartments and the transpiration stream. Sample series with variable tracer application periods allowed investigation of the dynamic aspect of the exchange. Such exchange dynamics can provide a wealth of information about the potential role of the different tissues in interactions regulating the axial flux at different time scales, but data interpretation poses a challenge of its own. The isotopic abundance maps calculated from cryo-SIMS isotope mapping are difficult to compare between experiments, due to anatomical differences between individual samples. Therefore a system was developed, where for all samples comparable regions were selected according to anatomical criteria (Metzner et al., sub 2009a) and labelling in the region was quantified as fractions originating from the applied tracer. This approach allowed a characterization of the *in planta* exchange extending our present knowledge about transport in individual cells from electrophysiological approaches (Wegner et al., 1994; Amtmann and Blatt, 2009) and uptake studies with slices of plant organs (Pitman et al., 1974; van Bel et al., 1981).

By varying speed of flow and tension of the transpiration stream, driving forces and dependence of the interactions on xylem flow parameters could be investigated. The driving forces are tightly linked to the pathways along which nutrients and water move, as each pathway (e.g. apoplastic or symplastic) has different potentials for flux regulations (Leigh and Storey, 1993; Steudle and Peterson, 1998).

Once equilibrium with the xylem vessel content is reached, the strength of labelling of tissues shows how much of the native nutrients and water can be replaced by tracer from the xylem vessels. This can be expressed as the exchangeable fraction of the specific tissue (Metzner et al., sub 2009a) and reveals how mobile the nutrient in the respective tissue is. High mobility is a prerequisite for fast release during regulation of the nutrient flow in the xylem vessels.

The labelling dynamics of water and nutrient in the xylem vessels offer a quite different type of information. Stable isotope tracer solution follows the transpiration stream, passing through the stem and upon reaching the sampling site its isotopic composition reflects any interactions with stem tissues along the way. Changes of isotopic abundance in stem shows effects of tissue interactions on xylem sap, allowing for estimation of nutrient concentrations at the sampling site (Metzner et al., sub 2009b), avoiding the necessity to sample xylem sap, which is generally a difficult task (Schurr, 1998).

In conclusion, stable isotope tracer localization with cryo-SIMS is well suited for characterizing interactions of water and nutrients between transpiration stream and stem tissues concerning localization of the tissues and pathways involved, speed and intensity of exchange and changes in xylem sap during passage of the stem xylem, without the difficulties associated with xylem sap sampling.

#### **1.4 Interactions between xylem vessels and stem tissues**

For understanding the role of the stem tissues in the regulation of axial flux of nutrients and water it is necessary to characterize the framework of the exchange of water and nutrients with the vessels.

The composite model for movement of water and nutrients through the root and into the xylem vessels (Steudle and Peterson, 1998) emphasizes the complex nature of this movement and the role of different tissues. No such model exists for the stem, but the root model may be appropriate in some respects, provided the different tissue structure and functions are not important.

The pathways for exchange are of special interest as the nature of the exchange and its regulation potential depends on the pathways. Since investigations on the root showed functional specialization of different tissues for radial transport (Steudle and Peterson, 1998), it is highly important to investigate the role of the different tissues in the stem in radial exchange. Another important aspect is the influence of environmental factors on the

radial exchange and the existence of a nutrient homeostasis in the xylem vessels by stem tissues. These aspects and their role for the regulation of the flux of nutrients and water in the stem will be discussed in the next sections.

### **1.4.1 Water and nutrient radial pathways**

Identification of the pathways along which nutrients and water move during exchange between the xylem vessels and the surrounding tissues reveals the structural framework for radial exchange and the possibilities of control mechanisms.

In contrast to the root and leaf xylem, where radial fluxes of water and nutrients are obvious, the stem xylem is often regarded as a set of closed off pipes with little contact to the surrounding tissues, channelling water movement in axial direction. But in fact it is a leaky tube with many contact points to the surrounding tissues (Canny, 1991). Major sites for the passage of water and nutrients across the xylem vessel walls are the non-lignified pit membranes (van Bel, 1990; Steudle and Peterson, 1998). These are tightly associated with the axial contact cells of the xylem parenchyma so a direct passage from the xylem vessels into the symplast of these cells appears to be possible (van Bel, 1990). On the other hand passage of water and nutrients directly across the xylem vessel walls is also likely, as they present no barrier comparable to the suberin-incrusted endodermis of roots. Movement within tissues can occur within the cell wall space (apoplastic), within the cytoplasm and plasmodesmata (symplastic) and from cell to cell via crossing of the plasma membranes (transcellular; Leigh and Storey, 1993; Steudle and Peterson, 1998). Each of the pathways has its own permeabilities and mechanisms of regulation. The actual contribution of the different pathways to exchange through tissues and organs differs between water and different nutrients, apparently related to their movement characteristics through cell walls and membranes.

#### **Water exchange**

The radial exchange of water is expected to be unhindered as well on the apoplastic as on the symplastic and transcellular pathways, since the hydraulic conductivity of cell membranes for water is very high (Steudle, 1997) and also of cell walls except at hydrophobic barriers like the casparian strip in the root endodermis (Steudle and Peterson, 1998). Such structures are uncommon in the stem, and if they are present, only enclosing the vascular cylinder (Lersten, 1997). Even in species like sugarcane, where solute

diffusion between the xylem and surrounding parenchyma is restricted (Walsh et al., 2005), there is fast radial equilibration of water (Bull *et al.*, 1972). In leaves many findings point to water movement from xylem vessels to the epidermis through the symplast (Sack and Holbrook, 2006; Ye et al., 2008).

The data presented in this study (Metzner et al., sub 2009b) certainly support that view, showing no sign of an isolated compartment anywhere in the stem. Since labelling with stable isotope tracer for water was almost uniform throughout our samples, including cell walls (see Fig. 3D-E in Metzner et al., sub 2009b), we conclude that the diffusivity of water was so high everywhere that the different pathways are indistinguishable in our system. Except, possibly, in some of the lignified walls of the xylem parenchyma where labelling is lower than in the cell lumina. This is in agreement with the symplastic pathways that occur in leaves, where suberized cell walls in the bundle sheath exists (Sack and Holbrook, 2006). Even though no clear differences were visible between pathways, the lateral resolution for water tracers was demonstrated to be sufficient for separation of the symplastic and the transcellular pathways (see Fig. 5B in Metzner et al., sub 2009b), which was not possible with other techniques so far (Steudle and Peterson, 1998). Furthermore we could show that the equilibration of water between xylem vessels and stem tissues holds at a much finer scale than has been seen previously, confirming that formulations for plant water relations taking for granted equilibration in all tissues of a plant (Steudle, 1989; Nobel, 1999) also hold true for large organs composed of several different tissues, like the stem.

### **Nutrient exchange**

Pathways for nutrient exchange are more restricted than for water. For nutrients the transcellular pathway, requiring many membrane passages, is usually negligible, due to the low membrane permeability (Steudle and Peterson, 1998). Movement of nutrients occurs therefore either along apoplastic or symplastic pathways with entrance and exit of the latter under strict metabolic control.

For the root and leaf these pathways were intensely studied (Leigh and Tomos, 1993; Steudle and Peterson, 1998). While different nutrients were shown to move along symplastic and / or apoplastic pathways through the root, nutrient loading into the xylem vessels in the root against a concentration gradient (e.g. for calcium; Karley and White, 2009) implies a transfer from the symplast of xylem parenchyma cells into the xylem

vessels. For leaves both direct uptake of solutes from the vessels into the symplast and apoplastic movement out of the xylem vessels have been found (Karley et al., 2000).

The stem has received less attention, focussing mainly on the transfer between xylem and phloem via the rays which is suggested to have an apoplastic and a symplastic component (van Bel, 1990). Both pathways are thought to start with solute diffusion out of the moving xylem sap into the adjoining cell wall apoplast (van Bel, 1990), but direct evidence for the pathways of nutrients is missing.

The subcellular localization of stable isotope tracer in this study shows that in the stem, potassium enters the cell wall apoplast directly from the xylem vessel lumina, without crossing the symplast of the xylem parenchyma cells enclosing the vessels (Metzner et al., sub 2009a). This is clearly in contrast to the purely symplastic pathway potassium moves along in the root (Karley and White, 2009), but in the root this may be favoured to circumvent the apoplastic barrier of the casparian strip.

Subsequent apoplastic spreading of potassium was observed for the pith and is also likely for the cambium and phloem. For calcium a symplastic pathway appears unlikely due to its very low symplastic free ion concentration (White, 2001), which is also true for magnesium (Yazaki et al., 1988). Therefore, the purely apoplastic spreading in the stem demonstrated for potassium in this study may be typical for all three cationic nutrients investigated. This agrees well with the fast and reversible diffusional equilibrium of radiolabelled amino acids between the xylem vessel lumina and the large apparent free space of the xylem translocation pathway (van Bel, 1978), which appears, in the light of our findings, to be identical with the cell wall apoplast of several stem tissues. This apoplastic pathway implies a non-limited exchange between the xylem vessel lumina and the apoplast of stem tissues, at least within the vascular cylinder as will be discussed later.

Exchange between the symplast of stem tissues and the xylem vessels appears to be indirect via exchange with the cell wall apoplast that is connected to the xylem vessels directly or through the cell wall apoplast of other tissues (Metzner et al., sub 2009a). The labelling in the cytoplasm and vacuoles is therefore strongly influenced by the nutrient turnover of the respective cells (uptake to replace loss by leaking of the plasmalemma e.g. potassium) and the leakiness of their membranes in the case of lower symplastic than apoplastic concentrations (e.g. calcium). This is in agreement with Fricke (2004), who found that the different ion content of leaf cells is caused mainly by different ion uptake from the apoplast rather than by different ion composition in the apoplast.



The purely apoplastic exchange between vessels and stem tissues implies that the nutrient concentrations in the cell wall apoplast are possibly not very different from the concentrations in the transpiration stream, due to constant equilibration with the xylem vessels. This is in agreement with the similar potassium concentrations found in the xylem vessels and apoplast of leaves (Lohaus, 2007) and the sensitivity of leaf apoplast potassium concentrations to changes of the xylem sap concentration (Long and Widders, 1990; Felle and Hanstein, 2007). Magnesium concentrations in the shoot apoplast are likewise expected to approximate that of the xylem sap (Karley and White, 2009). One may speculate that in the root the casparian strip limits the high permeability of the xylem vessels and cell wall apoplast to the stelar and thereby enables the build-up of higher solute concentrations in the xylem vessels than in the cortex-apoplast. However, if the concentration of solutes in the xylem vessels is in equilibrium with the apoplast of most of the plant, the question of nutrient homeostasis in the vessels becomes highly important as it is identical with homeostasis of the milieu for many living cells.

In conclusion, while water moves among all three pathways (apoplastic, symplastic and transcellular) or exchanges rapidly between them due to its high membrane permeability nutrients appear to move mainly along the apoplastic pathway and enter the symplast secondarily from the cell wall apoplast. This apoplastic, not metabolically controlled, exchange points to an equilibration of solute concentrations between the transpiration stream and the apoplast of stem tissues.

#### **1.4.2 Nature of radial movement**

Forces and flows of nutrient and water movement between xylem vessels and stem tissues are closely related to the pathways of movement and hint on the possibilities for regulations of axial flux. Along with their pathways the flows of water and nutrients show some differences caused by the different permeability through cell membranes and also different forces apply to their movements.

##### **Radial water movement**

Water moves in tissues by diffusion or by hydraulic flow along hydrostatic or osmotic gradients (Steudle and Peterson, 1998). Speed of diffusion depends on the resistance against water movement, but few hydrophobic structures within plants pose severe barriers against diffusion of water, like the casparian strip of the endodermis (Steudle, 2000).

Diffusion is negligible for water flow within the plant compared to hydraulic flows like the transpiration stream, but must be considered when interpreting isotope tracer data, where diffusion becomes visible (Link and Seelig, 1990). Diffusion may play, on the other hand, a large role for rewetting the tissues of resurrection plants (Boyer, 1985). Hydraulic water flows are driven by osmotic or hydrostatic forces, like those found in roots (e.g. Steudle and Peterson, 1998). In contrast to the root, large radial gradients are not to be expected due to a lack of water sources and sinks in the stem but small flows (compared to the transpiration stream) could possibly originate from a cross flow between xylem and phloem, from surface transpiration or during withdrawal of water from stem storage or refilling of this storage (Goldstein et al., 1998).

Cryo-SIMS measurements with  $\text{H}_2^{18}\text{O}$ -tracer showed that the resistance against radial movement in the stem is small, since even tissues 0.5 mm distant from the vessels were equilibrated with the tracer in the vessels within less than 5 minutes. The homogenous labeling of whole stem cross sections indicated no sign of mass flow of water through the symplast or the apoplast and spreading of tracer could well be explained by diffusion (Metzner et al., sub 2009b). Furthermore, radial equilibration was not influenced by axial flow rate (R. Metzner, unpublished data), which would influence radial hydrostatic gradients due to hydraulic coupling to the transpiration stream, also indicating diffusive movement instead of hydraulic flow.

The rapid radial equilibration of water also leads to a slow increase in the labelling of the xylem vessels some distance downstream of the tracer application site and corroborates other measurements using isotopic tracers (e.g. Meinzer et al., 2006; Ohya et al., 2008). This radial exchange must be kept in mind when using tracers to monitor water flow in plants (Waring and Roberts, 1979; Link and Seelig, 1990; Van der Weerd et al., 2002), either by waiting for a steady state or by an analysis that can account for the transient.

### **Radial nutrient movement**

Nutrients in tissues move by diffusion or are dragged along with water flows (Steudle and Peterson, 1998). Symplastic diffusion is limited by the generally low permeability of cell membranes to solutes (Steudle, 1989) and for some nutrients by low symplastic concentrations of free ions (e.g.  $\text{Ca}^{2+}$ ). In the apoplast of roots solvent drag with hydraulic water flows is thought to play an important role for movement of nutrients (Steudle and Peterson, 1998). Water flow in the apoplast of the stem tissues would be hydraulically coupled to the transpiration stream in the xylem vessels and therefore different

transpiration rates would be expected to show a strong impact on the movement of nutrients by solvent drag. But we found the radial movement of magnesium, potassium and calcium to be independent of the transpirational flux (Metzner et al., sub 2009a), except for a small tissue area between xylem vessels and cambium (discussed below). Therefore the radial movement of nutrients in the stem appears to be mainly diffusive. Resistance against the diffusion of cationic nutrient in the tissues could be the negative charges of the cell walls, preferentially binding divalent cations (Pitman, 1977; Tester and Leigh, 2000).

In the bean stem, the xylem parenchyma facing the cambium has the shape of a thin strip, one- or two cell-layers wide, of lignified, lowly vacuolated cells following the shape of the xylem vessels. These cells were the only ones in the cross sections for which radial exchange of nutrients showed a dependence on the axial flow rate. The radial exchange appeared to be inversely related to the axial flow rate in the xylem vessels (Metzner et al., sub 2009a). The inverse relationship between tracer spreading and the axial flow rate is consistent to the findings of van Bel (1974) for the radial escape of amino acids from the xylem, but findings in the present study (Metzner et al., sub 2009a) suggest that this effect is limited to the xylem parenchyma facing the cambium.

The nutrient movement by solvent drag implies that the xylem parenchyma facing the cambium may be especially important for the regulation of xylem nutrient fluxes as suggested in the literature for the whole xylem parenchyma (e.g. Karley and White, 2009). This tissue is also en route to the phloem which seems very likely to be important for nutrient cycling. Furthermore, a stronger radial exchange at lower transpiration flows may indicate a role in the regulation at very low transpiration (comparable to the slow speed of flow in the above mentioned experiments by van Bel) or possibly even flow in the absence of transpiration (e.g. Münch counterflow; Smith, 1991).

In conclusion, nutrients and water movement in most tissues appear to be diffusive with the exception of the xylem parenchyma facing the cambium which shows additional potential for exchange at low transpiration conditions, due to nutrient movement by solvent drag.

#### **1.4.3 Interaction of xylem with different surrounding tissues**

The various stem tissues showed different exchange characteristics with the xylem vessels for magnesium, potassium and calcium while for water no such differences were found. Since these characteristics are a strong hint suggesting different roles in the regulation of

nutrient distribution in the shoot, the different tissues in the stem were investigated in detail.

In the stem of dicotyledonous plants the xylem vessels are enclosed by the xylem parenchyma which is bordered towards the centre of the stem by the pith and in the peripheral direction by the cambium and the phloem. In many plants this concentric structure is crossed by rays running from the pith to the epidermis, linking xylem and phloem by a structure specialized on apoplastic and symplastic radial transport (van Bel, 1990), but in the climbing bean used in this study rays were absent (Metzner et al., 2008). Non-climbing cultivars of common bean do show the development of rays (Enright and Cumbie, 1973), and the absence in our model plant is possibly caused by the thinner stems and resulting short radial distances.

### **Xylem parenchyma**

The xylem parenchyma accompanies the xylem vessels and fills up the space between the different vessels, making it a key tissue for xylem vessel-stem tissue interaction.

Xylem parenchyma cells in direct contact to the xylem vessels show a distinct anatomy (Esau, 1977) and in many plants there are also specialized transfer cells with wall ingrowths enlarging membrane surface area or ray contact cells associated to very large pits in the xylem vessel walls (van der Schoot and van Bel, 1989). We did not find such specialized cells in the internodes, instead the xylem vessels are enclosed by an anatomically uniform sheath of xylem parenchyma cells which are smaller than the bulk of the tissue and in contrast to these only lowly vacuolated. Cells of such sheaths that are thought to play an important role within the xylem parenchyma due to their close association with the vessels are also termed axial contact cells (van der Schoot and van Bel, 1990). They are associated with the pit membranes, the areas of the xylem vessel walls most permeable for water (Steudle and Peterson, 1998) and thought to be the major pathway for radial exchange with the xylem vessels. In trees, more distant parenchyma cells were in contrast shown to be more specialized on storage of nutrients (van Bel, 1990). The axial contact cells were found to have a dense cytoplasm containing many mitochondria and high ATP-levels (van der Schoot and van Bel, 1989; van Bel, 1990), leading some authors to suggest that they play an important role in the regulation of axial nutrient flux (van Bel, 1990). The discovery of a multitude of ion channels in root xylem parenchyma cells that were suggested to play a role in xylem loading (Maathuis et al., 1997; Gambale and Uozumi, 2006) strengthen this view of the xylem parenchyma as an

important interface between long distance transport channels and other stem tissues but until now there was no direct evidence of the role of this tissue in mineral nutrient fluxes. We found that the xylem parenchyma cells in the axial sheath had the strongest labelling of all tissues in the stem within the shortest time, supporting their suggested role as interface for xylem vessel-stem tissue interactions (Metzner et al., sub 2009a). But this study also showed that the labelling of the bulk of the xylem parenchyma cells was only marginally slower and equally strong. Intense transmembrane trafficking of nutrients was suggested from the strong labelling of the cell lumina (Metzner et al., sub 2009a). Tracers need to pass only one membrane to enter the symplast but two to enter the vacuoles, therefore the faster labelling of the axial sheath compared to the bulk of the xylem parenchyma may be a result of their cytoplasm-dominated lumina, in contrast to the bulk tissue where the vacuoles dominate the cell lumina. Nevertheless, no clear functional differentiation in nutrient exchange between the axial contact cells and the bulk of the xylem parenchyma was found, in contrast to tree xylem parenchyma (van Bel, 1990). Islands of thin walled cells in the xylem parenchyma found occasionally associated with secondary xylem vessels are suggested to be sites of magnesium storage (Metzner et al., sub 2009a), similar to the endodermis in spruce needles (Stelzer et al., 1990).

The fast labeling was remarkable, and so was the extent of isotopic exchange for nutrients in the xylem parenchyma. Calcium, which is usually thought to be of low mobility within tissues, showed a full exchange within less than 20 minutes, demonstrating both high apoplastic mobility and high cellular turnover (Metzner et al., sub 2009a). Furthermore calcium in the cytosol (1-10 mM White et al., 1992) is mainly chemically bound leading to free cytoplasmic ion concentrations of 0.1-0.2 $\mu$ M (Clarkson, 1993), but all calcium in the cells was shown to be readily exchangeable (Metzner et al., sub 2009a). This high exchange was surprising, as in sugar beet plants more than three-quarter of the total tissue calcium was found to be firmly bound to pectates in cell walls and as phosphates (Marschner, 1995). Calcium in the bean stem appeared therefore to be highly mobile, and may be available for buffering of changes in the axial calcium flux. For magnesium and potassium also more than half of the nutrient in the xylem parenchyma was exchanged within 20 minutes, suggesting also high apoplastic mobility and intense transmembrane trafficking.

Phenomena where this transmembrane trafficking and its metabolic control are expected to play a key role are the resorption of sodium from the xylem stream (Jacoby, 1965; Marschner, 1995), which may help to keep shoot concentration low for natriophobic species

like the bean. The homeostasis of nutrients in the xylem vessels, found in perfusion experiments (e.g. for potassium Gilmer and Schurr, 2007), may also be explained by this ability of the xylem parenchyma symplast and vacuoles to sequester and release mineral nutrients. The tissue apoplast, open to the xylem vessels as discussed above, enables all cells of the xylem parenchyma to help regulate the xylem vessel content, extending regulation well beyond the axial contact cells.

Another phenomenon where the capacity of the xylem parenchyma for sequestration or release may play a key role is the enrichment of xylem and phloem streams supplying low transpiring organs like growing leaves and the stem apex (Jeschke et al., 1987; Jeschke and Pate, 1991; Jeschke and Hartung, 2000) by nutrient uptake, transfer and release, often against a concentration gradient. In plants with distinct rays these may also play an important role in the transfer between the two transport system (van Bel, 1990).

From the direct indication of apoplastic permeability and intense transmembrane trafficking gathered in this study, we suggest the xylem parenchyma in the stem to play a major role in the fast buffering of xylem mineral nutrient content and as a regulator for the axial nutrient fluxes in the stem.

### **Pith**

Storage of nutrients is a major function of the pith in herbaceous plants (van der Schoot and van Bel, 1990; Koroleva et al., 2000). In combination with its position close to the xylem vessels, this makes it an interesting candidate for xylem nutrient flow regulation.

Data presented in this study suggested storage of potassium and calcium in the vacuoles of the pith, but also showed fast exchange with the xylem vessels via the apoplast of pith and xylem parenchyma (Metzner et al., sub 2009a). The mainly apoplastic connection is compatible with findings for tomato (van der Schoot and van Bel, 1990), where the pith was symplastically isolated from the xylem parenchyma. Low labelling of the vacuoles which dominate the cell lumina in this tissue on the other hand, especially for potassium and calcium, suggested low transmembrane exchange rates. Local storage of nutrients was suggested to play an important role during times of high demand such as flowering and fruit onset in plants with an internal phloem in the pith like tomato (van der Schoot and van Bel, 1990). Many plants also take up nutrients needed for fruit growth long before fruiting (Mason and Maskell, 1931). Local storage associated to the xylem vessels is expected to be important, especially for nutrients with low phloem mobility (e.g. calcium; van der Schoot and van Bel, 1990).

In regulation of axial nutrient fluxes we suggest for the pith the role of a local storage tissue, involved in buffering larger changes in demand by the shoot or supply by the roots, especially for calcium, which is not circulated within the plant.

### **Cambium and Phloem**

Structure and function of the cambium and phloem differ from the parenchymatous tissues treated above. The meristematic cambium, situated between xylem and phloem, was shown to be notable sink for nutrients during growth activity (Kuhn et al., 1997) and also pathway for any exchange between the two transport systems. The phloem consists of sieve cells specialized on assimilate transport with associated companion cells and phloem parenchyma. Transfer from xylem to the phloem has been known about for a long time, such as the apoplastic transfer of xylem-borne radioactive potassium to the bark described by Stout and Hoagland in (1939). The actual transfer to the sieve cells of the phloem was demonstrated by Hoad and Peel (1965), with the appearance of the xylem -borne  $^{86}\text{Rb}$ -radiotracer in the honeydew of aphids. As the transfer of mineral nutrients from the xylem to the phloem is an important mechanism for the mineral supply of low-transpiring organs like shoot apices and fleshy fruits which receive most mineral nutrients via the phloem, this has been intensely investigated. Transfer of nitrogen (McNeil et al., 1979; Jeschke and Hartung, 2000), potassium (Wolterbeek and Debruin, 1986; Jeschke and Hartung, 2000), magnesium and calcium (Jeschke and Pate, 1991) have been demonstrated.

In parallel with the anatomical differences, this study showed much slower tracer movement into the cambium and phloem than into the xylem parenchyma and the pith (Metzner et al., sub 2009a). Though the labelling of cambium and phloem was comparable to the xylem parenchyma, it took at least 10 times as long to reach it (Metzner et al., sub 2009b). Such a difference was also found by van Bel (van Bel et al., 1981), who showed that in internode disks the uptake of amino acids by the extracambial tissues was a factor of eight lower than that of the xylem parenchyma.

The similarity, of the dynamics for magnesium and calcium labelling in the cambium and phloem, with uptake of external magnesium and calcium across the diffusion barrier of the endodermis into the root xylem (Kuhn et al., 2000), suggested an apoplastic barrier between the xylem parenchyma and the cambium. Furthermore the very similar and uniform labelling in both tissues also supports a free movement within and between cambium and phloem (Metzner et al., sub 2009a). A barrier hindering the apoplastic movement of nutrients between the xylem parenchyma and the cambium would separate

the stem apoplast into two distinct domains. The first one would be the open apoplastic space of the xylem, xylem parenchyma and pith, described above and the second one include the cambium, phloem and possibly all other peripheral tissues, in the absence of a stem endodermis around the vascular cylinder. Such a separation seems rational, as the considerable sugar concentration in the phloem apoplast were found in the climbing bean (Minchin and Thorpe, 1984), thought to buffer phloem sugar transport, but appearance in the xylem vessels was very low (Thorpe et al., 2006). Similarly in sugarcane, a barrier separates the vascular bundles from the surrounding storage tissue (Walsh et al., 2005), accessible to water but not sugar (Bull et al., 1972). For the cambium, these apoplastic domains imply an easy supply of the tissue with sugar and nutrients like magnesium, potassium and phosphate from the phloem, but may hinder the acquisition of calcium, which is not phloem mobile. It is unclear at the moment if the slow movement of calcium from the xylem to the cambium would transport enough calcium to supply an actively growing tissue. For the xylem, an enclosing apoplastic barrier, more permeable for water than for nutrients, might be related to the phenomenon of osmotic water lifting (Zimmermann et al., 2002).

An uncertainty in data interpretation is that the slower labelling of cambium and phloem compared to the xylem parenchyma cannot be attributed unambiguously to slow apoplastic diffusion. With the spatial resolution of the images available for these tissues at the moment it cannot be excluded that high apoplastic labelling might be masked by low labelling in the cell lumina. Low labelling in the cell lumina can be the result of low transmembrane trafficking of the cells in the cambium and phloem, and does not necessarily relate to low apoplastic labelling. Nevertheless, this explanation appears less likely in the light of the similar and homogenous labelling of both tissues, as in the case of strong apoplastic labelling all cells in both tissues would have to show very similar exchange between cell lumen and apoplast, which is not likely for two tissues as different as the cambium and phloem.

The possibility of a diffusion barrier against nutrient movement in the stem raises the question of its nature. The known diffusion barriers like the endodermis and casparian strip in the root and or the suberized bundle sheath cell walls in some leaf types are easily detected by light or electron microscopy, but no such structures are described for the stem so far, except for endodermal structures surrounding the vascular cylinder (Lersten, 1997). This may correlate with the fact that the radial movement of water in the stem was not



hindered, suggesting the barrier to be only effective against cationic nutrients, and does not require dense hydrophobic structures known from water barriers.

Whatever slows down movement of nutrients from the xylem to the lumina of the cambium and phloem cells it is clear that this slow exchange can only be a long-term regulation instrument for axial flux of nutrients in the xylem. The data obtained during this study call for further investigation of the specific interactions between xylem and phloem at the tissue level for a better understanding of these important interactions between the major transport systems of the plant.

In summary, the cambium appeared to be no strong sink for nutrients in contrast to the literature, which may be different for other experimental conditions (e.g. with roots still attached to the stem), species and developmental stages. Transfer to phloem was also quite weak, possibly because it is confined to some regions in the stem like departing leaf traces in nodes. Even though the data interpretation is not unambiguous it appears likely that the stem apoplast is separated in two domains by a (nutrient) diffusion barrier of unknown nature located between the xylem parenchyma and the cambium.

### **Stem tissues in regulation of the axial nutrient fluxes**

Different roles for regulation of axial fluxes of nutrients are suggested by the diverse interactions found for the different tissues with the xylem vessels. Based on labelling dynamics and strength of apoplastic and cell lumina labelling, we conclude that there are two functional groups of tissues in the stem:

- 1) The xylem parenchyma and pith, both showing fast exchange with the xylem vessels. The dynamics in the whole xylem parenchyma suggest that it functions as fast buffer and regulator for the axial nutrient flux. For the pith the dynamics suggest a role as a local storage tissue associated to the xylem vessels for regulating larger changes, especially for calcium which is not recycled in the plant.
- 2) The cambium and phloem, both showing slow exchange with the xylem vessels and possibly separated from the xylem by a barrier, playing a role in long term regulation of the axial nutrient flux.

The discovery of these two groups within stem tissues, due to their different dynamic interactions with the xylem vessels, emphasizes the need for localizing analysis of dynamic processes in plant stems at the tissue level.

#### 1.4.4 Nutrient exchange and water status

Environmental changes (e.g. light, temperature) have strong effects on transpiration rate and tension in the xylem vessels; hence the dependence of xylem vessel-stem tissue interactions on xylem vessel conditions shows their potential for regulating axial flux of nutrients under varying environmental conditions.

Tension in the xylem vessels, resulting from loss of water to the atmosphere, is the principal driving force of axial water flow according to the cohesion tension theory of water movement (Pickard and Melcher, 2005), although the tension may be only one of many forces for water lifting (Westhoff et al., 2009). For xylem vessel-stem tissue interactions the tension in the vessels is of special interest as it is reflected, at least in the roots, by radial turgor and osmotic pressure profiles (Rygel et al., 1993). Whenever tension changes abruptly, such as with cutting of the stem, marked changes in radial turgor and osmotic pressure profiles of roots occur (Wistuba et al., 2000; Schneider et al., 2007). The redistribution of water and solutes leading to the establishment of a new steady state in the radial gradients within 30 minutes (Zimmermann et al., 1992; Rygel et al., 1993) was therefore expected to show a strong effect on the radial movement of solutes.

This study showed, however, that the distribution patterns of nutrient tracers were similar (Metzner et al., sub 2009a), when applied by means of a microcapillary with little disturbance of xylem tension, or when applied via the cut stem when tension in the xylem was very different from undisturbed plants. Therefore we concluded that radial interactions of nutrients between xylem vessels and stem tissues were not significantly influenced by the tension in the xylem vessels. This makes it unlikely that radial water flow in the stem was involved in the radial movement of nutrients, as this water flow is expected to be coupled to the transpiration stream and vary according to its changes. This finding is consistent with recently published findings of Wegner and Zimmermann (2009) who showed that radial transport of potassium in maize roots showed little if any dependence on xylem pressure. Furthermore, if the radial movement of important osmotica like potassium and magnesium is not significantly affected by large differences in tension accompanied by reestablishment of osmotic gradients, it seems that mineral nutrients may not play a major role in establishing such radial osmotic gradients, especially potassium which is often an important osmoticum.

In conclusion it seems that the exchange of nutrients between stem tissues and xylem vessels and therefore regulation of axial nutrient flux, appears not to be significantly influenced by environmental conditions. This low dependence is in line with perfusion

experiments of Gilmer and Schurr (2007) who found no influence of the speed of flow in the xylem vessels on a regulation of the potassium content in the xylem vessels.

#### **1.4.5 Axial flux regulation by stem tissues**

Regulation of the flux of nutrients in the xylem vessels can be exhibited by the stem tissues by sequestration and release of nutrients. Since nutrients in the plant have a different isotopic signature, nutrients leaving or entering the transpiration stream during passage of the xylem vessels will affect the isotopic signature of the stable isotope tracer solution. Therefore the difference in the isotopic signature at the sampling site (measured by cryo-SIMS) from the original signature of the tracer is an indicator for the interactions along the stem.

The shoot critically depends for functioning and development on a sufficient supply of nutrients, therefore control over the fluxes of nutrients in the xylem vessels appears to be important for nutrient utilisation. The low dependence of nutrient flux to the shoot from external nutrient availability and water flow in the transpiration stream (Smith, 1991; Herdel et al., 2001) indicates that nutrient fluxes are under control of plant internal processes. Additionally the homeostasis of nutrients in the xylem is important for the upkeep of a constant inner milieu in the vessels and tissues tightly associated to them. Since potassium and other cationic nutrients are involved in the control of xylem vessels hydraulic resistance via swelling of hydrogels, (Zwieniecki et al., 2001) control over their concentrations is likely to affect proper functioning of the xylem. For the tissues closely associated to the xylem vessels like the bundle sheath in some leaves (Leigh and Storey, 1993; Karley et al., 2000) and the xylem parenchyma and pith in the stem as shown in this study (Metzner et al., sub 2009a). Nutrient homeostasis is important for sufficient uptake of nutrients for growth of cells, but also for maintenance of membrane potential and turgor pressure (Gierth and Maser, 2007).

The control of nutrient concentrations in the xylem vessels has been primarily attributed to the root loading of the xylem (Steudle and Peterson, 1998; Herdel et al., 2001; de Boer and Volkov, 2003; Köhler and Raschke, 2007). Specifically in the xylem parenchyma cells a variety of ion channels are suggested to be responsible for the loading of nutrients into the xylem for transport to the shoot (Wegner and De Boer, 1997; Gambale and Uozumi, 2006; Gierth and Maser, 2007; Karley and White, 2009). Few evidence about ion channels in the stem xylem parenchyma exists, except for sodium retention (Sunarpi et al., 2005), but it is

likely to assume that they have similar ion channels as found in the roots. Nevertheless, the mechanism and control of xylem loading, especially against concentration gradients (e.g. magnesium; Karley and White, 2009), remains to be demonstrated. Physiological relevance of exchange between xylem vessels and surrounding tissues influencing xylem vessel content has been demonstrated e.g. by perfusion experiments of roots (Clarkson, 1993) and has been interpreted as the result of a mechanism to establish ion homeostasis in the xylem (Lacan and Durand, 1996). Furthermore, it has been suggested that surrounding tissues are to be involved in the pH-homeostasis of the xylem (de Boer and Volkov, 2003). For the apoplast of leaves Lohaus et al. (2001) suggested homeostasis of potassium and calcium, after showing that during repeated extraction of fluid from leaf apoplast the concentration of potassium and calcium in the extracted fluid did not change. Nevertheless, this homeostasis may not apply to the whole leaf apoplast, as Felle and Hanstein (2007) found in the apoplastic fluid of the substomatal cavity after changes in potassium concentration no signs of a reestablishment of the initial concentration.

In comparison with root and leaves, the role of stem tissues in the regulation of plant nutrient transport has been demonstrated in very few cases. In perfusion experiments with internodes of castor bean, Gilmer and Schurr (2007) demonstrated that an upper limit for potassium concentration in the xylem existed, so that when a more concentrated solution was perfused, it was down-regulated to this value, presumably due to uptake by the stem tissues. When solution with lower concentration was perfused, they registered no change in concentration, but here we demonstrated an up-regulation of potassium concentration in the same situation (Metzner et al., sub 2009b). The results of Gilmer and Schurr (Gilmer and Schurr, 2007) can be explained when having a closer look at the potential origin of the nutrients. For the upkeep of these xylem potassium concentrations, the input from the stem tissues was similar to the total content of the perfused stem (Metzner et al., sub 2009b) which is present mainly in the symplast. Thus due to intracellular nutrient homeostasis (Leigh, 2001) it seems that most potassium delivered to the xylem must have been replaced by phloem transport from distal regions of the shoot in an example of nutrient cycling. This is also consistent with Zwieniecki et al (2004) showing that phloem-borne potassium may regulate the conductivity of the xylem along branches and is therefore important for homeostasis of potassium concentration in the local xylem vessels. In contrast, when Gilmer and Schurr (2007) perfused xylem of an *isolated* length of *Ricinus* stem (i.e. with no phloem connections from a shoot), they found hardly any up-regulation in the

potassium concentration during passage of the xylem vessels, suggesting that good phloem connections may be necessary for up-regulation of potassium in the xylem.

It remains an open question, if this transfer from phloem to xylem is mediated by a special structure like a node present between the tracer application and sampling site, which are considered to be key sites in radial exchange and often show the presence of transfer cells (Gunning, 1977) or if it is a transfer (supposedly symplastic) from the phloem to the xylem parenchyma and release from these into the xylem vessels, a task for which the xylem parenchyma cells seemed to be readily equipped. An apoplastic transfer appears unlikely in the light of the diffusion barrier suggested in this study between xylem parenchyma and the cambium.

In conclusion, xylem vessel-stem tissue interactions clearly allowed for an up-regulation at least of potassium concentration in the transpiration stream. This regulatory potential apparently involving transfer of cycled potassium from the phloem to the xylem vessels, illustrating complexity of nutrient utilization in the plant.

## 2 Synopsis

The aim of this thesis was to characterize interactions of the stem tissues with the transpiration stream in the xylem vessels in the stem of bean plants and to evaluate their potential for a regulation of axial nutrient fluxes. For this cryo-SIMS protocols were developed to allow diffusible stable isotope tracers to be used at cell and tissue level resolution, allowing for the first time a direct characterization of the nutrient and water exchange between the xylem transport system and the stem tissues (Metzner et al., 2008). This revealed a purely apoplastic pathway of nutrient movement from the xylem into the stem tissues and strong differences in exchange of individual tissues and between apoplast, symplast and vacuoles. There were two functional domains, one consisting of the xylem parenchyma and the pith, allowing fast exchange with the xylem and providing a major component for regulation of axial flux (Metzner et al., sub 2009a). The other domain consisted of cambium, phloem and other extracambial tissues showing slow exchange with the xylem. The findings suggested there may be an apoplastic barrier between the domains for nutrients. The ability of stem tissues to ensure potassium homeostasis in the xylem vessels was demonstrated (Metzner et al., sub 2009b). These findings suggest that the stem tissues may play an important role in regulating axial nutrient fluxes independent from xylem root loading and be one of the key factors for matching demand and delivery in shoot organs for optimal use of mineral nutrient resources.

### 3 Publications used for this dissertation

**Metzner R, Schneider HU, Breuer U, Schroeder WH** (2008) Imaging nutrient distributions in plant tissue using time-of-flight secondary ion mass spectrometry and scanning electron microscopy. *Plant Physiology* **147**: 1774-1787

**Metzner R, Schneider HU, Breuer U, Thorpe MR, Schurr U, Schroeder WH** (sub 2009a) Tracing cationic nutrients from xylem into stem tissues of *Phaseolus vulgaris* by stable isotope tracers and cryo-secondary ion mass spectrometry. *Plant Physiology* (*submitted*)

**Metzner R, Thorpe MR, Breuer U, Blümner P, Schurr U, Schroeder WH** (sub 2009b) Contrasting dynamics of water and mineral nutrients in stems shown by stable isotope tracers and cryo-SIMS. *Plant, Cell & Environment* (*submitted*)

## 4 References

- Amtmann A, Blatt MR** (2009) Regulation of macronutrient transport. *New Phytologist* **181**: 35-52
- Atkins C** (1999) Biochemical aspects of assimilate transfers along the phloem path: N-solutes in lupins. *In International Conference on Assimilate Transport and Partitioning (ICATP 99)*. C S I R O Publishing, Newcastle, Australia, pp 531-537
- Barbour MM** (2007) Stable oxygen isotope composition of plant tissue: a review. *Functional Plant Biology* **34**: 83-94
- Belu AM, Graham DJ, Castner DG** (2003) Time-of-flight secondary ion mass spectrometry: techniques and applications for the characterization of biomaterial surfaces. *Biomaterials* **24**: 3635-3653
- Boyer JS** (1985) WATER TRANSPORT. *Annual Review of Plant Physiology and Plant Molecular Biology* **36**: 473-516
- Bull TA, Gayler KR, Glasziou KT** (1972) Lateral movement of water and sugar across xylem in sugarcane stalks. *Plant Physiology* **49**: 1007-1011
- Canny MJ** (1991) The Xylem Wedge As A Functional Unit - Speculations on the Consequences of Flow in Leaky Tubes. *New Phytologist* **118**: 367-374
- Canny MJ** (1995) Apoplastic water and solute movement - New rules for an old space. *Annual Review of Plant Physiology and Plant Molecular Biology* **46**: 215-236
- Chandra S, Smith DR, Morrison GH** (2000) Subcellular imaging by dynamic SIMS ion microscopy. *Analytical Chemistry* **72**: 104A-114A
- Clarkson DT** (1993) ROOTS AND THE DELIVERY OF SOLUTES TO THE XYLEM. *Philosophical Transactions of the Royal Society of London Series B-Biological Sciences* **341**: 5-17
- Dasilva MC, Shelp BJ** (1990) XYLEM-TO-PHLOEM TRANSFER OF ORGANIC NITROGEN IN YOUNG SOYBEAN PLANTS. *Plant Physiology* **92**: 797-801
- de Boer AH, Volkov V** (2003) Logistics of water and salt transport through the plant: structure and functioning of the xylem. *Plant Cell and Environment* **26**: 87-101
- Derue C, Gibouin D, Demarty M, Verdus MC, Lefebvre F, Thellier M, Ripoll C** (2006) Dynamic-SIMS imaging and quantification of inorganic ions in frozen-hydrated plant samples. *Microscopy research and technique* **69**: 53-63
- Dickson RE, Vogelmann TC, Larson PR** (1985) Glutamine Transfer from Xylem to Phloem and Translocation to Developing Leaves of *Populus-Deltoides*. *Plant Physiology* **77**: 412-417
- Echlin P** (1992) *Low-Temperature Microscopy and Analysis*. Plenum Press, New York
- Enright AM, Cumbie BG** (1973) Stem Anatomy and Internodal Development in *Phaseolus-Vulgaris*. *American Journal of Botany* **60**: 915-922
- Esau K** (1977) *Anatomy of seed plants*. John Wiley & Sons, Inc.
- Felle H, Hanstein S** (2007) Probing apoplastic ion relations in *Vicia faba* as influenced by nutrition and gas exchange. *In B Sattelmacher, WJ Horst, eds, The apoplast of higher plants: Compartment of storage, transport and reactions*. Springer, Dordrecht, pp 295-306
- Fricke W** (2004) Solute sorting in grass leaves: the transpiration stream. *Planta* **219**: 507-514
- Gambale F, Uozumi N** (2006) Properties of Shaker-type potassium channels in higher plants. *Journal of Membrane Biology* **210**: 1-19
- Gartner BL**, ed (1995) *Plant stems: Physiology and functional anatomy*, Ed illustrated. Academic Press



- Gierth M, Maser P** (2007) Potassium transporters in plants - Involvement in K<sup>+</sup> acquisition, redistribution and homeostasis. *Febs Letters* **581**: 2348-2356
- Gilmer F, Schurr U** (2007) Dynamic and nutrient fluxes in the xylem. *In* B Sattelmacher, WJ Horst, eds, *The Apoplast of higher plants: Compartment of storage, transport, and reactions*. Springer, Dordrecht, pp 221-229
- Goldstein G, Andrade JL, Meinzer FC, Holbrook NM, Cavelier J, Jackson P, Celis A** (1998) Stem water storage and diurnal patterns of water use in tropical forest canopy trees. *Plant Cell and Environment* **21**: 397-406
- Goldstein JI, Romig AD, Jr., Newbury DE, Lyman CE, Echlin P, Fiori C, Joy DC, Lifshin E** (1994) *Scanning Electron Microscopy and X-Ray Microanalysis*. Plenum Press, New York
- Gunning BES** (1977) Transfer Cells and Their Roles in Transport of Solutes in Plants. *Science Progress* **64**: 539-568
- Hedrich R, Schroeder JI** (1989) The Physiology of Ion Channels and Electrogenic Pumps in Higher-Plants. *Annual Review of Plant Physiology and Plant Molecular Biology* **40**: 539-569
- Heeren RMA, McDonnell LA, Amstalden E, Luxembourg SL, Altelaar AFM, Piersma SR** (2006) Why don't biologists use SIMS? A critical evaluation of imaging MS. *Applied Surface Science* **252**: 6827-6835
- Herdel K, Schmidt P, Feil R, Mohr A, Schurr U** (2001) Dynamics of concentrations and nutrient fluxes in the xylem of *Ricinus communis* - diurnal course, impact of nutrient availability and nutrient uptake. *Plant Cell and Environment* **24**: 41-52
- Hoad GV, Peel AJ** (1965) Studies on Movement Solutes Between Sieve Tubes and Surrounding Tissues in Willow .2. Pathways of Ion Transport from Xylem to Phloem. *Journal of Experimental Botany* **16**: 742-&
- Jacoby B** (1965) Sodium Retention in Excised Bean Stems. *Physiologia Plantarum* **18**: 730-&
- Jahnke S, Menzel MI, van Dusschoten D, Roeb GW, Buhler J, Minwuyelet S, Blumler P, Temperton VM, Hombach T, Streun M, Beer S, Khodaverdi M, Ziemons K, Coenen HH, Schurr U** (2009) Combined MRI-PET dissects dynamic changes in plant structures and functions. *Plant Journal* **59**: 634-644
- Jeschke WD** (1970) On Application of Rb-86 As A Tracer for Potassium, Measurements of Light-Dependent K-42/K-Influx and Rb-86/Rb-Influx in *Elodea-Densa*. *Zeitschrift fur Naturforschung Part B-Chemie Biochemie Biophysik Biologie und Verwandten Gebiete* **B 25**: 624-&
- Jeschke WD, Hartung W** (2000) Root-shoot interactions in mineral nutrition. *Plant and Soil* **226**: 57-69
- Jeschke WD, Pate JS** (1991) Cation and Chloride Partitioning Through Xylem and Phloem Within the Whole Plant of *Ricinus-Communis* I Under Conditions of Salt Stress. *Journal of Experimental Botany* **42**: 1105-1116
- Jeschke WD, Pate JS** (1991) Modeling of the partitioning, assimilation and storage of nitrate within root and shoot organs of castor bean (*Ricinus-Communis* L.). *Journal of Experimental Botany* **42**: 1091-1103
- Jeschke WD, Pate JS, Atkins CA** (1987) PARTITIONING OF K<sup>+</sup>, NA<sup>+</sup>, MG<sup>++</sup>, AND CA<sup>++</sup> THROUGH XYLEM AND PHLOEM TO COMPONENT ORGANS OF NODULATED WHITE LUPIN UNDER MILD SALINITY. *Journal of Plant Physiology* **128**: 77-93
- Karley AJ, Leigh RA, Sanders D** (2000) Where do all the ions go? The cellular basis of differential ion accumulation in leaf cells. *Trends in Plant Science* **5**: 465-470

- Karley AJ, White PJ** (2009) Moving cationic minerals to edible tissues: potassium, magnesium, calcium. *Current Opinion in Plant Biology* **12**: 291-298
- Köhler B, Raschke K** (2007) Loading of ions into the xylem of the root. *In* B Sattelmacher, WJ Horst, eds, *The Apoplast of higher plants: Compartment of storage, transport and reactions*. Springer, Dordrecht, pp 181-200
- Koroleva OA, Davies A, Deeken R, Thorpe MR, Tomos AD, Hedrich R** (2000) Identification of a new glucosinolate-rich cell type in Arabidopsis flower stalk. *Plant Physiology* **124**: 599-608
- Kuhn AJ, Schroeder WH, Bauch J** (1997) On the distribution and transport of mineral elements in xylem, cambium and phloem of spruce (*Picea abies* [L.] Karst.). *Holzforschung* **51**: 487-496
- Kuhn AJ, Schroeder WH, Bauch J** (2000) The kinetics of calcium and magnesium entry into mycorrhizal spruce roots. *Planta* **210**: 488-496
- Lacan D, Durand M** (1996) Na<sup>+</sup>-K<sup>+</sup> exchange at the xylem/symplast boundary. *Plant Physiology* **110**: 705-711
- Lechene CP, Luyten Y, McMahon G, Distel DL** (2007) Quantitative imaging of nitrogen fixation by individual bacteria within animal cells. *Science* **317**: 1563-1566
- Leigh RA** (2001) Potassium homeostasis and membrane transport. *Journal of Plant Nutrition and Soil Science-Zeitschrift für Pflanzenernährung und Bodenkunde* **164**: 193-198
- Leigh RA, Storey R** (1993) Intercellular Compartmentation of Ions in Barley Leaves in Relation to Potassium Nutrition and Salinity. *Journal of Experimental Botany* **44**: 755-762
- Leigh RA, Tomos AD** (1993) ION DISTRIBUTION IN CEREAL LEAVES - PATHWAYS AND MECHANISMS. *Philosophical Transactions of the Royal Society of London Series B-Biological Sciences* **341**: 75-86
- Lersten NR** (1997) Occurrence of endodermis with a casparian strip in stem and leaf. *Botanical Review* **63**: 265-272
- Link J, Seelig J** (1990) COMPARISON OF DEUTERIUM NMR IMAGING METHODS AND APPLICATION TO PLANTS. *Journal of Magnetic Resonance* **89**: 310-330
- Lohaus G** (2007) Interaction between phloem transport and apoplastic solute concentrations. *In* B Sattelmacher, WJ Horst, eds, *The Apoplast of higher plants: Compartment of storage, transport, and reactions*. Springer, Dordrecht, pp 323-336
- Lohaus G, Pennewiss K, Sattelmacher B, Hussmann M, Muehling KH** (2001) Is the infiltration-centrifugation technique appropriate for the isolation of apoplastic fluid? A critical evaluation with different plant species. *Physiologia Plantarum* **111**: 457-465
- Long JM, Widders IE** (1990) Quantification of Apoplastic Potassium Content by Elution Analysis of Leaf Lamina Tissue from Pea (*Pisum-Sativum* l Cv *Argenteum*). *Plant Physiology* **94**: 1040-1047
- Maathuis JM, Ichida AM, Sanders D, Schroeder JI** (1997) Roles of higher plant K<sup>+</sup> channels. *Plant Physiology* **114**: 1141-1149
- Marschner H** (1995) *Mineral nutrition of higher plants*, Ed 2. Academic Press Limited, London
- Marschner H, Kirkby EA, Engels C** (1997) Importance of cycling and recycling of mineral nutrients within plants for growth and development. *Botanica Acta* **110**: 265-273
- Marschner H, Schimansky C** (1968) Differential Uptake of Potassium and Rubidium by Barley. *Naturwissenschaften* **55**: 499-&

- Mason TG, Maskell EJ** (1931) Further studies on transport in the cotton plant. I. Preliminary observations on the transport of phosphorus, potassium, and calcium. *Annals of Botany* **45**: 125-173
- McCully ME, Canny MJ, Huang CX** (2009) Cryo-scanning electron microscopy (CSEM) in the advancement of functional plant biology. Morphological and anatomical applications. *Functional Plant Biology* **36**: 97-124
- McNeil DL** (1980) THE ROLE OF THE STEM IN PHLOEM LOADING OF MINERALS IN LUPINUS-ALBUS L CV ULTRA. *Annals of Botany* **45**: 329-338
- McNeil DL, Atkins CA, Pate JS** (1979) UPTAKE AND UTILIZATION OF XYLEM-BORNE AMINO-COMPOUNDS BY SHOOT ORGANS OF A LEGUME. *Plant Physiology* **63**: 1076-1081
- Meinzer FC, Brooks JR, Domec JC, Gartner BL, Warren JM, Woodruff DR, Bible K, Shaw DC** (2006) Dynamics of water transport and storage in conifers studied with deuterium and heat tracing techniques. *Plant Cell and Environment* **29**: 105-114
- Minchin PEH, Thorpe MR** (1984) APOPLASTIC PHLOEM UNLOADING IN THE STEM OF BEAN. *Journal of Experimental Botany* **35**: 538-550
- Munns R, Tester M** (2008) Mechanisms of salinity tolerance. *Annual Review of Plant Biology* **59**: 651-681
- Nobel PS** (1999) *Physicochemical and environmental plant physiology*, Ed 2, illustrated. Academic Press
- Ohya T, Tanoi K, Hamada Y, Okabe H, Rai H, Hojo J, Suzuki K, Nakanishi TM** (2008) An analysis of long-distance water transport in the soybean stem using (H<sub>2</sub>O)-O-15. *Plant and Cell Physiology* **49**: 718-729
- Pickard WF, Melcher PJ** (2005) Perspectives of the biophysics of xylem transport. *In* NM Holbrook, MA Zwieniecki, eds, *Vascular transport in plants*. Elsevier Academic Press, Burlington, pp 3-18
- Pitman MG** (1977) ION-TRANSPORT INTO XYLEM. *Annual Review of Plant Physiology and Plant Molecular Biology* **28**: 71-88
- Pitman MG, Lutge U, Lauchli A, Ball E** (1974) ION UPTAKE TO SLICES OF BARLEY LEAVES, AND REGULATION OF K CONTENT IN CELLS OF LEAVES. *Zeitschrift Fur Pflanzenphysiologie* **72**: 75-88
- Reintanz B, Szyroki A, Ivashikina N, Ache P, Godde M, Becker D, Palme K, Hedrich R** (2002) AtKC1, a silent Arabidopsis potassium channel alpha-subunit modulates root hair K<sup>+</sup> influx. *Proceedings of the National Academy of Sciences of the United States of America* **99**: 4079-4084
- Rygel J, Pritchard J, Zhu JJ, Tomos AD, Zimmermann U** (1993) Transpiration Induces Radial Turgor Pressure-Gradients in Wheat and Maize Roots. *Plant Physiology* **103**: 493-500
- Sack L, Holbrook NM** (2006) Leaf hydraulics. *Annual Review of Plant Biology* **57**: 361-381
- Schneider HU, Wegner LH, Haase A, Zimmermann U** (2007) Long-distance water transport under controlled transpirational conditions: Minimal-invasive investigations by means of pressure probes and NMR imaging. *In* B Sattelmacher, WJ Horst, eds, *The apoplast of higher plants: Compartment of storage, transport and reactions*. Springer, Dordrecht, pp 251-264
- Schurr U** (1998) Xylem sap sampling - new approaches to an old topic. *Trends in Plant Science* **3**: 293-298

- Smith JAC** (1991) ION-TRANSPORT AND THE TRANSPIRATION STREAM. *Botanica Acta* **104**: 416-421
- Stelzer R, Lehmann H, Kramer D, Luttge U** (1990) X-ray microprobe analyses of vacuoles of spruce needle mesophyll, endodermis and transfusion parenchyma cells at different seasons of the year. *Botanica Acta* **103**: 415-423
- Steudle E** (1989) WATER-FLOW IN PLANTS AND ITS COUPLING TO OTHER PROCESSES - AN OVERVIEW. *Methods in Enzymology* **174**: 183-225
- Steudle E** (1997) Water transport across plant tissue: Role of water channels. *Biology of the cell* **89**: 259-273
- Steudle E** (2000) Water uptake by plant roots: an integration of views. *Plant and Soil* **226**: 45-56
- Steudle E, Peterson CA** (1998) How does water get through roots? *Journal of Experimental Botany* **49**: 775-788
- Storey R, Leigh RA** (2004) Processes modulating calcium distribution in citrus leaves. An investigation using x-ray microanalysis with strontium as a tracer. *Plant Physiology* **136**: 3838-3848
- Stout PR, Hoagland DR** (1939) Upward and lateral movement of salt in certain plants as indicated by radioactive isotopes of potassium, sodium, and phosphorus absorbed by roots. *American Journal of Botany* **26**: 320-324
- Sunarpi, Horie T, Motoda J, Kubo M, Yang H, Yoda K, Horie R, Chan WY, Leung HY, Hattori K, Konomi M, Osumi M, Yamagami M, Schroeder JI, Uozumi N** (2005) Enhanced salt tolerance mediated by AtHKT1 transporter-induced Na<sup>+</sup> unloading from xylem vessels to xylem parenchyma cells. *Plant Journal* **44**: 928-938
- Tester M, Leigh RA** (2000) Partitioning of nutrient transport processes in roots. *In Annual Meeting of the Society-of-Experimental-Biology*. Oxford Univ Press, Exeter, England, pp 445-457
- Thellier M, Derue C, Tafforeau M, Le Sceller L, Verdus MC, Massiot P, Ripoll C** (2001) Physical methods for in vitro analytical imaging in the microscopic range in biology, using radioactive or stable isotopes (review article). *Journal of Trace and Microprobe Techniques* **19**: 143-162
- Thorpe MR, Ferrieri AP, Herth MM, Ferrieri RA** (2007) C-11-imaging: methyl jasmonate moves in both phloem and xylem, promotes transport of jasmonate, and of photoassimilate even after proton transport is decoupled. *Planta* **226**: 541-551
- Thorpe MR, Minchin PEH, Gould N, J M** (2006) The Stem Apoplast: A potential communication channel in plant growth regulation. *In NM Holbrook, MA Zwieniecki, eds, Vascular transport in plants*. Academic press, pp 201-220
- van Bel AJE** (1974) Absorption of L-alpha-alanine and L-alpha-amino-iso-butyric acid during their movement through xylem vessels of tomato stem segments *Acta Botanica Neerlandica* **23**: 305-313
- van Bel AJE** (1978) Free space of xylem translocation pathway of tomato stem. *Journal of Experimental Botany* **29**: 295-303
- van Bel AJE** (1990) Xylem-phloem exchange via the rays - the undervalued route of transport. *Journal of Experimental Botany* **41**: 631-644
- van Bel AJE, Vanleeuwenkamp P, van der Schoot C** (1981) AMINO-ACID-UPTAKE BY VARIOUS TISSUES OF THE TOMATO PLANT - EFFECTS OF THE EXTERNAL PH AND LIGHT. *Zeitschrift Fur Pflanzenphysiologie* **104**: 117-128
- van der Schoot C, van Bel AJE** (1989) Architecture of the internodal xylem of tomato (*Solanum-lycopersicum*) with reference to longitudinal and lateral transfer. *American Journal of Botany* **76**: 487-503

- van der Schoot C, van Bel AJE** (1990) Mapping membrane-potential differences and dye-coupling in internodal tissues of tomato (*Solanum-lycopersicon* L.). *Planta* **182**: 9-21
- Van der Weerd L, Claessens M, Efde C, Van As H** (2002) Nuclear magnetic resonance imaging of membrane permeability changes in plants during osmotic stress. *Plant Cell and Environment* **25**: 1539-1549
- Vickerman JC, Briggs D** (2001) ToF-SIMS Surface Analysis by Mass Spectrometry. IM Publication and Surface Spectra Limited
- Walsh KB, Sky RC, Brown SM** (2005) The anatomy of the pathway of sucrose unloading within the sugarcane stalk. *Functional Plant Biology* **32**: 367-374
- Waring RH, Roberts JM** (1979) ESTIMATING WATER FLUX THROUGH STEMS OF SCOTS PINE WITH TRITIATED-WATER AND P-32. *Journal of Experimental Botany* **30**: 459-471
- Wegner LH, De Boer AH** (1997) Properties of two outward-rectifying channels in root xylem parenchyma cells suggest a role in K<sup>+</sup> homeostasis and long-distance signaling. *Plant Physiology* **115**: 1707-1719
- Wegner LH, Deboer AH, Raschke K** (1994) Properties of the K<sup>+</sup> Inward Rectifier in the Plasma-Membrane of Xylem Parenchyma Cells from Barley Roots - Effects of Tea(+), Ca<sup>2+</sup>, Ba<sup>2+</sup> and La<sup>3+</sup>. *Journal of Membrane Biology* **142**: 363-379
- Wegner LH, Zimmermann U** (2009) Hydraulic conductance and K<sup>+</sup> transport into the xylem depend on radial volume flow, rather than on xylem pressure, in roots of intact, transpiring maize seedlings. *New Phytologist* **181**: 361-373
- Westhoff M, Zimmermann D, Schneider H, Wegner LH, Gessner P, Jakob P, Bamberg E, Shirley S, Bentrup FW, Zimmermann U** (2009) Evidence for discontinuous water columns in the xylem conduit of tall birch trees. *Plant Biology* **11**: 307-327
- White PJ** (2001) The pathways of calcium movement to the xylem. *Journal of Experimental Botany* **52**: 891-899
- White PJ, Banfield J, Diaz M** (1992) UNIDIRECTIONAL CA<sup>2+</sup> FLUXES IN ROOTS OF RYE (*SECALE-CEREALE* L) - A COMPARISON OF EXCISED ROOTS WITH ROOTS OF INTACT PLANTS. *Journal of Experimental Botany* **43**: 1061-1074
- Windt CW, Vergeldt FJ, De Jager PA, Van As H** (2006) MRI of long-distance water transport: a comparison of the phloem and xylem flow characteristics and dynamics in poplar, castor bean, tomato and tobacco. *Plant Cell and Environment* **29**: 1715-1729
- Wistuba N, Reich R, Wagner HJ, Zhu JJ, Schneider H, Bentrup FW, Haase A, Zimmermann U** (2000) Xylem flow and its driving forces in a tropical liana: concomitant flow-sensitive NMR imaging and pressure probe measurements. *Plant Biology* **2**: 579-582
- Wolterbeek HT, Debruin M** (1986) Xylem and phloem import of Na<sup>+</sup>, K<sup>+</sup>, Rb<sup>+</sup>, Cs<sup>+</sup> and Sb(SO<sub>4</sub>)<sup>2-</sup> in tomato fruits - differential contributions from stem and leaf. *Journal of Experimental Botany* **37**: 928-939
- Yazaki Y, Asukagawa N, Ishikawa Y, Ohta E, Sakata M** (1988) ESTIMATION OF CYTOPLASMIC FREE MG-2+ LEVELS AND PHOSPHORYLATION POTENTIALS IN MUNG BEAN ROOT-TIPS BY INVIVO P-31 NMR-SPECTROSCOPY. *Plant and Cell Physiology* **29**: 919-924
- Ye Q, Holbrook NM, Zwieniecki MA** (2008) Cell-to-cell pathway dominates xylem-epidermis hydraulic connection in *Tradescantia fluminensis* (Vell. Conc.) leaves. *Planta* **227**: 1311-1319

- 
- Zierold K** (1992) Comparison of Cryopreparation Techniques for Electron-Probe Microanalysis of Cells As Exemplified by Human Erythrocytes. *Scanning microscopy* **6**: 1137-1145
- Zimmermann U, Rygol J, Balling A, Klock G, Metzler A, Haase A** (1992) Radial Turgor and Osmotic-Pressure Profiles in Intact and Excised Roots of Aster-Tripolium - Pressure Probe Measurements and Nuclear Magnetic-Resonance-Imaging Analysis. *Plant Physiology* **99**: 186-196
- Zimmermann U, Schneider H, Wegner LH, Wagner HJ, Szimtenings M, Haase A, Bentrup FW** (2002) What are the driving forces for water lifting in the xylem conduit? *Physiologia Plantarum* **114**: 327-335
- Zwieniecki MA, Melcher PJ, Feild TS, Holbrook NM** (2004) A potential role for xylem-phloem interactions in the hydraulic architecture of trees: effects of phloem girdling on xylem hydraulic conductance. *Tree Physiology* **24**: 911-917
- Zwieniecki MA, Melcher PJ, Holbrook NM** (2001) Hydrogel control of xylem hydraulic resistance in plants. *Science* **291**: 1059-1062

## 5 Publications of the dissertation

### 5.1 First publication: Imaging of nutrients in plant tissues using cryo-SIMS

Status: **Published** (August 2008)

Metzner R, Schneider HU, Breuer U, Schroeder WH (2008)

**Imaging nutrient distributions in plant tissue using time-of-flight secondary ion mass spectrometry and scanning electron microscopy.** *Plant Physiology* 147: 1774-1787

#### **Own contribution**

- Development of analytical protocol
- Experiments
- Sample preparation
- Cryo-SIMS analysis
- Data analysis
- Preparation of manuscript (with co-authors)

---

**Breakthrough Technologies**


---

# Imaging Nutrient Distributions in Plant Tissue Using Time-of-Flight Secondary Ion Mass Spectrometry and Scanning Electron Microscopy<sup>[OA]</sup>

Ralf Metzner, Heike Ursula Schneider, Uwe Breuer, and Walter Heinz Schroeder\*

Central Division of Analytical Chemistry (R.M., U.B.) and Phytosphere Institute (H.U.S., W.H.S.),  
Research Center Jülich, 52425 Jülich, Germany

A new approach to trace the transport routes of macronutrients in plants at the level of cells and tissues and to measure their elemental distributions was developed for investigating the dynamics and structure-function relationships of transport processes. Stem samples from *Phaseolus vulgaris* were used as a test system. Shock freezing and cryo-preparation were combined in a cryogenic chain with cryo-time-of-flight secondary ion mass spectrometry (cryo-ToF-SIMS) for element and isotope-specific imaging. Cryo-scanning electron microscopy (cryo-SEM) was integrated into the cryogenic workflow to assess the quality of structural preservation. We evaluated the capability of these techniques to monitor transport pathways and processes in xylem and associated tissues using supplementary sodium (Na) and tracers for potassium (K), rubidium (Rb), and <sup>41</sup>K added to the transpiration stream. Cryo-ToF-SIMS imaging produced detailed mappings of water, K, calcium, magnesium, the K tracers, and Na without quantification. Lateral resolutions ranged from 10 μm in survey mappings and at high mass resolution to approximately 1 μm in high lateral resolution imaging in reduced areas and at lower mass resolution. The tracers Rb and <sup>41</sup>K, as well as Na, were imaged with high sensitivity in xylem vessels and surrounding tissues. The isotope signature of the stable isotope tracer was utilized for relative quantification of the <sup>41</sup>K tracer as a fraction of total K at the single pixel level. Cryo-SEM confirmed that tissue structures had been preserved with subcellular detail throughout all procedures. Overlays of cryo-ToF-SIMS images onto the corresponding SEM images allowed detailed correlation of nutrient images with subcellular structures.

Monitoring nutrient distributions in higher plant tissues is an important task for plant physiology. A selection of potent methods is available by analysis of single-cell samples, giving information on nutrient ion content of cell vacuoles (Rygel et al., 1993; Fricke et al., 1996; Tomos and Leigh, 1999). Fluorescent-dye ratio imaging can monitor free ions at the cell and tissue levels, giving symplastic or apoplastic concentrations (Mühlhling and Läuchli, 2000; Halperin and Lynch, 2003). However, as for measurements with ion-selective microelectrodes (Leigh, 2001), only a limited range of ions can be imaged, most commonly Ca<sup>2+</sup> or K<sup>+</sup> ions in solution, but the total element contents, including bound species, are not detected.

At the tissue level, distributions of nutrients can be best revealed by microbeam analysis techniques, but they have been severely limited because satisfactory sample preparation methods have not yet been developed or detection sensitivities were not adequate. Our aim is to meet this challenge. It is essential that sample preparation preserves the original distribution of dif-

fusible analytes. Chemical fixation or embedding leads to exchange or loss of material and must be avoided. By contrast, shock freezing can preserve the authentic distribution of solutes with minimal risk of redistribution because a sufficiently rapid solidification of water stops diffusion (Goldstein et al., 1992). Hypothetically, the shock-frozen, hydrated tissues may be simply freeze dried and then sectioned. However, besides possible relocation of solutes, freeze drying causes pronounced topography of the sectioned surfaces that will interfere dramatically with microbeam analysis. Therefore, the use of shock-frozen hydrated samples followed by the preparation of sample surfaces by fracturing and planing to eliminate surface topography is the method of choice for microbeam techniques that are currently available. If, and only if, samples are maintained below -80°C throughout all analytical procedures, this offers the best method to preserve in vivo ion distributions. A major limitation of this approach for samples much larger than a few cell layers (where vitrification is possible) is the formation of ice crystals during shock freezing. For samples with diameters as large as 2 mm that are needed for transport studies in complex tissues, ice crystal formation can only be minimized, but not avoided, and the structural preservation must be examined. Ice crystal formation is also responsible for the difficulties in obtaining cryo-sections under these conditions. The low temperatures are necessary to avoid recrystallization of water that may lead to redistribution of ana-

---

\* Corresponding author; e-mail w.schroeder@fz-juelich.de.

The author responsible for distribution of materials integral to the findings presented in this article in accordance with the policy described in the Instructions for Authors ([www.plantphysiol.org](http://www.plantphysiol.org)) is: Walter Heinz Schröder ([w.schroeder@fz-juelich.de](mailto:w.schroeder@fz-juelich.de)).

<sup>[OA]</sup> Open Access articles can be viewed online without a subscription.

[www.plantphysiol.org/cgi/doi/10.1104/pp.107.109215](http://www.plantphysiol.org/cgi/doi/10.1104/pp.107.109215)



lytes and severe tissue damage. Most previous microbeam analyses on frozen-hydrated plant specimens have been obtained by energy-dispersive x-ray analysis (EDXA). With this technique, distributions of several nutrient elements at the cellular level were obtained (Canny, 1993; Williams et al., 1993). However, the detection sensitivity of cryo-EDXA for physiologically relevant elements is rather limited (approximately 10–20 mM for the usual macro- and micronutrients; Enns et al., 1998; Rowan et al., 2000) and often restricted to elements that are of high natural abundance or hyperaccumulated as, for example, in the analysis of zinc in leaves of *Thlaspi caerulescens* (Küpper et al., 1999).

Time-of-flight secondary ion mass spectrometry (ToF-SIMS) offers exceptional sensitivity that can, in principle, detect all elements and isotopes. ToF-SIMS is a surface analytical technique that is well established in material sciences (Vickerman, 2001). A pulsed scanning primary ion beam is used to sputter secondary ions from the surface of a solid sample. These secondary ions are transferred to a mass spectrometer to produce mass-resolved maps of element distributions. The immediate atomic vicinity of the analyte (the matrix) influences the efficiency to produce secondary ions. Cryo-ToF-SIMS on frozen-hydrated samples has rarely been employed, especially in plant physiology. So far, attempts to implement an uninterrupted cryo-chain were successful only in a few cases of biological suspensions (Colliver et al., 1997; Cliff et al., 2003) and only in three cases for the analysis of plant tissues (Dérue et al., 1999, 2006a; Dickinson et al., 2006). First successful cryo-SIMS studies on frozen-hydrated plant tissues used stems of flax (*Linum usitatissimum*) to localize sodium (Na), magnesium (Mg), calcium (Ca), and potassium (K; Dérue et al., 2006a) and leaf blades of *Pteris vittata* to map arsenic (Dickinson et al., 2006).

Allocation and transport of nutrients are typically dynamic processes related to changes in source-sink relationships and depend, for example, on growth and environmental conditions. Transport can be studied by use of tracers provided their transport properties reflect the nutrient of interest. Many investigations with techniques other than cryo-SIMS used a variety of element tracers based on the assumption that their chemical properties are similar to the element of interest (e.g. rubidium [Rb] for K or strontium [Sr] for Ca; Storey and Leigh, 2004). The interpretation of the resulting distribution patterns, however, can be problematic if a tracer does not mimic the respective nutrient completely (Marschner and Schimansky, 1968; Jeschke, 1970). Also, the similarities may depend on the context. For example, the similarity of Rb to K may be sufficient to trace apoplastic transport of K; on the other hand, it is known that transport of Rb and K across membranes depends on the selectivity of the K channels (Hedrich and Schroeder, 1989; Reintanz et al., 2002). Chemically identical isotopes are always preferable because of their identical transport characteristics (Schroeder et al., 1980; Schroeder and Fain, 1984).

Isotope tracers and Rb have been used in the past for transport studies involving MS, including SIMS (Lazof et al., 1992; Goldsmith et al., 1993).

In this feasibility study, we implemented a completely cryogenic workflow to measure the distribution of nutrients in stem cross sections of French bean (*Phaseolus vulgaris* 'Shiny Fardenlosa') plants. The workflow is a sequence of shock freezing, cryo-preparation, cryo-ToF-SIMS, and cryo-scanning electron microscopy (cryo-SEM). Two tracers for K, Rb and enriched  $^{41}\text{K}$ , were added to the transpiration stream to test the utility of the technique to measure their transport in xylem vessels and into surrounding tissues.

## RESULTS AND DISCUSSION

### Cryo-SEM Imaging as Control of Sample Preparation and Support for Cryo-ToF-SIMS Analysis of Frozen-Hydrated Stem Samples of French Bean

An important prerequisite for microbeam analysis is adequate tissue sample preparation. We therefore imaged the shock-frozen samples both before and after cryo-ToF-SIMS analysis. Because cryo-ToF-SIMS is a surface analytical technique, we planed cross-sectional fracture faces and evaluated their quality for element mapping by cryo-SEM. The fracture faces represent stem cross sections. Following the cryo-ToF-SIMS analysis, the sample surfaces were imaged again by cryo-SEM to evaluate for possible beam damage. Further, after cryo-ToF-SIMS analysis, it was possible to remove a thin layer of ice from the sample surfaces by freeze etching and examine the structural details that were invisible in the fully hydrated state. In this way, the structural preservation of tissues and cells could be verified.

### Quality Control of Sample Surfaces Prepared for Cryo-ToF-SIMS

Fracture faces of frozen-hydrated samples were imaged by cryo-SEM prior to cryo-ToF-SIMS analysis. A typical image of a French bean stem segment is shown in Figure 1. The micrograph represents about 15% of the total surface area of the sample. As judged by cryo-SEM imaging, large surface areas of the samples appeared sufficiently flat for cryo-ToF-SIMS analysis. Almost no structural details of the tissue under investigation can be recognized, except for a few semicircular white lines delineating the lumina of some xylem vessels (the largest marked with X in Fig. 1) by local sample charging due to the conductivity of the underlying structures and not by topography. Minor knife marks running from bottom left to top right are visible (marked by arrows in Fig. 1), indicating that no water sublimation from the surface had occurred during sample preparation. Minor knife marks were not detectable in cryo-ToF-SIMS images; however, larger marks could result in topography

Metzner et al.

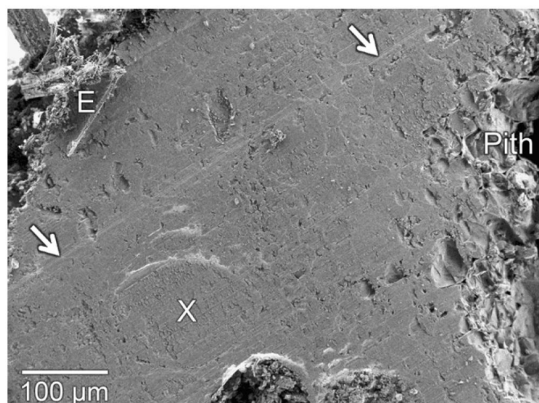


**Figure 1.** Cryo-SEM micrograph of a cross-sectional face of a shock-frozen, hydrated stem segment of French bean. The surface was planed for cryo-ToF-SIMS analysis and imaged by cryo-SEM to ascertain that large enough areas of little topography were available for analysis. Some minor knife marks are visible (arrows). E, Epidermis; Pith, pith cells; X, xylem vessel.

effects. The lack of water loss is also confirmed by a lack of prominent cell structures above the ice plane. Confined areas of pronounced topography could be occasionally detected, such as in the part of the sample surface labeled as pith in Figure 1, where cells are missing or damaged. Figure 1 also shows two xylem vessels lacking water (bottom middle) and protruding uncut fibers (top left corner) near the epidermis. Once the planing procedure was optimized, pronounced surface irregularities could be recognized by light microscopy (data not shown). Consequently, surface quality control prior to cryo-ToF-SIMS analysis was reduced to light microscopic monitoring of the sample surface during the planing process and in the cryo-ToF-SIMS instrument.

#### Cryo-SEM Imaging after Cryo-ToF-SIMS Analysis

Sample surfaces were routinely imaged by cryo-SEM after completion of the cryo-ToF-SIMS analysis, maintaining an uninterrupted cryo-chain. Scanned areas were undistinguishable from surrounding unscanned areas, indicating that no beam damage had occurred during cryo-ToF-SIMS analysis that was detectable by the field emission cryo-SEM (data not shown).

For quality control of tissue preservation, the cellular and tissue structures buried in the ice had to be revealed by freeze etching of the sample surfaces. To this end, the temperature of the sample holder was transiently elevated to approximately  $-90^{\circ}\text{C}$ . Water sublimation from the specimen surface was monitored by continuous imaging. The image shown in Figure 2A is typical of a total number of 30 shock-frozen samples of French bean stems analyzed by cryo-ToF-SIMS and

cryo-SEM. One assembly of proto- and metaxylem vessels and several secondary xylem vessels, as well as the phloem, cambium, and pith, are distinguishable due to cell shapes and sizes and cell wall thickness. Despite the large size of the stem samples with diameters of 2 to 2.5 mm that will lead to at least some structural damage due to ice crystal formation during shock freezing, subcellular structures (vacuoles and organelles) were preserved in many tissue areas (Fig. 2B). The structural preservation within the block faces therefore appears sufficient for tissue level and, to some extent, even subcellular cryo-ToF-SIMS analysis. Ice crystal formation had obviously occurred in most vessels and cells during shock freezing. Ice crystals can be detected by the striped appearance in the lumina (Fig. 2A). Such structures are typical for sample areas of high water content. Solutes interfere with the crystalline structure of pure water and therefore are often squeezed out during crystal growth. This results in the accumulation of solutes between the ice crystals in so-called interdendritic channels. Whereas the water is removed from the sample surface by sublimation, the solutes remain and become apparent in ordered structures.

No indication of ice crystal growth traversing cell walls was found. Structural damage at the tissue level was absent in most areas of the samples, but local tissue defects, as indicated by arrows in Figure 2A, were occasionally visible. Areas of such imperfections were in retrospect excluded from interpretation of the cryo-ToF-SIMS data.

An interesting finding of cryo-SEM during freeze etching the samples was that sublimation was not homogeneous, but different rates of sublimation could be observed during the process of freeze etching. This resulted in a variety of final ice levels in different tissues as visible in Figure 2 and may be caused by local differences in solute or free water concentrations and/or water-binding capacities that might be specific for cells or tissues. Some cells in the phloem region still contained frozen cell sap up to the plane of cutting, whereas the xylem vessels exhibited ice levels well below this plane. Even lumina belonging to the same tissue type could exhibit different sublimation properties. This applies to xylem vessels as well as to phloem cells. Note, for example, the slightly different ice level of xylem vessel X1 as opposed to those of vessels X2 and X3 and the very deep etching of the very small vessels adjacent to X2 and X3. Qualitative evaluation of seven similar cryo-SEM images indicated that there may be a general tendency to stronger etching of smaller vessels (data not shown). However, there may be a more complex situation and further study is needed before conclusions can be drawn.

#### Evaluation of Cryo-ToF-SIMS Imaging of Naturally Occurring Elements and Tracers

To test the suitability of our analytical protocols to study the distribution and the transport of nutrient

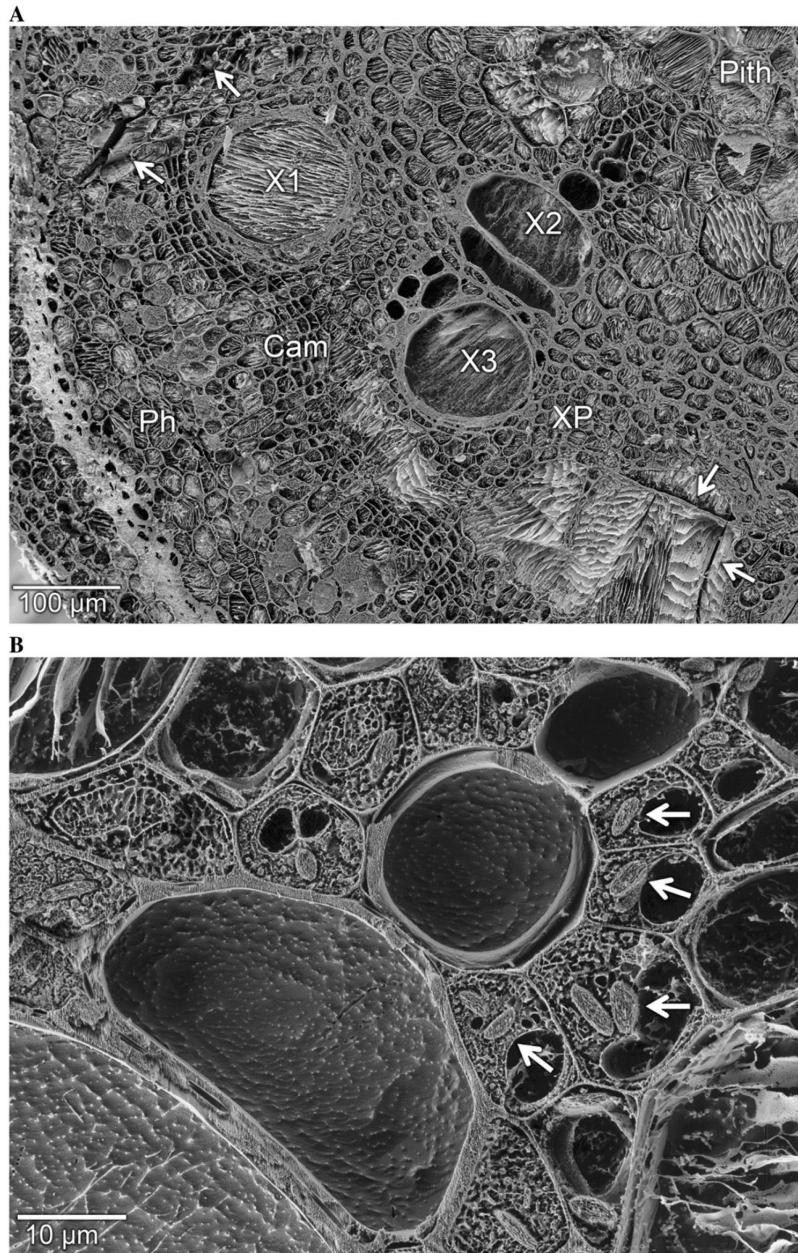


**Figure 2.** Cryo-SEM micrographs of cross-sectional faces of frozen-hydrated internodal stem segments of French bean obtained after cryo-ToF-SIMS analysis. Freeze etching was applied to reveal details of tissues and cell structures for quality control of the structural preservation, as well as reference to cryo-ToF-SIMS ion images. A, Overview of the tissue types in the vascular tissues, from an area that was already analyzed by cryo-ToF-SIMS. Starting from the lower left corner of the image, the phloem (Ph) can be seen, separated by the cambium (Cam) from the xylem. The xylem is in the secondary state of growth as indicated by the presence of large secondary vessels (X1–X3) as well as smaller vessels, and metaxylem vessels are bordering X2 (probably metaxylem) on the top right side and small secondary vessels bordering X3 on the top. All vessels are enclosed by xylem parenchyma (XP). Toward the pith (Pith) thicker cell walls are visible, while toward the cambium, the xylem parenchyma is more thin walled. Occasional local tissue defects are visible (arrows). B, Detailed view of xylem and surrounding tissues, including subcellular structural details, such as the fine structure of xylem walls, vacuoles, and organelles in xylem parenchyma cells. The arrows are placed in vacuoles and point to organelles in the cytoplasm.

elements, we examined whether (1) the most abundant isotopes of some common cationic nutrient elements could be localized in the frozen-hydrated sample surfaces with a satisfactory quality; and (2) Rb and  $^{41}\text{K}$  distribution from xylem vessels into the surrounding tissues could be traced satisfactorily.

In this pilot study, we used freshly detached shoots of French bean plants that were fed from their cut end with tracer solutions. Tracers added to the transpiration stream were either applied in half-strength Hoagland solution (solution 1) containing 10 mM Rb or in a stable isotope solution (solution 2) containing

Metzner et al.

2.5 mM enriched  $^{41}\text{K}$ . The tracer concentrations were near physiological concentrations found in other plant species (Lohaus et al., 2000; Herdel et al., 2001; Wegner and Zimmermann, 2002). After a 20-min application of the solution to the transpiration stream, stem samples were harvested approximately 50 cm apical of the application site for subsequent processing for cryo-ToF-SIMS.

#### Cryo-ToF-SIMS Imaging of Naturally Occurring Elements at 10- $\mu\text{m}$ Lateral Resolution

The first cryo-ToF-SIMS images shown are recorded in the high-current bunched mode, which has two advantages. First, it allows imaging of large tissue areas up to  $500 \times 500 \mu\text{m}^2$  within a reasonable measurement time, typically 3 to 4 h. Second, it offers a high mass resolution of  $m/\Delta m = 3,500$ . This allows the necessary unambiguous identification of the ion species of interest and separation from potentially interfering ions (e.g. hydrocarbons and water clusters). The lateral resolution of 10  $\mu\text{m}$  permits the recognition of individual tissues based on differences in cell shape that was verified by cryo-SEM images obtained from the same sample.

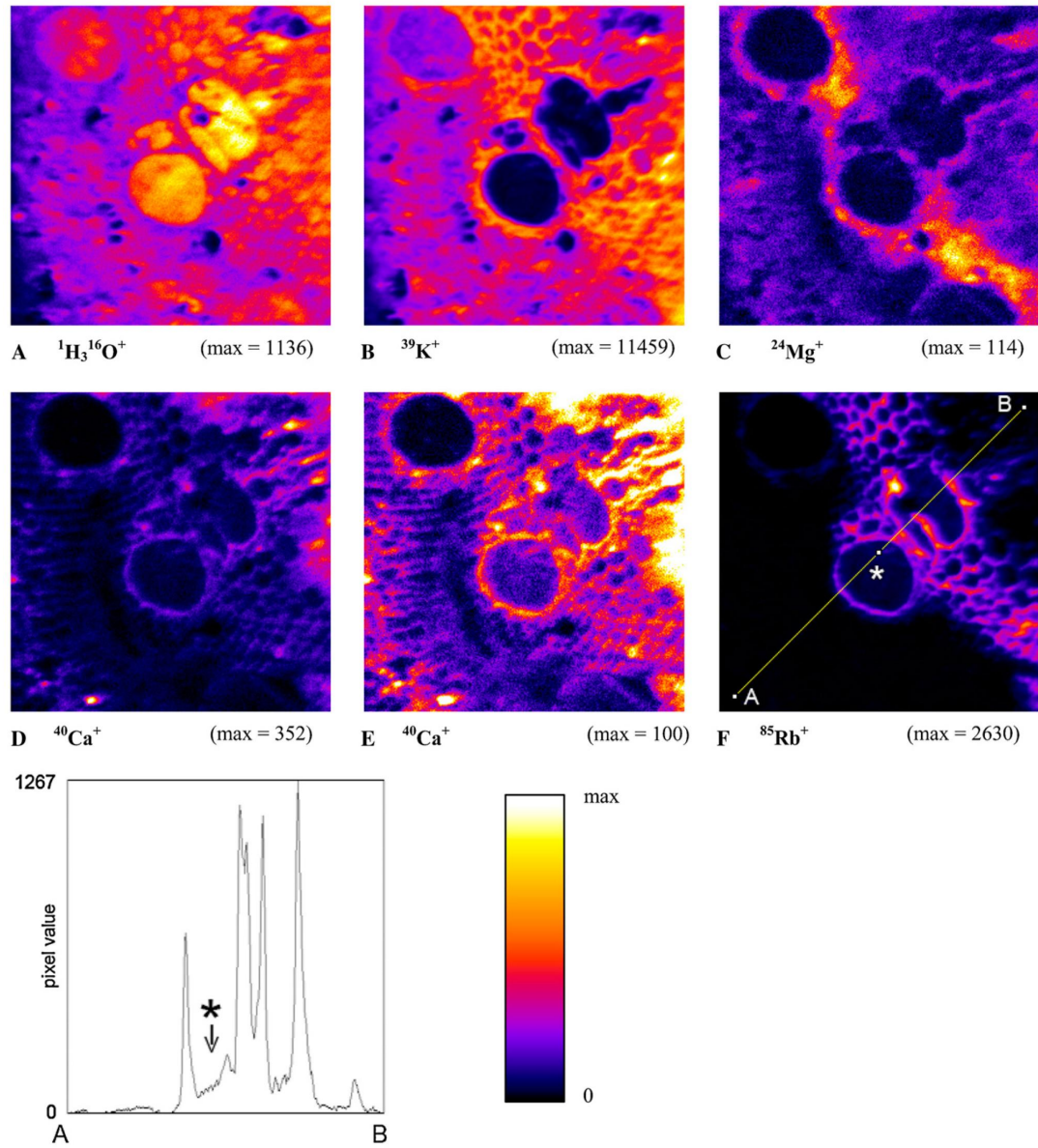
An example of a set of cryo-ToF-SIMS images is shown in Figure 3. These images were obtained from the same area that was subsequently imaged after freeze etching by cryo-SEM (Fig. 2A). The analyzed sample was obtained after feeding with a Rb tracer (solution 1).

Contrast in such SIMS images is derived from (1) the local variation in concentration of the analyte; (2) the topography of the specimen surface (Rangarajan and Tyler, 2006); and (3) the local matrix composition (Vickerman, 2001). The surface topography in our sample preparation was sufficiently reduced to avoid interference with the imaging process because minor knife marks that were detectable by cryo-SEM never appeared in ion images. Matrices of biological tissues are highly complex and inhomogeneous and this may modulate the local ion signal leading to artefacts. Despite this general caveat, it is plausible that within the hydrated tissue the matrix is similar throughout the imaged area. Another caveat is that different signals between elements (Wilson et al., 1989) in an unknown matrix do not allow relative quantification of the elements. In the well-studied case of pure silicon, the yields of elements of the first main group in the periodic table are by a factor of 3 to 5 higher than those of the second main group (Wilson et al., 1989; due to the higher ionization energy of the second group). Dérue et al. (2006b) determined sensitivity factors for Na, Mg, and Ca relative to K using frozen-hydrated reference solutions and found factors for Na/K as 0.67; Mg/K as 0.22; Ca/K as 0.31. These sensitivity factors were obtained under different SIMS conditions and may not be applicable to our conditions. Nevertheless the prospects for quantification are promising for cryo-ToF-SIMS due to the lower erosion depth as compared to dynamic SIMS.

The distribution of water in this sample is represented in Figure 3A by  $^1\text{H}_3^{16}\text{O}^+$ , the most abundant water-related ion species. The image confirms the hydrated state of the sample because  $^1\text{H}_3^{16}\text{O}^+$  ions were detected in almost the entire imaged area. Several xylem vessels, including the large vessels termed X1 to X3 in Figure 2A and a number of larger and smaller cells, are prominent in Figure 3A due to contrast between higher signals in lumina compared to cell borders. Pronounced differences in ion signals between different tissue areas of the sample are visible. The highest signals are found in xylem vessels X2 and X3 and adjacent smaller vessels, as well as in pith cell lumina. Xylem parenchyma, cambium, phloem, and xylem vessel X1 exhibit lower signals. This is compatible with the speculations about the different tissue components derived from the differences in ice levels observed by cryo-SEM after freeze drying (Fig. 2).

In addition to water, we show the major naturally occurring isotopes of K ( $^{39}\text{K}^+$ ; Fig. 3B), Mg ( $^{24}\text{Mg}^+$ ; Fig. 3C), and Ca ( $^{40}\text{Ca}^+$ ; Fig. 3, D and E). K (Fig. 3B) could be imaged with particularly high sensitivity because of its high ionization probability. Together with the high abundance of this major cation in living plant tissues, this resulted in K images of especially high signals. The highest  $^{39}\text{K}^+$  signals originate from the thick-walled xylem parenchyma and some hot spots in the pith. Some cells abutting xylem vessel X2 also reveal particularly high signals. Lower signals are found in most areas of the pith, the thin-walled xylem parenchyma, the cambium, and the phloem. The contents of xylem vessels X2 and X3 appear as dominating dark structures. Compared to these xylem vessels, the lumen of vessel X1 exhibits 4-fold higher  $^{39}\text{K}^+$  signals (440–1,750 mean counts/pixel). Likewise, Enns et al. (1998) found higher concentrations of K in certain xylem vessel elements compared to the bulk of vessels analyzed in a study on frozen-hydrated maize (*Zea mays*) roots with EDXA. They suggested that these high K concentrations indicate that these vessel elements were not fully mature, which we assume applies as well for vessel X1.

The particularly differentiated distribution of  $^{24}\text{Mg}^+$  (Fig. 3C) shows a high signal in a distinct band of the thin-walled xylem parenchyma cells close to the vessels and the cambium. Also, cells abutting xylem vessels X1 and X2 and facing toward the cambium and phloem exhibit markedly higher signals compared to the neighboring tissues. Lowest  $^{24}\text{Mg}^+$  signals are found in the xylem vessels, phloem, pith, and cambium. The confined distribution pattern may indicate a specialization of these cells for Mg uptake and accumulation. A similar assumption was made by Shaul et al. (1999) on the basis of a study on *Arabidopsis* (*Arabidopsis thaliana*), which showed an enrichment of mRNA for the  $\text{Mg}^{2+}/\text{H}^+$  exchanger AtMHX in close association with the vascular elements. They hypothesized that this exchanger may be responsible for creating a vacuolar pool of  $\text{Mg}^{2+}$ .



### G linescan of Figure 3 F

**Figure 3.** Cryo-ToF-SIMS images of several ion species from the surface of a frozen-hydrated sample. A slightly larger area of the same sample is shown in Figure 2A for orientation. The stem sample was taken 50 cm apical from the feeding site, 20 min after feeding Rb in a concentrated half-strength Hoagland solution to the xylem. Water (A) is represented by its highest-intensity ion, whereas K (B), Mg (C), Ca (D and E), and Rb (F) are mapped by elemental ions of the naturally most abundant isotopes. Images were acquired in the high-current bunched mode. Imaged areas are  $500 \times 500 \mu\text{m}^2$  at a resolution of  $256 \times 256$  pixels. Like all subsequent cryo-ToF-SIMS images below, each image was linearly scaled (equalized) from zero to its maximal counts per pixel, with the maximal value indicated (max =) and mapped to the indicated palette. Note that the  $^{40}\text{Ca}^+$  image in E is the same image as shown in D, but equalized to a reduced max = 100 to reveal further details of lower signals. The linescan (G) was computed from the image dataset of the Rb image (F) along the path from A to B. The largest xylem vessel in the line is marked in both figures by an asterisk (\*). It is the same vessel that is marked as X3 in Figure 2A.

Metzner et al.

that could be used in times of deficiency in the xylem parenchyma.

By contrast,  $^{40}\text{Ca}^+$  images exhibited particularly high ion signals in only a few spots in the pith region in the neighborhood of the xylem vessels and in the phloem region (Fig. 3D). When the image was scaled to a fraction of the maximal signal allowing highlight clipping in these hot spots (Fig. 3E), the highest  $^{40}\text{Ca}^+$  signals were found in the pith. Lower signals are found in the thick-walled xylem parenchyma and the phloem. Because the  $^{40}\text{Ca}^+$  signal pattern resembles the cellular structure of the tissues, it may originate mainly from the large pools of Ca found in the cell walls (Marschner, 1995). Still lower signals originate from the cambium, the thin-walled xylem parenchyma, and the xylem vessels. Interestingly, xylem vessels X2 and X3 exhibit higher signals than vessel X1. This finding would be expected if X2 and X3 were conducting xylem vessels in which the half-strength Hoagland solution moved, whereas X1 as a nonconducting vessel remained free of the additional Ca.

Despite the fact that Na should be detectable with a relative sensitivity factor similar to that of K (Dérue, 2006b), Na could not be imaged in these samples. The results for mapping of  $\text{Na}^+$  were variable and signals, if any, yielded only faint and poorly structured images that could not properly be evaluated (data not shown). This must be due to low Na concentrations in the stem tissues of this natrophobic *Leguminosae* species (Marschner, 1995).

Despite the caveat regarding the unknown strength of a possible matrix effect, the specific element mappings provided indications for differences in functional specialization and degrees of maturation within different tissues. Attribution of signals to different tissue types was possible at this level of lateral resolution and image contrast. Qualitatively similar distribution patterns for  $^{39}\text{K}^+$ ,  $^{24}\text{Mg}^+$ , and  $^{40}\text{Ca}^+$  were acquired for 30 of 30 analyzed surface areas regardless of the feeding solution (data not shown). In none of the analyzed samples did we witness an indication of element redistribution due to the surface planing during sample preparation (e.g. along knife marks in cases where these were visible by cryo-SEM).

#### Cryo-ToF-SIMS Imaging of Rb as an Element Tracer for K at 10- $\mu\text{m}$ Lateral Resolution

Studies of dynamic processes, such as the loading and unloading of xylem vessels, require the use of appropriate tracers. The suitability of Rb as an element tracer for K (e.g. in transport studies) was tested in the next step of evaluation of the cryo-ToF-SIMS imaging protocols. Figure 3F shows the cryo-ToF-SIMS image of the major isotope of Rb from the same experiment as described in Figure 3, A to E. One reason to choose Rb as an element tracer for K was the fact that it is naturally present in very low amounts in plant tissues (e.g. 2,000-fold lower compared to K in tomato [*Solanum lycopersicum*] leaves; National Institute of

Standards and Technology standard reference material 1573a). Despite this low natural background, Rb could be detected in our measurements of frozen-hydrated tissue samples when no tracer was added (data not shown). Because of this combination of high detection sensitivity and low natural background, Rb tracer should be detectable in the cryo-ToF-SIMS images even in very small amounts near the background of 1/2,000 of the local K concentration. Figure 3F demonstrates that the major isotope,  $^{85}\text{Rb}^+$ , could be imaged after the 20-min feeding time in the walls of xylem vessels X2 and X3 and radial from these vessels in the surrounding thick-walled xylem parenchyma 50  $\mu\text{m}$  apical of the application site. However, a clear-cut attribution of the ion signals to the apoplast and/or symplast would require a higher lateral resolution.

The wide dynamic range of the Rb signal cannot show detailed steps of signal in the limited dynamic range of the print medium. Therefore, an intensity profile derived from the dataset of this image (from bottom left A to top right corner B, plotted in Figure 3G) gives a more quantitative presentation of the Rb signals. The tracer is present in the lumen of vessel X3, as well as in the lumen of X2, but not in X1, as determined from regions of interest (data not shown). This indicates differences in xylem transport of the tracer between these vessels. In the cambium and phloem, Rb was not detectable at levels above natural background.

#### Cryo-ToF-SIMS Imaging of the Enriched Stable Isotope Tracer $^{41}\text{K}$

Matrix effects can be ruled out when enriched stable isotopes are employed as tracers because the ratios of the isotopes are the basis for detection and quantification. Naturally occurring K is mainly composed of  $^{39}\text{K}$  (93.2581%) and  $^{41}\text{K}$  (6.7302%; Böhlke et al., 2005). Our own measurements obtained from entire cryo-ToF-SIMS images from three independent samples yielded a mean abundance of 93.75%  $^{39}\text{K}$  and 6.25%  $^{41}\text{K}$  with  $3\sigma = 0.54\%$  for each of the two isotopes. With these error margins, we assume in first approximation that we can detect a  $^{41}\text{K}$  tracer if the measured abundance exceeds our measured natural abundance by 0.54%. For the  $^{41}\text{K}$  used in this study (enriched to 97%), this corresponds to the presence of 0.6% of the tracer in total K. On the single-pixel level or regions of interest, however, this detection sensitivity will be reduced and primarily limited by the statistical variation of the number of counts per pixel.

#### Cryo-ToF-SIMS Imaging at Enhanced Lateral Resolution

The distribution of the stable isotope  $^{41}\text{K}$  supplemented as a tracer for K was investigated at increased lateral resolution to facilitate analysis at the cellular level. Higher lateral resolution was attempted in two different ways. (1) In the low-current bunched mode, the lateral resolution was improved to 6  $\mu\text{m}$  at a mass

resolution of  $m/\Delta m = 5,000$ . (2) The burst-align mode offers the potential to obtain enhanced lateral resolution up to a specified value of 300 nm. However, in this measuring mode, the mass resolution is reduced to nominal mass. Therefore, it was necessary to acquire isotope images in both modes. The high mass resolution was necessary to detect the possible presence of mass interference by different ion species that might be superimposed at the mass of the selected ions and unnoticed at low mass resolution. At high mass resolution, it was possible to quantify their possible contribution to determine possible errors in images obtained at high lateral resolution.

As a point of reference for the following cryo-ToF-SIMS images within the tissue (yellow box), a cryo-SEM image is shown in Figure 4. An assembly of protoxylem and metaxylem vessels can be seen with decreasing diameters from bottom left to top right surrounded by thick-walled xylem parenchyma. Figure 4, A and B, show typical distributions of  $^{39}\text{K}^+$  and  $^{41}\text{K}^+$  measured in the low-current bunched mode.

Both isotope images contain a mixture of the naturally occurring isotope originating from the plant and the isotope originating from the tracer (because the tracer is not pure  $^{41}\text{K}^+$ , a fraction is present in the  $^{39}\text{K}^+$  image). Highest  $^{39}\text{K}^+$  signals originate from perimeters of the xylem vessels, the thick-walled xylem parenchyma, and the pith.

The distribution of  $^{41}\text{K}^+$  signals is similar, with the remarkable exception in some the protoxylem and metaxylem elements that show very high signals of  $^{41}\text{K}^+$ , but lower signals for  $^{39}\text{K}^+$ . In the case of  $^{41}\text{K}^+$ , the highest signals were detected in the tangential walls of the smaller xylem vessels (Fig. 4B, center) and the xylem parenchyma, especially close to the vessels. Interestingly, the tangential parts of these vessels exhibited higher signals of  $^{41}\text{K}^+$  than of  $^{39}\text{K}^+$  isotope, suggesting that a substantial amount of K detected in these structures originated from the  $^{41}\text{K}$  tracer. The image of the  $^{41}\text{K}$  isotope fraction is calculated from Figure 4, B and C, and is displayed in Figure 4D. The maximal value per pixel of total  $^{41}\text{K}^+$  was 47%. This corresponds to a maximal fraction of the tracer of 45% if the small amount of  $^{39}\text{K}$  in the tracer solution is also corrected for (see "Materials and Methods"). Figure 4D shows that the largest fraction of  $^{41}\text{K}$  is found in the xylem lumina. Additional signals originate from the xylem parenchyma left and top left of the central vessel. These distribution patterns were typical of all four images from three plants fed with solution 2. In control samples where no  $^{41}\text{K}$  had been applied, the ratio of  $^{41}\text{K}^+$  to ( $^{39}\text{K}^+ + ^{41}\text{K}^+$ ) was homogeneous and no relevant contrast was visible (data not shown).

We checked for possible mass interferences for the K isotopes in the spectra taken at nominal mass resolution by inspecting high mass resolution spectra from entire images being recorded in the low-current bunched mode in samples where  $^{41}\text{K}$  tracer was not used. The signal at nominal mass resolution was 98.75% identified as  $^{39}\text{K}$  and 1.25% in one interfering

peak, most likely  $\text{C}_3\text{H}_3$ . There were three peaks at the position of  $^{41}\text{K}$  at nominal mass resolution.  $^{41}\text{K}$  contributed about 83% and the interfering peaks (presumably carbohydrates) contributed about 17%. This demonstrated that  $^{39}\text{K}$  can be imaged at high lateral resolution in our samples at the nominal mass resolution of the burst-align mode, with only minor mass interferences. Images of  $^{41}\text{K}$  must be interpreted with some caution and may require verification of  $^{41}\text{K}$  distribution patterns by complementary high mass resolution imaging in the low-current bunched mode.

#### Imaging at 1- $\mu\text{m}$ Lateral Resolution with Nominal Mass Resolution

Images of the same sample area acquired with the burst-align mode are displayed in Figure 5. Limiting the measuring time to a 4-h time period per image set required a restriction in image area, in this example to  $195 \times 195 \mu\text{m}^2$ . This still supplied a view covering the protoxylem and metaxylem with surrounding tissues. The lateral resolution was slightly better than  $1 \mu\text{m}$  as suggested by line scans across cell walls of frozen-hydrated tissue samples (data not shown). This improved resolution can give a more detailed view of the element distributions not yet visible in Figure 4. For example, the very small xylem parenchyma cells abutting the xylem vessels, which could not be identified as individual cells in Figure 4, can be identified in the images of  $^1\text{H}_3^{16}\text{O}^+$  (Fig. 5A). Interestingly, subcellular dendritic ice crystal structures could be imaged in this measuring mode as demonstrated in Figure 5A.

The improved resolution refines the results already seen in the images in Figures 3 and 4, as exemplified by the K images. High  $^{39}\text{K}^+$  signals (Fig. 5C) are found especially in very small parenchyma cells directly adjacent to the xylem vessels. The high signal apparently originates from the cell borders, although the contributions from the cytoplasm and/or the cell walls cannot be allocated precisely. Interestingly the tangential walls of the xylem vessels display rather low  $^{39}\text{K}^+$  signals (Fig. 5C). By contrast, these structures were particularly prominent in the  $^{41}\text{K}^+$  image (Fig. 5D), confirming the findings of Figure 4C. The corresponding map of  $^{41}\text{K}/(^{39}\text{K} + ^{41}\text{K})$  (Fig. 5E) shows the maximal fraction of total  $^{41}\text{K}$  as 53%, corresponding to a maximal fraction of the tracer of 51%. It is more clearly visible in Figure 5E than in Figure 4D that the tracer of K transport was located predominantly in the xylem vessels, but that it had also spread into the neighboring tissue. Seemingly equal fractions of  $^{41}\text{K}$  were present in the vessel lumina and walls. Lower, but visible,  $^{41}\text{K}$  percentages delineate the cell borders of the xylem parenchyma.

#### Imaging of Supplemented Na

Interestingly, there is no mass interference at  $^{23}\text{Na}^+$ . Because Na is extremely difficult to map using micro-beam techniques unless present in high concentra-

Metzner et al.

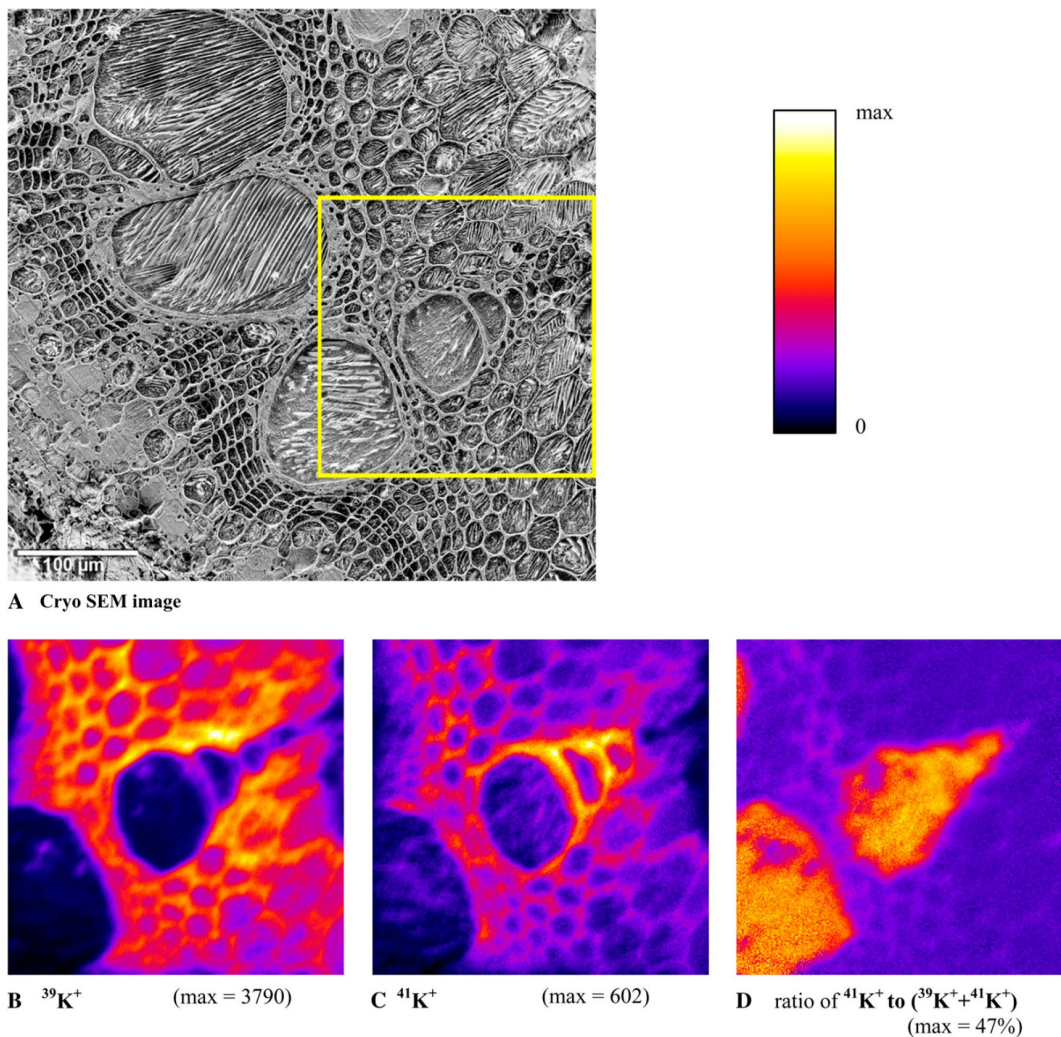


**Figure 4.** A to D, Cryo-SEM image (A) and cryo-ToF-SIMS images (B–D) of the surface of a bean stem cross section. The SEM image (A) was obtained after analysis with cryo-ToF-SIMS and freeze etching. The tissue details described in Figure 2A can be seen here as well. The stem sample was taken 50 cm apical from the feeding site 20 min after feeding enriched  $^{41}\text{K}$  as a tracer to the xylem. The isotope maps show the two major isotopes  $^{39}\text{K}^+$  (B) and  $^{41}\text{K}^+$  (C). The analyzed area is indicated by the yellow box in A and was selected to cover the protoxylem and metaxylem. The images were acquired in the low-current bunched mode. The imaged area is  $229 \times 229 \mu\text{m}^2$  with  $256 \times 256$  pixels. The calculated map of the ratio  $^{41}\text{K}^+$  to  $(^{39}\text{K}^+ + ^{41}\text{K}^+)$  that indicates the distribution of the  $^{41}\text{K}$  tracer expressed in percent is shown in D.

tions, it was straightforward to test whether imaging of  $^{23}\text{Na}^+$  was possible at high lateral resolution. Whereas we were again unable to image Na in control plants, we tested whether supplemented Na could be detected. Sodium was supplemented to the transpiration stream as 2.5 mM NaCl in the stable isotope tracer solution (solution 2). Figure 5B shows a highly de-

tailed distribution of  $^{23}\text{Na}^+$  with high signals in the xylem parenchyma. This finding is compatible with the previously published assumption that Na accessing in the transpiration stream of natriophobic species, especially in *Phaseolus*, is relocated into xylem parenchyma (Jacoby, 1965; Rains, 1969; DeBoer and Volkov, 2003).



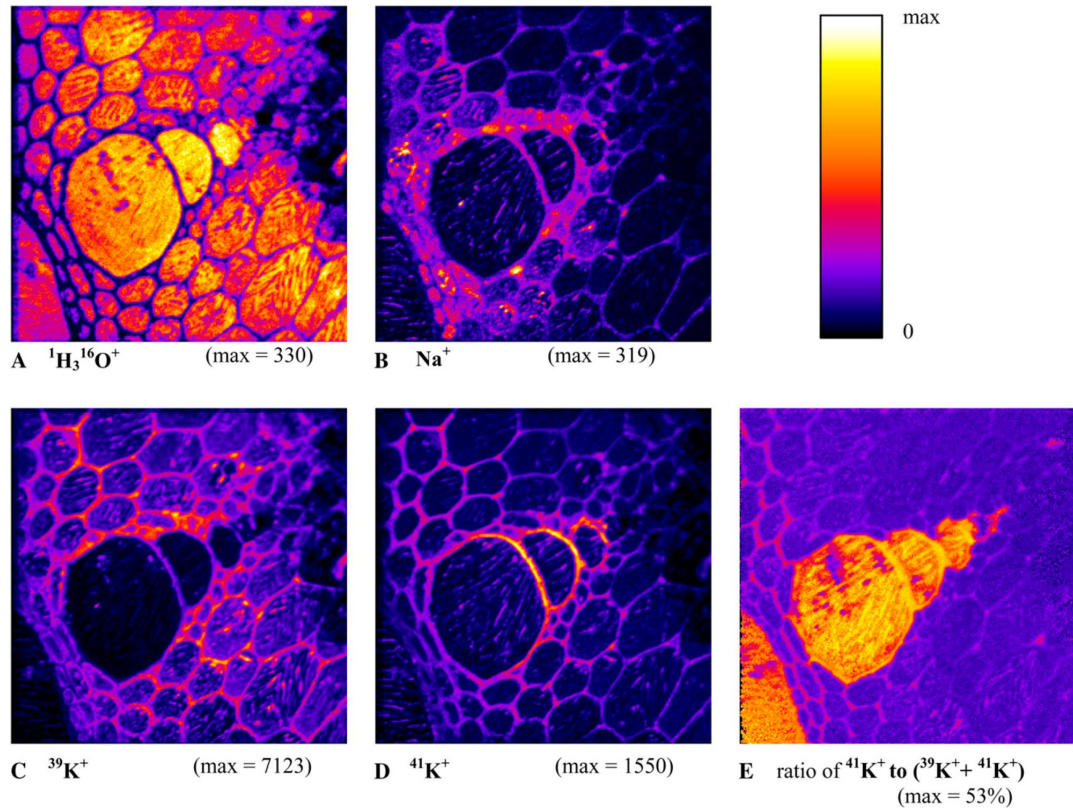


**Figure 5.** Cryo-ToF-SIMS mappings of the sample shown in Figure 4, but at higher magnification and enhanced lateral resolution obtained in the burst-align mode. A to D, Maps of  $^1\text{H}_3^{16}\text{O}^+$ ,  $^{23}\text{Na}^+$ ,  $^{39}\text{K}^+$ , and  $^{41}\text{K}^+$ , respectively. E, Calculated map of the ratio  $^{41}\text{K}^+$  to  $(^{39}\text{K}^+ + ^{41}\text{K}^+)$  expressed in percent. Note that in the selected measuring mode mass interferences on mass 41 could contribute up to 17% to the  $^{41}\text{K}^+$  ion signal. The area was imaged with  $256 \times 256$  pixels covering  $195 \times 195 \mu\text{m}^2$ .

#### Assigning Ion Distributions to Detailed Anatomical Structures

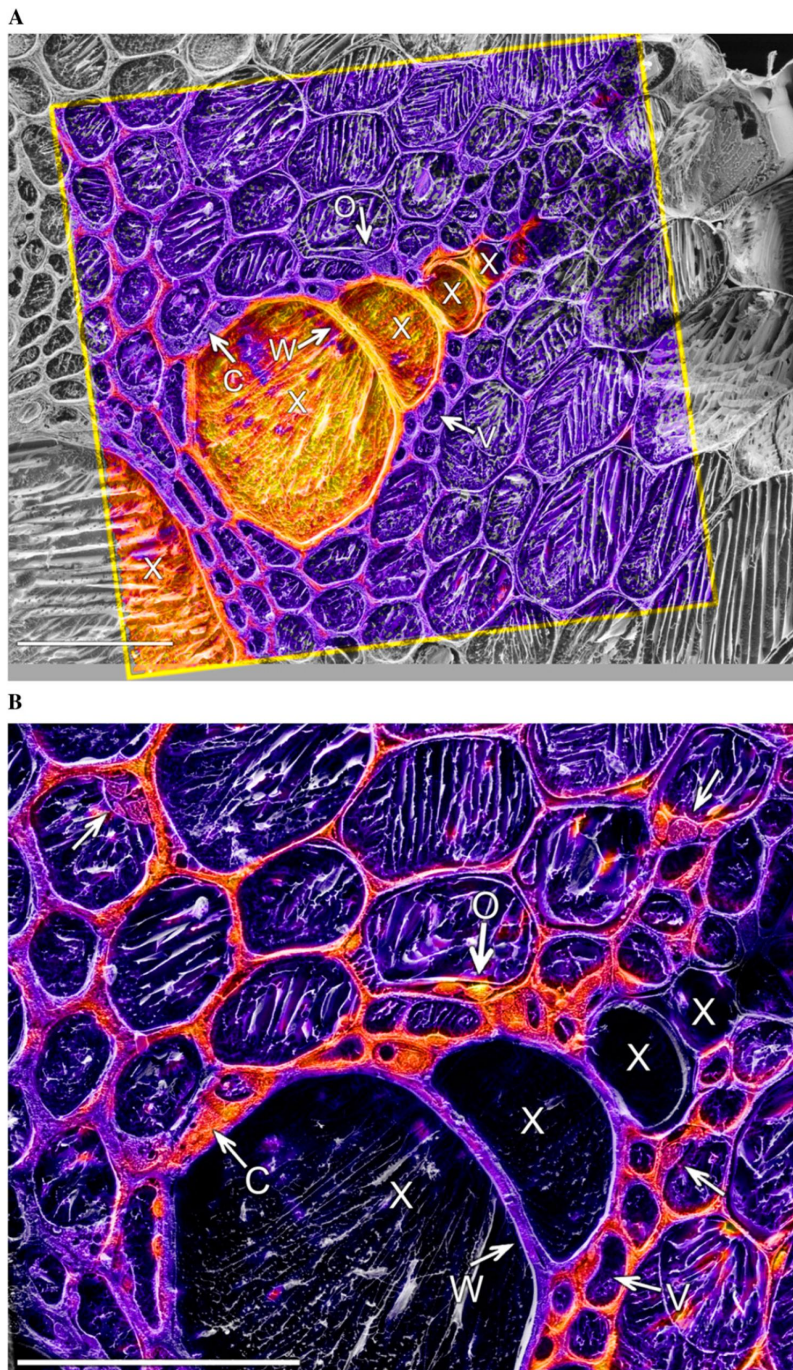
The cryo-ToF-SIMS images obtained at the high lateral resolution contain such a high level of detail that analysis of subcellular structures appeared possible. However, because each image relates to only one single ion in the tissue, the unambiguous identification of structures within the ion images still proved difficult. We therefore superimposed ion images onto cryo-SEM images of the same areas after freeze etching. Two such overlays are shown in Figure 6. Two different magnifications originating from the same cryo-ToF-SIMS and cryo-SEM datasets are shown to allow orientation within the tissue, as well as an optimal view of cellular and subcellular details. Figure 6A shows an overlay of the K isotope ratio image already shown in Figure 5E over the corresponding cryo-SEM. It is already possible to marginally distinguish between symplastic and apoplastic areas. This confirms the finding from Figure 5E that large fractions of  $^{41}\text{K}^+$

were found in the cell borders of thick-walled xylem parenchyma, but now these signals can be clearly attributed to the cell walls of this tissue.

Zooming in to a higher magnification (Figure 6B) reveals subcellular structures in more detail (e.g. cytoplasm and cell walls). In this case, the overlaying cryo-ToF-SIMS image shows the  $^{39}\text{K}^+$  isotope (from Fig. 5C) that represents predominantly the K in the plant before onset of the labeling.  $^{39}\text{K}^+$  is not primarily detected in the apoplast, but high signals originate from the cytoplasm, especially pronounced in the cytoplasm-rich parenchyma cells abutting the xylem vessels. Subcellular differences (e.g. differentiation between cytoplasm, vacuole, and organelles) can be observed in these cells. Several larger parenchyma and pith cells show extended vacuoles and narrow rims of cytoplasm together with plasma pockets around the organelles. Figure 6B reveals that  $^{39}\text{K}^+$  signals found in the vacuoles are lower than in the cytoplasm. This is consistent with reported findings (Leigh, 2001) with a

Metzner et al.

**Figure 6.** Cryo-ToF-SIMS, superimposed onto corresponding cryo-SEM images of the same area, presented as overlays. The cryo-SEM image was obtained after cryo-ToF-SIMS analysis and subsequent freeze etching. Figure 6A shows the ratio  $^{41}\text{K}^+$  to  $(^{39}\text{K}^+ + ^{41}\text{K}^+)$ . It covers the entire area analyzed by cryo-ToF-SIMS plus a small margin for better orientation within the tissue. The ratio image was already shown separately in Figure 5E. Figure 6B images the isotope  $^{39}\text{K}^+$  that was also shown above as separate image in Figure 5C. The view was zoomed in for this figure to better visualize the structural details at the print size. Among the subcellular structures visible are the xylem vessels (X), cell walls (W), vacuoles (V), and cytoplasm (C) with contained organelles (O). For clarity of the underlying structures, background subtraction and transparency adjustment were applied. The unlabeled arrows indicate thin rims of cytoplasm with plasma pockets. The micron markers in both images represent  $50\ \mu\text{m}$ .



different experimental approach (triple-barreled ion-sensitive microelectrodes), showing high levels of K (80–100 mM) in the cytoplasm and up to 100 mM in the vacuoles.

#### CONCLUSION AND FUTURE PERSPECTIVE

Three cryogenic techniques, namely (1) specimen preparation of shock-frozen tissue samples, (2) cryo-ToF-SIMS, and (3) cryo-SEM were improved and combined for the task of nutrient element imaging and tracer analysis in tissues for the study of transport processes in plants.

1. Specimen preparation by cryo-fracturing and planing surfaces produced samples adequate for cryo-ToF-SIMS analysis. This avoids the necessity to produce cryo-sections, which is considered difficult, if not impossible, for many tissues.
2. High-quality images were obtained by cryo-SEM, allowing tissue identification and recognition of subcellular structures. Thus, despite the large sample sizes of approximately 2 mm, sufficient structural preservation could be obtained by shock freezing and maintained throughout the cryogenic workflow, including shuttle transfers from sample preparation through cryo-ToF-SIMS to cryo-SEM.
3. Lateral resolution of cryo-ToF-SIMS at high mass resolution ranged in large area nutrient surveys from 10 to 6  $\mu\text{m}$ . The high mass resolution was required for the unambiguous identification of the major isotopes of nutrient cations and their separation from possibly interfering ions.
4. High lateral resolution cryo-ToF-SIMS at reduced mass resolution allowed ion imaging at tissue details, such as assemblies of xylem vessels and surrounding xylem parenchyma with subcellular details at 1- $\mu\text{m}$  resolution. Possible uncertainties of mass interferences were quantified from images at high mass resolution of the same areas.
5. The combination of high lateral resolution cryo-ToF-SIMS with cryo-SEM images in overlay images allowed the mapping of selected ions to cellular and subcellular structures, including a distinction between apoplastic and symplastic localization.
6. The elemental tracer Rb was applied to the transpiration stream and could be detected with high sensitivity by cryo-ToF-SIMS apical of the application site. Na supplemented at 2.5 mM could be detected, yielding images of high detail. However, quantification is not advisable due to a possible matrix effect.
7. The isotopic tracer  $^{41}\text{K}$  could be imaged at a lower sensitivity of detection than Rb, but ratio images of  $^{41}\text{K}$  can be used to quantify the percentage of total K, thus providing a powerful tool to track K movement.

The study revealed that cryo-ToF-SIMS is well suited to monitor distributions of nutrients in plant tissue

samples and to detect tracers down to the subcellular level. Both types of tracer could be imaged after transport within the xylem and radially translocated into the surrounding tissue. Enriched (stable) isotope tracers can be imaged with cryo-ToF-SIMS to trace nutrients unaffected by matrix effects and topography effects, thus allowing quantification of the tracer fraction. Physiological effects of tracer addition can be completely eliminated when the tracer is applied at unchanged concentration by changing isotopic composition only. Besides  $^{41}\text{K}$  used in this pilot study, suitable enriched stable isotopes are available for most elements. For several nutrients, such as Mg and Ca, more than one isotope is available to allow for simultaneous multi-element multitracer analysis. To our knowledge, no other technique can detect several tracers simultaneously at a similar lateral resolution and sensitivity.

Possible future applications in plant nutrition studies could focus on loading and unloading sites of the long-distance transport systems or on the penetration of diverse tissues by different nutrients from conducting tissue. Another field of application is in plant phenotyping, especially ecotypes and mutants obtained by genetic engineering. Studies on the movement of mineral nutrients (e.g. across the endodermis) or on the accessibility of different tissues for specific elements traveling in the xylem can be helpful in characterization particularly of mutants modified in ion transport.

#### MATERIALS AND METHODS

##### Plant Material

French bean (*Phaseolus vulgaris* 'Shiny Fardenlosa') plants were grown from seeds in 1.7-L pots with standard soil substrate (type ED 73; Einheitserde) in a growth chamber with a 12-h light/12-h dark cycle, a temperature of 20°C to 25°C, and a relative humidity of 35% to 45%. Illumination with photosynthetically active radiation (PAR) of 300  $\mu\text{mol m}^{-2} \text{s}^{-1}$  was obtained with commercial fluorescent lamps (15  $\times$  36-W; Fluora). Alternatively, plants were grown throughout the year under controlled greenhouse conditions with a day/night regime of 26°C/18°C and 45%/80% relative humidity. During the 16-h photoperiod, irradiance was enhanced by movable high-pressure sodium lamps, if required, to ensure that the natural light intensity never fell below a PAR value of about 390  $\mu\text{mol m}^{-2} \text{s}^{-1}$ . Automatic watering of all plants occurred twice a day. Plants were used for experiments at an age of approximately 4 weeks when at least three mature trifoliate leaves had developed.

##### Tracer Application

Two different tracer solutions containing either the elemental tracer Rb or the isotope tracer  $^{41}\text{K}$  were used. The Rb tracer (solution 1) consisted of 10 mM RbCl and 5 mM CsCl in half-strength Hoagland solution (modified after Hoagland and Arnon, 1950) containing 2.5 mM  $\text{KNO}_3$ , 2.5 mM  $\text{Ca}(\text{NO}_3)_2$ , 1 mM  $\text{MgSO}_4$ , and 0.5 mM  $\text{KH}_2\text{PO}_4$  at pH 5.1 and trace elements as 5  $\mu\text{M}$   $\text{MnCl}_2$ , 0.5  $\mu\text{M}$   $\text{CuSO}_4$ , 0.5  $\mu\text{M}$   $\text{ZnSO}_4$ , 25  $\mu\text{M}$   $\text{H}_3\text{BO}_3$ , and 0.25  $\mu\text{M}$   $\text{NaMoO}_4$ . The enriched-stable isotope tracer solution (solution 2) was a multielement tracer solution consisting of  $^{26}\text{MgCl}_2$  (enriched to 96%  $^{26}\text{Mg}$ ; natural abundance 10.0%),  $^{41}\text{KCl}$  (enriched to 97%  $^{41}\text{K}$ ; natural abundance 6.7%),  $^{44}\text{CaCl}_2$  (enriched to 96%  $^{44}\text{Ca}$ ; natural abundance 2.1%), and  $\text{Na}^{15}\text{NO}_3$  (enriched to 94%  $^{15}\text{N}$ ; natural abundance 0.4%), each at 2.5 mM concentration in deionized water.  $\text{Na}^{15}\text{NO}_3$  was obtained from Sigma-Aldrich, whereas all other stable isotopes were purchased from Medgenix.

In separate experiments, either of the tracer solutions was fed into the transpiration stream by cutting the shoot of a bean plant under water a few

Metzner et al.

centimeters above the root and rapidly transferring the wet cut end into the tracer solution. The Rb tracer solution was applied in the laboratory at a PAR of  $100 \mu\text{mol m}^{-2} \text{s}^{-1}$  (400-W HQI lamp; Osram), a temperature of  $24^\circ\text{C}$ , and a relative humidity of 45%, whereas the stable isotope and combined tracer solutions were fed in the growth chamber. During a subsequent feeding period of 20 min, the shoot usually took up about 2 to 3 mL of the Rb tracer solution and 4 mL of the stable isotope tracer solution, respectively. We found similar uptake as measured by weight losses due to transpiration using comparable control plants placed next to the experimental plants.

### Preparation of Frozen-Hydrated Tissue Samples

As termination of the feeding procedure, stem samples of approximately 4-cm length were quickly excised with a scalpel blade from the first and second internode above the primary leaves and mounted in tightly fitting copper rivets by the aid of 0.6 M Suc solution (Sigma-Aldrich). These sample-rivet assemblies were rapidly shock frozen by plunging them into melting propane ( $-189^\circ\text{C}$ ). The time period from excision to freezing was less than 30 s.

During the subsequent procedures of sample preparation and measurement, the ambient temperature was continuously controlled, not exceeding  $-130^\circ\text{C}$ . Frozen samples were trimmed at liquid nitrogen temperature to protrude  $<3$  mm from the rivets and stored under liquid nitrogen. Clean and even surfaces, as needed for cryo-ToF-SIMS analysis, were obtained by planing the samples with the aid of a microtome. To this end, a sample-rivet assembly was mounted under liquid nitrogen on a modified commercial sample holder (BU 012092-T; BAL-TEC) that had been mechanically adapted to receive the rivet. The sample holder was transferred from the liquid nitrogen storage container to the freeze-fracturing unit (MED 020/GBE; BAL-TEC) by use of a so-called cryo-shuttle (VCT-100; BAL-TEC). The shuttle was filled with dry cryogenic nitrogen gas and the sample holder introduced through a dry cryogenic nitrogen atmosphere. The shuttle was closed and the sample moved to the freeze-fracturing unit. After connection to the MED 020, the shuttle was evacuated and the sample holder transferred to the precooled sample stage of the MED 020. At a temperature of approximately  $-150^\circ\text{C}$  and a pressure of  $10^{-3}$  Pa, the sample was planed with a hard metal knife of a built-in microtome under stereomicroscopic control by first removing a few  $10\text{-}\mu\text{m}$  slices from the top of the sample and then removing  $5\text{-}\mu\text{m}$ -thick slices until the surface was reasonably flat. After planing, the sample was again introduced into the cryo-shuttle while maintaining high vacuum and protecting the specimen from heating and surface contamination by a liquid nitrogen-cooled cryo-shield. The sample was subsequently transferred to the cryo-SEM and/or the cryo-ToF-SIMS via the shuttle across the respective airlock systems. Upon arrival on the cryo-stages of both instruments typically after approximately 15-min transfer time, the temperature of the sample holder never exceeded  $-130^\circ\text{C}$ . The shuttle vacuum was always below  $1 \times 10^{-3}$  Pa after transfer.

### Cryo-SEM

A LEO Gemini VP 1550 SEM (Zeiss) with a cold-field emission electron source was used for imaging of the surfaces of frozen-hydrated samples. The instrument is equipped with a BAL-TEC cryo-stage (BAL-TEC) and an airlock for the cryo-shuttle. The samples were imaged at an acceleration voltage of 1.8 keV at a stage temperature below  $-120^\circ\text{C}$  and a pressure of  $2 \times 10^{-3}$  Pa.

If freeze etching was required, the temperature of the sample stage was transiently raised to  $-90^\circ\text{C}$ . The etching process was monitored by continuous scanning of the sample and stopped as required for imaging of the tissue structure by interrupting the stage heating, typically after 2 to 5 min. Overlays of ion images superimposed over SEM images were produced using Adobe Photoshop CS3 and overlay mode for image blending. SEM images were optimized for printing using limits and curves settings in Photoshop.

### Cryo-ToF-SIMS

For the element and isotope imaging performed in this study, a ToF-SIMS IV mass spectrometer (IONTOF) was used. A separate airlock system allowed the transfer of a sample between the shuttle and the cryo-stage. The cryo-stage was based on the IONTOF heat/cool sample holder that had been modified to reach and maintain temperatures down to  $-150^\circ\text{C}$ . For all reported measurements, the sample temperature was kept below  $-130^\circ\text{C}$ .

To remove a possibly deposited thin layer of ice or other possible surface contamination, an area of  $750 \times 750 \mu\text{m}^2$  was presputtered with an  $\text{O}_2^+$  ion beam at 2 keV and 400 nA for 90 s, resulting in an ion dose density of  $4 \times 10^{16}$  ions  $\text{cm}^{-2}$ . In a silicon sample, assuming a sputter yield of one sputtered

particle from each primary ion, this would presumably remove 10 nm from the surface of the sample.

For cryo-ToF-SIMS analysis a pulsed mass-filtered 25 keV  $\text{Bi}^+$  ion beam was used. The ion beam current was between 0.2 and 1.2 pA and resulted in a primary ion dose density between  $1.3 \times 10^{13}$  and  $6.9 \times 10^{13}$  ions  $\text{cm}^{-2}$ . In a silicon sample, this would result in the removal of less than 1 nm from the surface of the sample during analysis. The sputtered secondary ions were extracted with 2 kV into a reflectron ToF mass analyzer. Only positively charged ions were analyzed. A complete secondary ion spectrum was recorded for each pulse and each pixel. To prevent charging of the sample surface, a low-electron energy flood gun was used.

Three different modes of operation were used with differently weighted compromises for the counteractive parameters of mass resolution, lateral resolution, and time of measurement required for a sufficient signal:

1. The high-current bunched mode was used for large area views ( $500 \times 500 \mu\text{m}^2$ ; see Fig. 3). To achieve high mass resolution in this mode, the primary ion pulses (5 to 15 ns) were compressed by a bunching device to produce shorter pulses of 1 to 2 ns. This resulted in a mass resolution  $m/\Delta m$  of 3,500 (at mass 41). As a trade-off, the energy spread introduced by the buncher and the resulting chromatic aberration limited the lateral resolution to  $10 \mu\text{m}$  as determined by knife edge scans. This mode employs the highest primary ion density (875 ions/pulse) of all modes and therefore offers the highest ion yield per primary ion pulse.
2. The low-current bunched mode was preferred for imaging with high lateral and high mass resolution (see Fig. 4). It is identical to the high-current bunched mode described above, but with a reduced primary ion density (190 ions/pulse). Therefore, the lowered ion yield per pulse allowed only for smaller raster sizes without extensive prolongation of the measurement time, thereby improving the mass resolution  $m/\Delta m$  to 5,000 (at mass 41). The advantage is the improved lateral resolution of  $6 \mu\text{m}$  (determined by knife edge scans).
3. The burst-align mode was used for detailed mapping (see Fig. 5). Pulses were not bunched, which allowed for an improved lateral resolution of approximately  $1 \mu\text{m}$  (knife edge scans), but limited the mass resolution to nominal mass. The low primary ion density (120 ions/pulse), resulting in low ion yield per pulse, allowed only small raster sizes without extensive prolongation of the measurement time.

A Poisson correction algorithm (Stephan et al., 1994) as part of the ion-image software (IONTOF) was used in all modes for compensation of dead-time effects of the detector at high count rates. Based on the number of measurement cycles and the number of detected counts, the probability of a missed count event was calculated and added to the counted number. The resulting number of counts per pixel within the indicated mass window integrated over all measurement is referred to as signal in the text.

To compute the true percentage of the  $^{41}\text{K}$  isotope tracer ( $C_{\text{tracer}}$ ) based on the measured  $^{39}\text{K}$  and  $^{41}\text{K}$  images, we used the following formula:

$$C_{\text{tracer}} = (41_{\text{measured fraction}} - 41_{\text{natural fraction}}) / (41_{\text{fraction of the tracer}} - 41_{\text{fraction of natural isotope}}).$$

This corrects for the  $^{41}\text{K}$  fraction present in the total K in the plant and the  $^{39}\text{K}$  fraction in the enriched tracer.

### ACKNOWLEDGMENTS

We are very grateful to Alexandra Ley for performing light microscopy on bean stem cross sections as a valuable aid for orientation in the cryo-ToF-SIMS instrument. We thank Hans-Peter Bochem and the Institute of Bio- and Nanosystems 2 for the liberal use of their SEM facilities. Special support came from Marion Roeb and Beate Uhlig for plant cultivation. Andreas Aversch and the ICG workshop, especially Elmar Mommertz, contributed general technical assistance. Michael Thorpe, Hinrich Lüthring, and Vicky Temperton helped with critical reading of the manuscript.

Received September 14, 2007; accepted May 26, 2008; published June 20, 2008.

### LITERATURE CITED

Böhlke JK, de Laeter JR, De Bièvre P, Hidaka H, Peiser HS, Rosman KJ, Taylor PD (2005) Isotopic composition of the elements, 2001. *J Phys Chem Ref Data* 34: 57–67

## Mapping Nutrients by Secondary Ion Mass Spectrometry

- Canny MJ (1993) The transpiration stream in the leaf apoplast: water and solutes. *Philos Trans R Soc Lond B Biol Sci* **341**: 87–100
- Cliff B, Lockyer NP, Corlett C, Vickerman JC (2003) Development of instrumentation for routine ToF-SIMS imaging analysis of biological material. *Appl Surf Sci* **203-204**: 730–733
- Colliver TL, Brummel CL, Pacholski ML, Swanek FD, Ewing AG, Winograd N (1997) Atomic and molecular imaging at the single-cell level with ToF-SIMS. *Anal Chem* **69**: 2225–2231
- DeBoer AH, Volkov V (2003) Logistics of water and salt transport through the plant: structure and functioning of the xylem. *Plant Cell Environ* **26**: 87–101
- Dérue C, Gibouin D, Demarty M, Verduc MC, Lefebvre F, Thellier M, Ripoll C (2006a) Dynamic-SIMS imaging and quantification of inorganic ions in frozen-hydrated plant samples. *Microsc Res Tech* **69**: 53–63
- Dérue C, Gibouin D, Lefebvre F, Rasser R, Robin A, Le Sceller L, Verduc MC, Demarty M, Thellier M, Ripoll C (1999) A new cold stage for SIMS analysis and imaging of frozen-hydrated biological samples. *J Trace Microprobe Tech* **17**: 451–460
- Dérue C, Gibouin D, Lefebvre F, Studer D, Thellier M, Ripoll C (2006b) Relative sensitivity factors of inorganic cations in frozen-hydrated standards in secondary ion MS analysis. *Anal Chem* **78**: 2473–2477
- Dickinson M, Heard PJ, Barker JH, Lewis AC, Mallard D, Allen GC (2006) Dynamic SIMS analysis of cryo-prepared biological and geological specimens. *Appl Surf Sci* **252**: 6793–6796
- Enns LC, McCully ME, Canny MJ (1998) Solute concentrations in xylem sap along vessels of maize primary roots at high root pressure. *J Exp Bot* **49**: 1539–1544
- Fricke W, Leigh RA, Tomos AD (1996) The intercellular distribution of vacuolar solutes in the epidermis and mesophyll of barley leaves changes in response to NaCl. *J Exp Bot* **47**: 1413–1426
- Goldsmith JG, Lazof DB, Schroeder WH, Kuhn AJ, Ruffly TW, Linton RW (1993) Application of secondary ion image analysis for quantification of isotope and elemental nutrient tracers in plant tissues. In A Benninghoven, Y Nihei, R Shimizu, HW Werner, eds, *Secondary Ion Mass Spectrometry SIMS IX*. John Wiley & Sons, Chichester, UK, pp 824–827
- Goldstein JI, Romig AD, Newbury DE, Lyman CE, Echlin P, Fiori C, Joy DC, Lifshin E (1992) *Scanning Electron Microscopy and X-Ray Microanalysis*, Ed 2. Plenum Press, New York
- Halperin SJ, Lynch JP (2003) Effects of salinity on cytosolic Na<sup>+</sup> and K<sup>+</sup> in root hairs of *Arabidopsis thaliana*: *in vivo* measurements using the fluorescent dyes SBFI and PBFI. *J Exp Bot* **54**: 2035–2043
- Hedrich R, Schroeder JI (1989) The physiology of ion channels and electrogenic pumps in higher plants. *Annu Rev Plant Physiol* **40**: 539–569
- Herdel K, Schmidt P, Feil R, Mohr A, Schurr U (2001) Dynamics of concentrations and nutrient fluxes in the xylem of *Ricinus communis*—diurnal course, impact of nutrient availability and nutrient uptake. *Plant Cell Environ* **24**: 41–52
- Hoagland DR, Arnon DI (1950) The water-culture method for growing plants without soil. *Calif Agr Exp Sta Cir* **347**: 1–39
- Jacoby B (1965) Sodium retention in excised bean stems. *Physiol Plant* **18**: 730–739
- Jeschke WD (1970) Über die Verwendung von <sup>86</sup>Rb als Indikator für Kalium, Untersuchungen am lichtgeförderten <sup>42</sup>K/K- und <sup>86</sup>Rb/Rb-Influx bei *Elodea densa*. *Z Naturforsch* **25**: 624–630
- Küpper H, Zhao FJ, McGrath SP (1999) Cellular compartmentation of zinc in leaves of the hyperaccumulator *Thlaspi caerulescens*. *Plant Physiol* **119**: 305–311
- Lazof D, Linton RW, Volk RJ, Ruffly TW (1992) The application of SIMS to nutrient tracer studies in plant physiology. *Biol Cell* **74**: 127–134
- Leigh RA (2001) Potassium homeostasis and membrane transport. *J Plant Nutr Soil Sci* **164**: 193–198
- Lohaus G, Hussmann M, Pennewiss K, Schneider H, Zhu JJ, Sattelmacher B (2000) Solute balance of a maize (*Zea mays* L.) source leaf as affected by salt treatment with special emphasis on phloem re-translocation and ion leaching. *J Exp Bot* **51**: 1721–1732
- Marschner H (1995) *Mineral Nutrition of Higher Plants*, Ed 2. Academic Press, London
- Marschner H, Schimansky C (1968) Unterschiedliche Aufnahme von Kalium und Rubidium durch Gerste. *Naturwissenschaften* **55**: 499
- Mühlhling KH, Läubli A (2000) Light-induced pH and K<sup>+</sup> changes in the apoplast of intact leaves. *Planta* **212**: 9–15
- Rains DW (1969) Cation absorption by slices of stem tissue of bean and cotton. *Experientia* **25**: 215–216
- Rangarajan S, Tyler BJ (2006) Topography in secondary ion mass spectrometry images. *J Vac Sci Technol A* **24**: 1730–1736
- Reintanz B, Szyroki A, Ivashikina N, Ache P, Godde M, Becker D, Palme K, Hedrich R (2002) AtK1, a silent *Arabidopsis* potassium channel alpha-subunit modulates root hair K<sup>+</sup> influx. *Proc Natl Acad Sci USA* **99**: 4079–4084
- Rowan A, McCully ME, Canny MJ (2000) The origin of the exudate from cut maize roots. *Plant Physiol Biochem* **38**: 957–967
- Rygel J, Pritchard J, Zhu JJ, Tomos D, Zimmermann U (1993) Transpiration induced radial turgor pressure gradients in wheat and maize roots. *Plant Physiol* **103**: 493–500
- Schroeder WH, Fain GL (1984) Light-dependent calcium release from photoreceptors measured by laser micro-mass analysis. *Nature* **309**: 268–270
- Schroeder WH, Frings D, Stieve H (1980) Measuring calcium uptake and release by invertebrate *Astacus leptodactylus* photoreceptor cells by laser microprobe mass spectrometry. *Scan Electron Microsc* **606**: 647–654
- Shaul O, Hilgemann DW, de-Almeida-Engler J, Van Montagu M, Inzé D, Galili G (1999) Cloning and characterization of a novel Mg<sup>2+</sup>/H<sup>+</sup> exchanger. *EMBO J* **18**: 3973–3980
- Stephan T, Zehnpfennig J, Benninghoven A (1994) Correction of dead time effects in time-of-flight mass spectrometry. *J Vac Sci Technol A* **12**: 405–410
- Storey R, Leigh RA (2004) Processes modulating calcium distribution in citrus leaves. An investigation using x-ray microanalysis with strontium as a tracer. *Plant Physiol* **136**: 3838–3848
- Tomos AD, Leigh RA (1999) The pressure probe: a versatile tool in plant physiology. *Annu Rev Plant Physiol* **50**: 447–472
- Vickerman JC (2001) ToF-SIMS—an overview. In J Vickerman, D Briggs, eds, *TOF-SIMS: Surface Analysis by Mass Spectrometry*. IM Publishing, Charlton and Surface Spectra Limited, Manchester, UK, pp 1–40
- Wegner LH, Zimmermann U (2002) On-line measurements of K<sup>+</sup> activity in the tensile water of the xylem conduit of higher plants. *Plant J* **32**: 409–417
- Williams ML, Thomas BJ, Farrar JF, Pollock CJ (1993) Visualizing the distribution of elements within barley leaves by energy dispersive X-ray image maps (EDX maps). *New Phytol* **125**: 367–372
- Wilson RG, Stevie FA, Magee CW (1989) *Secondary Ion Mass Spectrometry*. John Wiley & Sons, New York

## 5.2 Second publication: Radial movement of cationic nutrients in stems

Status: **Submitted** (June 28, 2009; Revision requested September 19, 2009)

Metzner R, Schneider HU, Breuer U, Thorpe MR, Schurr U, Schroeder WH (sub 2009a)  
**Tracing cationic nutrients from xylem into stem tissues of *Phaseolus vulgaris* by stable isotope tracers and cryo-secondary ion mass spectrometry.** *Plant Physiology* (submitted)

### Own contribution

- Experiments (except pressure probe measurements and capillary tracer application)
- Sample preparation
- Cryo-SIMS analysis
- Data analysis and interpretation
- Preparation of manuscript

**Running title:**

Radial movement of cationic nutrients in stems

**Corresponding author:**

Ralf Metzner

Phytosphere Institute (ICG 3)

Forschungszentrum Jülich

Leo Brandt Straße

52425 Jülich, Germany

Phone: +49 (0) 2461-612652

Fax: +49 (0) 2461-612492

Email: [r.metzner@fz-juelich.de](mailto:r.metzner@fz-juelich.de)

**Proposed journal research area:**

Whole Plant and Ecophysiology

**Tracing cationic nutrients from xylem into stem tissue of *Phaseolus vulgaris* by stable isotope tracers and cryo-secondary ion mass spectrometry**

*Ralf Metzner<sup>1,2,\*</sup>, Heike Ursula Schneider<sup>2</sup>, Uwe Breuer<sup>1</sup>, Michael Robert Thorpe<sup>2</sup>, Ulrich Schurr<sup>2</sup> and Walter Heinz Schroeder<sup>2</sup>*

<sup>1</sup>Central Division of Analytical Chemistry, <sup>2</sup>Phytosphere Institute (ICG-3),  
Forschungszentrum Jülich, Leo Brandt Straße, 52425 Jülich, Germany



<sup>1</sup>financial source

<sup>2</sup>corresponding author

---

<sup>1</sup> \_

<sup>2</sup> Ralf Metzner, [r.metzner@fz-juelich.de](mailto:r.metzner@fz-juelich.de)

**Abstract**

The movement of organic and inorganic nutrients in the stem xylem is not confined to the vessels. A role for other tissues (e.g. N-transfer towards phloem) has been shown by perfusion of stem segments, and by collection of xylem and phloem sap at various sites, but a direct localization of these processes at the tissue level has not been possible. An important basis for understanding the function of these processes in the intact stem and their mechanisms, is the localization of the tissues providing pathways from the xylem vessels, and the nature of the pathways. Using our newly developed technique, which combines cryogenic sample preparation, cryo-secondary ion mass spectrometry (cryo-SIMS) and cryo-scanning electron microscopy (cryo-SEM), we used enriched  $^{26}\text{Mg}$ ,  $^{41}\text{K}$  and  $^{44}\text{Ca}$  as stable isotope tracers supplied continuously to the transpiration stream of excised shoots of *Phaseolus vulgaris* and imaged them in the xylem vessels and surrounding tissues after continuous feeding for 20 or 240 minutes. All stem tissues showed the presence of at least two tracers after 20 minutes. The fast exchange of large fractions of the native element in the thick-walled xylem parenchyma with the xylem vessels supported it as a freely exchanging region of storage while exchange with the pith was equally fast but, similar to the cambium and phloem, much smaller fractions of element were exchanged although these tissues harbored lots of element that was not exchangeable within 240 minutes. The tension in the xylem vessels showed only marginal influence on these spreading patterns.

**Key words:** *Phaseolus vulgaris*; cryo-secondary ion mass spectrometry (SIMS); cryo-scanning electron microscopy (SEM); potassium; magnesium; calcium; stem xylem and tissue; thick-walled xylem parenchyma; mineral nutrition

## **Introduction**

After uptake from the soil by the root, water and solutes are distributed within the stem of higher plants mainly by the xylem. In stems the long distance transport is strongly influenced by the interaction of the moving xylem sap with the surrounding tissues as demonstrated e.g. by the stem-piece perfusion experiments of Thompson and Zwieniecki (2006). Gilmer and Schurr (2007) and many others also showed that xylem sap composition is changed by the action of adjacent living cells. Therefore the stem xylem cannot be viewed as a hermetic pipeline connecting roots with leaves. Van Ieperen (2007), however, showed that perfusion experiments with detached stem segments or isolated vascular bundles may be an inappropriate for elucidating solute exchange between xylem and neighbouring tissues. He argued that unlike in the *in planta* situation, where xylem tension prevents a radial movement of water and solutes out of the xylem, in perfusion experiments lateral solute movement is possible and even promoted if slight hydrostatic overpressures are employed to reach perfusion. This argument would even apply to the small number of studies made so far with the root pressure chamber technique, which have all indicated that there are strong interactions between shoot xylem and adjacent tissues (Siebrecht et al., 2003; Gilmer and Schurr, 2007).

Radial transfer of solutes from xylem to phloem was shown very early e.g. by the work of Stout and Hoagland (1939) and exchange in the opposite direction by Biddulph and Markle (1944). The importance of this exchange between xylem and phloem in the stem of herbaceous plants was emphasized by Pate et al. (1979) in studies of C/N budgets of plants based on the analysis of xylem and phloem fluids and bulk analyses of several organs. A similar importance of “leaky” stem xylem for the partitioning of mineral nutrients such as potassium, magnesium and calcium between different organs was shown shortly thereafter by several authors using similar experimental approaches (Jeschke et al., 1985; Jeschke and Pate, 1991; Wolf et al., 1991). To appropriately account for the high potential of xylem-surrounding tissues to exchange with the xylem sap, the apparent free space of the xylem translocation pathway was estimated by several authors such as van Bel (1978) and Wolterbeek (1985). The functioning of this space, with rapid and reversible diffusional equilibrium with the xylem vessels, was demonstrated by the use of radiolabeled amino acids and mineral elements. Both van Bel (1978) and Wolterbeek et al. (1985) showed that this space for several nutrient species is much larger than the volume of the xylem vessels but its location has not been demonstrated yet.

While these studies clearly demonstrated the importance of the exchange of the solutes transported in the xylem with the surrounding tissues, no technique of sufficient quality existed to identify the structures of the pathways and the compartments at the tissue level. Furthermore, no analytical protocol was able to detect physiological concentrations of mineral nutrients at the tissue level in a plant stem without the risk of redistribution of diffusible elements during sample preparation. In order to understand the role of the stem xylem in the longitudinal and radial translocation of nutrients, and the interactions between xylem and phloem, a localization of the nutrients moving out of the xylem vessels among the surrounding tissues is clearly essential.

Our new technique (Metzner et al., 2008) combines cryogenic sample preparation with cryo-scanning electron microscopy (cryo-SEM) and cryo-time of flight secondary ion mass spectrometry (cryo-SIMS) to monitor authentic distribution of nutrient elements in frozen-hydrated plant tissues. Being mass spectrometric, cryo-SIMS can show stable isotope tracers as well as isotopes naturally present in the tissue. The tracer movement is identical to the naturally occurring nutrient isotope, even when transport mechanisms may be highly selective, such as in membrane transport. Shock freezing of the samples after tracer application and subsequent sample processing at cryogenic temperatures physically immobilizes the solutes and thereby preserves the distribution of the nutrients within the tissue during the entire analytical process. Cryo-SEM images taken after cryo-SIMS analysis provide a control of the quality of the freezing and preparation processes as well as high-resolution structural information of the samples.

Here we used this cryogenic workflow of sample preparation and analysis to examine stem tissue of common bean (*Phaseolus vulgaris*) after application of stable isotope tracers of the cationic nutrients potassium, calcium and magnesium to the transpiration stream, in order to identify the tissues and pathways involved in radial spreading of solutes within the stem tissue. Based on earlier microanalytical studies on the diffusion kinetics of cationic nutrients moving into roots (Kuhn et al., 2000; Horst et al., 2007) we selected two different periods of tracer application, namely 20 minutes to show any potential diffusion barriers, and 240 minutes to evaluate distribution patterns after equilibration of nutrients between xylem and surrounding tissue. To better understand the underlying mechanisms of radial nutrient distribution we evaluated the influence of axial flow rates on the distribution patterns. By means of the xylem pressure probe, we investigated the effects of xylem tension comparing the distributions of nutrient tracers as applied either to the cut stem or directly to a xylem vessel via microcapillary.

## **Results**

To show magnesium, potassium and calcium in *Phaseolus vulgaris* xylem vessels and after spreading into the surrounding tissues we used tracer solutions with stable isotopes of naturally minor abundance ( $^{26}\text{Mg}$ ,  $^{41}\text{K}$  and  $^{44}\text{Ca}$ , respectively) highly enriched to >95% total element. The tracer solution, containing 2.5 mM of each of the three elements, entered the cut transpiring shoot (Fig. 1) until samples were cut from the first internode above the primary leaves, ca. 25 cm from the application site (Fig. 1) and immediately shock-frozen to preserve ion distribution.

The high quality of tissue preservation is demonstrated by the cryo-SEM image of a cryo-planed surface after cryo-SIMS analysis and freeze-etching (Fig. 2A). The cryo-SEM images are used to identify tissues in the frozen-hydrated samples to help assigning the cryo-SIMS signals to the structure of individual samples. Stained cross-sectional light micrograph (Fig. 2B) are used to help identify tissues.

### **Tracer signal distribution after 20 min**

Cryo-SIMS maps at high mass resolution give unambiguous identification of the individual isotopes in an image  $500 \times 500 \mu\text{m}^2$  and a lateral resolution of 10 to  $7 \mu\text{m}$ . At low mass resolution (presented later) there is higher spatial resolution at the expense of some ambiguity of signal assignment to individual isotopes. In these images signal ( $S^I$ , counts of isotope I per pixel) shows isotope from both the plant (at natural abundance) and also from the tracer solution. Taking potassium as example, K from the plant contains 6.7%  $^{41}\text{K}$  and 93.3%  $^{39}\text{K}$ . K in the tracer solution in contrast contains >94%  $^{41}\text{K}$  and an impurity of <6%  $^{39}\text{K}$  (Table I). An  $S^{39\text{K}}$  image therefore contains a plant-originating and a tracer-originating  $S^{39\text{K}}$ , and similarly for the corresponding  $S^{41\text{K}}$  image.

Signal distribution maps (Fig. 3), are laid over the corresponding cryo-SEM image (i.e. Fig. 2A) of tissue structure. The signal may not show isotope concentrations because signal generation (i.e. ionization) depends on the specific element imaged (e.g. higher for potassium than calcium), and the local probability depends on the matrix, the immediate atomic vicinity of the analyte which is particularly inhomogenous for biological tissues. Rather, the signal maps provide information on the extent of tracer distribution within the tissues. Nevertheless, signals in a pixel from isotopes of the same element are equally influenced by the matrix, so that if the images of different isotopes of an element are not

the same tracers are present. These maps (Fig. 3) are representative of 10 samples from 9 plants with tracer applied via the cut stems. The tracer solution uptake rate of ca.  $0.2 \text{ ml min}^{-1}$  resembled the transpiration rate of uncut control plants and, with a xylem vessel volume of  $46 \pm 19 \mu\text{l}$  (measured by centrifugation,  $n = 7$ ), would have been replaced 87-fold.

Concerning magnesium, the highest  $S^{24\text{Mg}}$  values occurred in a distinct area of thin-walled xylem parenchyma (lower right of Fig. 3A), in parts of the thick-walled xylem parenchyma towards the pith from the vessels, and in part of the phloem. The highest  $S^{26\text{Mg}}$  values occurred in thick-walled xylem parenchyma cells enclosing the vessels, and neighboring thick-walled xylem parenchyma facing the pith (Fig. 3B). Both potassium isotope images (Figs 3C and 3D) showed high signal throughout the area of thick-walled xylem parenchyma. Slight differences and thus indications for the presence of the K tracer in the imaged area are indicated for the pith and some restricted regions of thick-walled xylem parenchyma between the metaxylem vessels. Interestingly, one vessel lumen (XV1 in Fig. 2A) showed higher signals of  $^{39}\text{K}$  than the other vessels, but  $^{41}\text{K}$  did not. For calcium, there are also prominent differences between the two images (Fig. 3E and 3F):  $S^{40\text{Ca}}$  and  $S^{44\text{Ca}}$  were both high in thick-walled xylem parenchyma, but  $S^{40\text{Ca}}$  showed maximum values both in the pith but also in phloem “hot spots”.

### Tracer fractions after 20 min

The isotope maps (Fig. 3) show tracer signal in the vessels and many tissues in the stem cross-section after 20 min uptake of tracer solution to the cut stem; but they will not reflect tracer from the solution where the natural element had a high concentration - even though the natural abundance of the tracer isotopes is low. This problem, and that of matrix effects, were resolved by calculating  $F_E$ , the fraction of element E originating from the tracer solution (see Methods, equation 1).  $F_E$  is zero where tracer isotope has natural abundance, and 100% where isotopic composition is the same as the applied tracer solution, so that contrast in the  $F_E$  images shows local differences in the fractions. Samples from controls, where no tracer solution was applied, gave images with no contrast (data not shown). Interpretation of the  $F_E$  must recognize that a low value for  $F_E$  can arise from a low amount of tracer or a large amount of natural element.

Figures 4B-D show large fractions of all tracers in the vessel lumina, from where all tracers obviously spread into the surrounding tissues (identified by an anatomical map:

Figure 4A). Potassium  $F_K$  values clearly declined outside the vessels, but magnesium  $F_{Mg}$  showed only a small decline and calcium  $F_{Ca}$  was similar in lumina, in part of the thin-walled xylem parenchyma, and in nearly all the thick-walled xylem parenchyma. The pith, phloem and cambium showed markedly lower tracer fractions compared to the xylem parenchyma. One vessel (asterisk in Fig. 4A, XV1 in Fig. 2A) displayed negligible tracer fractions for all three elements. This vessel also showed high  $^{39}K$  signals (Figure 3C), suggesting that such vessels were non-conducting and probably immature. The average of these  $F_K$ ,  $F_{Mg}$  and  $F_{Ca}$  values for phloem (Ph), cambium (Cm), xylem parenchyma (XP), conducting xylem vessel lumina (XV) and the pith (Pi) (Figure 5A-D, black columns), with xylem parenchyma subdivided: a half ring of thick-walled cells facing the cambium (XP-cm), (2) a half ring of thick-walled cells facing the pith (XP-pi), (3) thick-walled cells between vessels (XP-xv) and (4) islands of thin-walled cells (Xp-is) within the thick-walled cells.

Tracer fractions in vessel lumina were significantly below 100%, but were different with  $F_{Mg}$  at 78%,  $F_{Ca}$  at 60%, and  $F_K$  as low as 30%. In eight of the ten samples scanned after 20min tracer uptake, the largest potassium tracer fraction  $F_K$  was in vessel lumina, and in two samples (including that in Figures 4B-D) the tangential walls of the metaxylem bundles showed the largest fractions, by a small margin (Fig. 4C, right-hand side). Vessel  $F_K$  was lower on the outer rims (green arrows in Fig. 4C) with larger fractions towards the center. In contrast,  $F_{Mg}$  and  $F_{Ca}$  values were quite homogeneous within the vessel lumina (Figs. 4B and D).

In parenchyma surrounding the vessels facing the pith (XP-pi) calcium,  $F_{Ca}$  was identical to that in the vessels and only slightly lower in the parenchyma facing the cambium (XP-cm) and the parenchyma more distant from the vessels (XP-xv), whereas magnesium and potassium were lower in the parenchyma than in the vessels (Figs 5B-D). In fact the tracer fractions for the different elements showed strong differences amongst tissues with XP-pi showing the largest fractions for all elements amongst all the living tissues.  $F_{Mg}$  reached there two thirds of the  $F_{Mg}$  in the vessels, in XP-xv it was slightly lower, and in XP-cm  $F_{Mg}$  reached only one third of the vessel values. Potassium showed the same pattern; with  $F_K$  in XP-pi one-third of  $F_K$  in the vessels, which was twice that in XP-cm.

The islands of thin-walled xylem parenchyma displayed similar  $F_{Ca}$  values as XV and XP-pi, whereas  $F_K$  and  $F_{Mg}$  were much lower. Other parts of the thin-walled xylem

parenchyma (XP-th in Fig. 2A) between XP-cm and the cambium showed smaller fractions for all elements which were, however, for calcium still markedly higher than those of the cambium (Fig. 4D). The pith bordering the xylem parenchyma towards the center of the stem showed large magnesium fractions,  $F_{Mg}$  (almost one-third of vessel values; Fig. 5B) while potassium and calcium fractions were again very low (Figs 5C and D).

Tracer fractions for all three elements in the cambium and phloem were much lower than for the neighboring XP-cm (Figs. 5B-D).  $F_{Mg}$  for cambium and phloem was about half of the corresponding thick-walled xylem parenchyma values, while  $F_K$  was below the detection limit (Fig. 5C). On the other hand,  $F_{Ca}$  in cambium was about half of the XP-cm values, and larger than in phloem.

### **Distributions of potassium at high-lateral resolution**

More detail of transport pathways was gained with additional cryo-SIMS images at a higher lateral resolution, better than 1  $\mu\text{m}$ , allowing us to differentiate between borders and lumina of individual cells (Metzner et al., 2008). The high lateral resolution, however, sacrificed mass resolution, so no useful images for magnesium and calcium tracers were possible, and even potassium data are uncertain within about 20% (Metzner et al., 2008). Since this uncertainty is mainly related to carbohydrates it may tend to be higher in areas with high organic background.

For the sample presented in Figures 2A and 4 the area including metaxylem vessels, the xylem parenchyma and the pith (next to V4 in Fig. 2A) was chosen for the high-lateral resolution imaging as displayed in Figure 6A. This enabled us to evaluate the spreading of tracer from the xylem towards the stem center in more detail. The largest vessel lumen shown in Figure 6A displayed an  $F_K$  value of 20% (Fig.6B; XV), which is very close to the 18% determined for the same vessel lumen in the overview image (Fig. 4C) where no uncertainty due to mass resolution existed. The fractions in the cell walls of the thick-walled xylem parenchyma (XW) were half of this value (9%; Fig. 6B), while in the lumina of the thick-walled xylem parenchyma cells adjacent to the vessel (XL) we found only 3%. Similar fractions were found for the cell walls of the pith (PW) and only 1% in the lumina of the pith cells (PL).

### **Transpiration rate**



Tracer fractions of all three elements gave very similar images to those in Figures 4B-D (data not shown) where transpiration (and tracer uptake) rate was almost halved by increasing air humidity. The results from three independent experiments at this low rate (Fig. 5B-D white columns) showed that the fractions of tracer for all three elements in most tissues were hardly affected. The only difference between the two situations occurred for magnesium and potassium in the XP-cm, where their tracer fractions had doubled at the low transpiration rate and calcium fractions were identical to those in the vessels.

### **Xylem tension**

Xylem tension, monitored by xylem pressure probe, was stable at 0.107 MPa relative to atmosphere (Figure 7A), until the stem was cut under water (osmolality 6 mosmol kg<sup>-1</sup>; “#” in Fig. 7A) prior to tracer application (Fig. 1). Cutting caused a reduction to 0.02 MPa, an 81% loss of tension. In contrast, tracer application via microcapillary led to a much smaller tension loss of 8% (downward-arrow, Figure 7B). Subsequent withdrawal of the application capillary (upward arrow, Fig. 7B) tension returned to its initial value, confirming the probe’s fidelity, and showing that the small measured tension loss was due to solution entry to the xylem.

Tension loss measured for a total of six cut-stem and four capillary applications (Fig. 7C) revealed that the loss of tension for cut-stem application was significantly higher ( $81 \pm 7\%$ ) than by capillary ( $11 \pm 8\%$ ), so it can be expected that the pressure equilibrium between the xylem and the adjacent cells was more severely disturbed by cutting the stem.

### **Tracer distribution with micropillary delivery**

In samples where tracer solution was delivered via microcapillary to a xylem vessel of intact plants the uptake was 90-200  $\mu\text{l}$  which results in a 450-1000 fold replacement of xylem sap in the vessel (for a xylem vessel diameter of 100 $\mu\text{m}$ ). This value may be overestimated as fraction maps (e.g. potassium; Fig. 8) showed tracer to be present in a small number of vessel lumina demonstrating an exchange of sap between the punctured and neighboring xylem vessels along the 2.5 cm internode between application and sampling site. Tracer fractions in the vessel lumina were smaller than those in cut stems, but the tracer distribution patterns were similar (Figs 5B-D and 8). In the xylem vessel lumina,  $F_{\text{Mg}}$  is only slightly smaller after microcapillary application than after cut-stem application while  $F_{\text{K}}$  and  $F_{\text{Ca}}$  are barely half as large as after cut-stem application. Likewise

the fractions in the different tissues were also lower than after cut-stem application. The thick-walled xylem parenchyma again showed the largest fractions of all tissues and  $F_{Ca}$  was equal to the xylem vessels, with  $F_{Mg}$  and  $F_K$  showed much smaller fractions than in the vessel lumina.  $F_K$  in the other tissues was barely detectable while  $F_{Mg}$  values in the pith, cambium and phloem were similar to the fractions detected after cut-stem application for 20 minutes and therefore relative to the vessels much larger than in the cut-stem application experiments (black and white columns in Fig. 5C) The same was shown for  $F_{Ca}$  in the pith and cambium, but in all these cases the standard deviations are exceptionally high.

### **Tracer distribution after 240-min cut-stem delivery**

Since a steady state is expected to occur at some stage during tracer application, we took samples after 240 min to compare with the 20 min application. Transpiration rates in these experiments started at 0.10-0.13 ml min<sup>-1</sup> and decreased with application time to values around 0.04 ml min<sup>-1</sup>, so that total solution uptake was 12 ml, a 260 fold replacement of the xylem fluid within the stem segment. Typical images of tracer fractions and the corresponding anatomical map are in Figures 9A-D. In this example three vessels (asterisks in Fig. 9A) appear to be non-conducting and immature, going by the negligible fraction of all tracers in their lumina (Figs. 9B-D). The images for all three elements (Fig. 9B-D) were qualitatively very similar at 20 and 240 min (Fig. 4B-D) with the exception of  $F_{Ca}$  showing markedly increased fractions in the cambium and phloem after 240 minutes. Vessel tracer fractions after 240 minutes were very similar to those after 20-min (compare hatched with black and white columns in Figs 5B-D), as were all tracer fractions in the different types of xylem parenchyma, and the pith. However, tracer fractions in the cambium and phloem were at least twice as large after 240 minutes of tracer application as after 20 minutes.

High-lateral resolution images of  $F_K$  from metaxylem areas comparable to those shown in Figure 6A for 20-min experiments were also acquired after 240-min of cut-stem tracer application. Figure 10A shows a map of  $F_K$  overlaid onto the corresponding cryo-SEM image, which represents a close-up of the structure shown in Figure 9C in the overview mode.

$F_K$  in the vessel lumen (XV) is with 20% (Fig. 10B) close to the fraction found in the overview image for the same vessel (26%; Fig. 5C) and identical to the fraction found at

---

high lateral resolution after 20 minutes application (Fig. 6B). Fractions of the surrounding tissues were much larger at 240 minutes (Fig. 9B) even though data from overview images showed an increase for the xylem parenchyma but none for the pith (Fig. 4C). Largest increase was found for the cell lumina of the thick-walled xylem parenchyma (XL) that were five times larger after 240 as after 20 minutes but still below the fractions in the cell walls (XW). In the pith both cell walls and lumina were three times larger after 240 than after 20 minutes.

## **Discussion**

In this study we utilized a new protocol combining cryo-SIMS and cryo-SEM (Metzner et al., 2008) to show stable isotope tracers of magnesium, potassium and calcium in stem xylem some distance from where they entered the transpiration stream at an excision, and to show their location in the neighboring stem tissues. We demonstrate that this methodological combination is well suited to help elucidate the mode and pathways of cation exchange between living tissues and the xylem sap within a plant stem. After tracer solution was fed to the transpiration stream for 20 min, all tracer elements at a 25 cm distance were easily detectable in the xylem vessels, and strong radial spreading into surrounding tissues had also occurred by then.

The distribution patterns of tracer were similar for delivery to cut-stems or by microcapillary, despite a pronounced difference in tension loss in the xylem between the two protocols. This finding seems to be in contrast with conclusions from the use of the pressure-probe where marked changes in radial turgor and osmotic pressure profiles of roots occurred whenever tension changed abruptly, such as with cutting (Wistuba et al., 2000; Schneider et al., 2007). The redistribution of water and solutes leading to the establishment of a new steady state within 30 minutes (Zimmermann et al., 1992; Rygol et al., 1993) was expected to show a strong effect on the radial movement of solutes, which we did not find for magnesium, potassium or calcium. Our results are, however, consistent with recently published findings of Wegner and Zimmermann (2009) who showed that radial potassium transport of maize roots showed little if any dependence on xylem pressure. Therefore we must caution that mineral nutrients may not play a major role in establishing such radial osmotic gradients, especially potassium which is often an important osmoticum.

When the flow rate in the xylem vessels was decreased twofold, there was very little change in the radial distribution patterns of the nutrient tracers (Fig. 5B-D) with one notable exception: labelling in the xylem parenchyma towards the cambium, was lower at higher transpiration rates. This inverse relationship between tracer spreading and the axial flow rate is consistent to the findings of van Bel (1974) for the radial escape of amino acids from the xylem. The only tissue showing the effect of axial flow rate, the one type of xylem parenchyma, may therefore have a different nature of spreading than other regions. In contrast to solely diffusive spreading of nutrients nutrient movement in a radial flow of water caused by solvent drag, as found for roots (Steudle and Peterson, 1998), would

depend on the axial flow rate. Radial water flows in stems could originate from a cross flow between xylem and phloem, or from surface transpiration. Therefore we conclude that tracer movement by solvent drag most likely played a role in the xylem parenchyma facing the cambium only and that movement to other tissues in the stem was diffusive. Movement by solvent drag and the implied radial flow of water show that the xylem parenchyma facing the cambium may be especially important for the regulation of xylem nutrient fluxes as suggested in the literature for the whole xylem parenchyma (e.g. Karley and White, 2009). This tissue is also en route to the phloem which seems very likely to be for nutrient cycling

### **Interpreting tracer fractions**

For investigating the movement of nutrients within plant tissues the cryo-SIMS technique offers the unique possibility to map isotopes with tissue-level lateral resolution (Metzner et al., 2008). The differences in the maps of the natural and tracer isotopes of the elements investigated give first insight into the distribution of natural and tracer element in the stem cross section. But these maps may not be quantitative, due to the dependency of the signal on the local chemical environment (matrix) which is expected to be very inhomogeneous within tissues. Therefore our interpretation of the data is based on the fraction of element originating from the tracer solution ( $F_E$ ), which is calculated from the relative isotopic abundance of the tracer isotope and is independent of any matrix-effect because all isotopes would be affected by it in exactly the same way.

The value for  $F_E$  in the tissues depends on 1) the  $F_E$  in the xylem vessels which are the source for radial spreading, 2) on the process of exchange with the xylem vessels and 3) on the fraction of element that can exchange with the xylem vessels. For tissues which were found to have reached an equilibrium with the xylem vessels (i.e. similar  $F_E$  after 20 and 240 min of tracer application) the value of  $F_E$  depends on the fraction of element in the tissues that can be exchanged against element from the tracer solution. At equilibrium the element of the exchangeable (unbound) fraction will have equal abundance to the xylem vessels, but the non-exchangeable material will remain at natural abundance. Thus if element (E) in the xylem sap is all unbound, we can calculate from the tracer fraction in the xylem vessels and in the tissue the exchangeable fraction of element of the tissue ( $e_E$ ) according to equation 4. The size of this exchangeable fraction is usually lower than 100% for two reasons: 1) physical isolation of natural element in the tissue from the tracer (e.g.

compartmentation in vacuoles) and 2) chemical binding of the natural element within the tissue (e.g. Mg in Mg-ATP or Ca in pectins).

For tissues that are not in equilibrium with the vessels (i.e. show unequal fractions between 20 and 240 min)  $e_E$  shows the transient exchanged fraction, and  $F_E$  will increase with time. The time until equilibrium is reached depends on the amount of element in the exchangeable pool and on the rate of exchange.

The fraction of all three elements tracers in the vessels was significantly below that of the applied tracer solution even after longer feeding periods. The explanation for lower fractions is that a significant influx of solutes to the xylem, from surrounding tissues along the pathway from the point of tracer solution application to our sampling site, 25 cm downstream. Elements from the stem tissue at natural isotope abundance entered the vessels and reduced the proportion of the tracer isotopes on the total elements. Because xylem vessel isotope fractions did not change very much with time (from 20 min to 240 min), we can conclude that material entered the xylem at a relatively constant rate and isotopic composition, suggesting that it came from a pool so large that tracer isotope entering this pool did not change its isotopic composition significantly. This dilution inflow of natural element differed strongly between the studied elements, so that the fraction of applied solution reduced to 80% for magnesium, and 60% for calcium to 30% for potassium (Fig. 5B-D). Because the concentration of each element supplied in the tracer solution was the same, we can infer that the element fluxes into the vessels were largest for potassium and smallest for magnesium. This is clearly consistent with a larger amount of potassium for exchange within the plant stem than of magnesium, which can be expected because potassium concentration within the symplast is expected to be ten times higher than that of magnesium and this is the largest storage for both elements in the tissue (Marschner, 1995). The lower fractions of potassium at the rim of larger vessels compared to the centre as seen in Figures 4C and 9C is consistent with a potassium influx.

### **Tracer flows from the xylem vessels to the surrounding tissues**

Our results showed radial spreading of tracer fractions within the stem but giving significantly different degrees of labeling across the stem for the three elements, and also pronounced differences for different tissues (Fig. 5B-D). In the following section we will discuss which tissues contribute to the bidirectional flows of nutrients with the xylem vessels. To address these flows and their pathways in further detail we compared spreading

of nutrients after different application periods. Our sampling times were selected based on kinetics of calcium and magnesium entering spruce roots from the rhizosphere, across cortex and endodermis into the stele (Kuhn et al., 2000), where the radial distances for tracer movement were roughly similar to our system. The half time ( $t_{1/2}$ ) for calcium and magnesium entry into the root cortex apoplast was approximately three minutes, indicating almost free movement up to the endodermis. The endodermis, separating external cortex and internal stele, provided a diffusion barrier that gave  $t_{1/2}$  for externally added calcium and magnesium of 240 minutes in the stele. Therefore we used an exposure time of 240 min to detect the effects of any significant diffusion barrier, and a short exposure time (20 minutes) to report on any fast movement without barriers.

### *Xylem parenchyma*

The thick-walled xylem parenchyma, in direct contact with the xylem vessels, showed the strongest labeling for all elements. After 20 minutes, calcium in this tissue had equal fractions of tracer to the xylem vessel lumina (Fig. 5D), indicating a readily exchangeable fraction of 100%, showing that calcium exchange was not limited e.g. chemically bound, or a significant diffusion barrier. This high exchangeable fraction was surprising, as more than three-quarter of the calcium in sugar beet plants was found to be firmly bound to pectates in the cell walls and as phosphates (Marschner, 1995). Clearly a much lower fraction of calcium is bound in the stem tissue of bean, and mixes completely with calcium in the xylem within less than 20 min.

In contrast, magnesium did not show an equal fraction to the vessels, although it had reached an equilibrium with an  $F_{Mg}$  of 50% at both 20 and 240 minutes (Fig. 5B), significantly below the 80% detected in the vessel lumina. Potassium fractions in the xylem parenchyma increased from 8% to 15% in samples fed for 20 or 240 minutes, but were still lower than the 30% in the xylem vessels, showing that there was non-exchangeable magnesium and potassium in this tissue. These large gradients in tracer fractions between xylem vessels and xylem parenchyma in the samples confirm the successful immobilization and imaging of the diffusible cations by our protocols. From the fractions in the xylem vessels and the fractions in the tissues we calculated (eq 4) the exchangeable fraction of magnesium in the thick-walled xylem parenchyma to be ca. 60% and for potassium to be ca. 30% during 20 minutes with a larger fraction of 60% after 240 minutes. In contrast to magnesium the exchangeable fractions of potassium represent only

transient values since the increase between 20 and 240 min of tracer application indicates that no equilibrium with the xylem vessels was reached.

For potassium, which is not expected to be chemically bound (Marschner, 1995) this exchangeable fraction may equate to potassium in the apoplast-very extensive in this tissue- and the nonexchangeable fraction consisting to symplastic potassium isolated behind cellular membranes. The large size of the exchangeable fraction on the other hand makes it unlikely that it is confined to the apoplast but also the symplast is partly exchangeable since by far the largest proportions of potassium in tissues are typically found in the symplast (Marschner, 1995). A likely non-exchangeable compartment is the vacuole which is enclosed by two membrane systems. This is also consistent with the high lateral resolution images of potassium showing tracer in the apoplast and cell lumen although fractions were three times higher in the apoplast after 20 minutes (Fig. 6B). Since symplastic potassium concentrations are high (cytoplasm 100 mM) and a little lower in the vacuoles (e.g. Leigh, 2001) a detectable symplastic potassium fraction after 20 min indicates a fast turnover of potassium in the symplast, maybe in compensation for loss by membrane leakage. After 240 minutes of tracer application we found higher tracer fractions with a markedly smaller difference between apoplast and symplast (Fig. 10B) showing that the symplastic potassium obviously was slower to reach equilibrium with the xylem vessels than the apoplast.

Obviously the tracer in the apoplast of the xylem parenchyma must have been transported from the xylem vessels by an apoplastic route, and could not have passed through the symplast of the thick-walled xylem parenchyma cells, since these contain lower tracer fractions. This is obvious since  $F_E$  can never exceed  $F_E$  in the source of tracer, so the source of tracer detected in the apoplast can only be the vessels which show a higher  $F_E$  than the apoplast but not the symplast with its lower  $F_E$ . In contrast to concentration measurements where tracer may become concentrated (e.g. due to selective binding) in the sample the isotopic abundance on which  $F_E$  is based could only increase by selective enrichment of a single isotope due to an isotope effect. Even though small isotope effects in plants are known e.g. for magnesium (Black et al., 2008) they are more than two orders of magnitude too small to account for the 6% by which the fractions in the apoplast are larger than in the symplast.

Imaging at subcellular resolution is at the moment only possible for potassium, due to lower signal for magnesium and calcium and interferences in the mass spectrum. The striped appearance of the xylem vessel lumina in the high lateral resolution image may be a



result of concentrating within the vessel due to growth of ice crystals (Metzner et al., 2008).

The concept of a fast exchangeable xylem parenchyma fits well with the large and rapidly exchanging (<15 minutes) apparent free space associated with the xylem proposed by van Bel (1978) and Wolterbeek et al. (1985).

For magnesium the exchangeable fraction is 60% of the element in the tissue and since the largest proportion of the magnesium in tissues is symplastic (Marschner, 1995) it is likely that the tracer is not physically excluded from the symplast but that non-exchangeable fraction of magnesium is chemically bound (e.g. as phosphate in vacuoles; (Marschner, 1995).

The thick-walled xylem parenchyma shows particularly high signals of natural isotopes of magnesium and potassium (Fig. 3A and C) which may indicate large concentrations in this tissue. This implies that the large exchanged fractions are the result a massive exchange of nutrients with the xylem parenchyma, which is consistent with a role as a reservoir for xylem-tissue exchange, although the signal images are subject to matrix artefacts. "Islands" of thin-walled xylem parenchyma within the thick-walled xylem parenchyma show fast equilibration of calcium and magnesium with the vessels, like the thick-walled xylem parenchyma, but only  $F_{Ca}$  was equal to the vessels while  $F_{Mg}$  was half as large as in the thick-walled xylem parenchyma (Figure 5B-D). Fractions of potassium were consistently not in equilibrium and also half as large as in the thick-walled parenchyma. For potassium this finding is consistent with the suggestion of a smaller apoplastic compartment due to the thinner cell walls that may result in a smaller fast exchangeable fraction of element than in the thick-walled parenchyma. For magnesium on the other hand the high signal of major natural magnesium isotope found for this tissue (Fig. 3A) suggests large amounts of stored magnesium, as a functional homologue to the magnesium storage in the endodermis of spruce needles found by Stelzer et al. (1990). This magnesium storage may represent a larger nonexchangeable fraction than present in the thick walled xylem parenchyma.

### *Pith*

All the nutrient elements in the pith are clearly less exchangeable than in the xylem parenchyma. Tracer fractions for potassium and calcium were very low (3% and 5%), even after 240 minutes of tracer application indicating that only ca 10% element were

exchangeable. In contrast magnesium fractions were almost as large as in the xylem parenchyma indicating that there can be no blockage of nutrient movement between the xylem vessels and the pith. The low fractions of tracer (and very low exchangeable fractions in this tissue) for potassium and calcium therefore probably reflect large amounts of potassium and calcium that do not exchange during our experiments. This is consistent with the suggestion of the pith as a storage tissue for nutrients (van der Schoot and van Bel, 1990; Koroleva et al., 2000), and indeed we found high signal for the natural isotopes of potassium and calcium (Fig. 3C and E) but not for magnesium (Fig. 3A) in the pith. The pathway for nutrient movement between the xylem vessels and the pith is most likely apoplastic as demonstrated by the much larger fractions of potassium in the cell walls of both the xylem parenchyma and the pith compared to the cell lumina (Fig. 6B). This is compatible with findings for tomato (van der Schoot and van Bel, 1990) where dye movement between cells and membrane potential mappings showed that there was symplastic isolation of the pith from the xylem parenchyma.

#### *Cambium and phloem*

There were low tracer fractions in cambium and phloem for all three nutrients, but a distinct increase in tracer fractions between 20 minutes to 240 minutes of tracer application shows that there is no equilibrium between the vessels and these tissues. The low values after 20 min are striking since the cambium is only separated from the xylem vessels by one or two cell layers of xylem parenchyma (that also show strong labeling). For calcium, the large values of  $F_{Ca}$  after 240 minutes tracer application suggest that the equilibrium fraction may be as large as in the thick-walled xylem parenchyma and the exchangeable fraction may be also 100%. Therefore the small fractions after 20 minutes of tracer application likely represent a slow exchange rate between the xylem vessels and the cambium. Because fractions in the cambium and phloem are almost equal for potassium and magnesium this slow exchange is expected to be located on the interface between xylem parenchyma and cambium. An explanation may be either a diffusion barrier or a large very slow exchangeable fraction or possibly a combination of both.

The values for calcium (16-22%) and magnesium (15%) tracer in the cambium and phloem found in this study (Figs. 5B and D) are very similar to the values in the root xylem (enclosed by the diffusion barrier of the endodermis) found by Kuhn et al. (2000)

after 20 minutes tracer uptake. In analogy to the root this is consistent with the existence of an apoplastic barrier, despite the lack of structural indications.

## **Conclusions**

The labelling of all tissues in the stem by magnesium, potassium and calcium originating from tracer solution in the xylem vessels within 20 min shows that no strong barriers against radial movement of these cations exist in the stem comparable to the endodermis in the root. Nevertheless the time for reaching equilibrium with the element in the xylem vessels and also the exchangeable fraction of element showed strong differences between the individual tissues, regardless of the distance from the xylem vessels. Equilibration within 20 minutes for calcium and magnesium, and large exchangeable fractions of all three elements, showed that the xylem parenchyma had the most intense exchange with the xylem vessels of all tissues, supporting a role as the interface between tissue-level and long-distance transport. Fast equilibrium and complete exchange of calcium showed a higher mobility of calcium than of potassium and magnesium in the xylem parenchyma. This is quite puzzling since the mobility of monovalent ions is usually faster than of divalent ions. It may reflect that magnesium and potassium were mostly in the symplast while largest amounts of calcium are located in the apoplast. The pith showed a fast equilibration with the xylem vessel lumina but only very small exchangeable fractions of potassium and magnesium, which fits with their role as a storage tissue for these nutrients. In contrast the cambium and phloem were slower to equilibrate than the xylem parenchyma and the pith, suggesting to a barrier to diffusion slowing down apoplastic movement from the xylem parenchyma to the cambium. Direct application of tracers into the transpiration stream showed similar distribution patterns of the tracers in stem tissues as after cut-stem application showing cut transpiring shoots can be used for studying mineral nutrient movement in intact plants.

For the nutrient cycling within plants these findings have several implications. For regulation of xylem nutrients, the intense exchange with the surrounding tissues provides a buffering system with reservoirs of various sizes and exchange properties. Rapid exchange with the thick-walled xylem parenchyma enlarges the storage volume of the xylem translocation pathway, and provides short-term buffering of fluctuations in xylem sap concentration, especially for calcium. A slower exchange, but with a larger nutrient pool, is provided by the pith, cambium and phloem. Of these the phloem is a route for many nutrients to be exchanged with other parts of the plant (Marschner et al., 1997; Jeschke and Hartung, 2000), for coordinating the distribution of ions as tissues and organs need them, and to avoid their delivery to organs where excesses could be harmful. But because

calcium is hardly mobile in phloem, it appears that its storage is purely local, with fast access in the xylem parenchyma, and long-term storage in the pith.

## **Material and Methods**

### **Plant material**

Plants of French bean (*Phaseolus vulgaris* L. cv. Shiny Fardenlosa) were grown from seeds in 1.7 l pots with standard soil substrate (ED 73, Einheitserde, Fröndenberg, Germany) in a growth chamber with 12 h / 12 h light / dark cycle. Illumination with photosynthetically active radiation (PAR) of  $300 \mu\text{mol m}^{-2} \text{s}^{-1}$  was obtained with fluorescent lamps (15 x 36-W Fluora, Osram, Munich, Germany). Temperature was between 21°C and 23°C and automatic watering was carried out twice a day. Plants approximately four weeks old were used for experiments, when they had about three mature trifoliate leaves .

### **Tracer application**

The multi-element tracer solution contained 2.5 mM  $^{26}\text{MgCl}_2$ ,  $^{41}\text{KCl}$ ,  $^{44}\text{CaCl}_2$  and  $\text{NaNO}_3$  (Sigma-Aldrich, Steinheim, Germany) in water.  $^{26}\text{MgCl}_2$  and  $^{44}\text{CaCl}_2$  were purchased from Medgenix (Düsseldorf, Germany).  $^{41}\text{KCl}$  for 20-min experiments at low transpiration was obtained from Isoflex (Moscow, Russia). For the other experiments  $^{41}\text{KCl}$  was purchased from Medgenix. The isotopic enrichment of the tracers is shown in Table I. Solution osmolality was  $24 \text{ mosmol kg}^{-1}$ . Osmolality was determined by a freezing point osmometer (Micro-Osmometer Model 210, Fiske® Associates, Mass., USA).

We used two protocols to supply tracer to the transpiration stream. For cut-stem applications (Experiments type 1, 2 and 4 in Table II), the bean shoot was cut under tap water ( $6 \text{ mosmol kg}^{-1}$ ) directly above soil and the wet end rapidly transferred into the tracer solution, which was then taken up by the transpiration stream for 20 or 240 minutes. For minimally invasive application (type 3 in Table II) the tracer solution entered a xylem vessel of the first internode above the primary leaves via a glass microcapillary (maximum outer diameter ca.  $20 \mu\text{m}$ ) attached to Tygon® tubing (internal diameter 0.8 mm). A micromanipulator slowly moved the capillary tip radially into the shoot tissue while observing the meniscus formed within the tubing by the tracer solution continuously in a microscope. Forward movement of the tip was immediately stopped when the meniscus moved suddenly towards the plant. This microcapillary application extended for 20-min only. Environmental conditions during both protocols are displayed in Table II.

Transpiration rate was measured as weight loss of plants under the same environmental conditions as in the respective experiments with pots wrapped in plastic to prevent evaporation.

### **Pressure probe**

Xylem pressure probe measurements (Benkert et al., 1991) used parallel experiments with tracer-free solutions. Experimental conditions were with 5-20  $\mu\text{mol m}^{-2} \text{s}^{-1}$  PAR, 20-25°C and 47-70% relative humidity, more variable than for the tracer application experiments. After inserting the xylem pressure probe into the xylem of the first stem internode, and reading a reasonably constant xylem tension for several minutes, the two solution application protocols was undertaken while measuring the tension. When the tension rose to 0.0977 MPa relative to atmosphere (corresponding to water vapor pressure at room temperature), it was provoked to drop below that critical value to demonstrate a firm hydraulic coupling, ie absence of water vapor or air bubbles, which would have falsified the measurement.

### **Preparation of frozen-hydrated tissue samples**

Frozen-hydrated tissue samples were prepared as follows ( see (Metzner et al., 2008). In short, ca. 4-cm-long samples from the first internode above the primary leaves were excised, mounted in copper rivets by the aid of a sucrose solution, and shock-frozen by plunging into melting propane (-189°C), all within 30 s after excision. During subsequent preparation and measurement the ambient temperature was continuously kept below -130°C. Frozen samples were trimmed and their surfaces planed prior to the cryo-ToF-SIMS analysis with the aid of a cryo-microtome (MED 020/GBE with BU 012092-T and VCT-100, BAL-TEC, Witten, Germany). The samples were subsequently transferred via the VCT-100 cryo-shuttle through the respective airlock systems to the cryo- SIMS and/or the cryo-SEM.

### **Cryo-SIMS measurements**

Surface isotope mapping on the cryo-planed frozen-hydrated bean stem samples was performed with a ToF-SIMS IV mass spectrometer (IONTOF, Münster, Germany) equipped with an airlock system, a modified cryostage and a pre-sputtering  $\text{O}_2^+$ -ion beam with 2keV as described in detail by (Metzner et al., 2008). A mass-filtered 25 keV pulsed

$\text{Bi}^+$  - or  $\text{Bi}^{3+}$ -ion beam was used for generation of the secondary ions. The ion beam current was between 0.1 and 1.2 pA resulting in a primary ion dose density between  $1.3 \times 10^{13}$  and  $6.9 \times 10^{13}$  ions  $\text{cm}^{-2}$ . The sputtered secondary ions were extracted with 2 kV into a reflectron-type time-of-flight mass analyzer. A complete secondary-ion mass spectrum was recorded for each pulse and pixel. To prevent charging of the sample surface a low-energy electron flood gun was used.

Two types of measurements were conducted during the 6-8 hours measuring time for the same sample. (1) Overview images acquired with the high-current bunched mode with  $\text{Bi}^+$  (Figs. 3+4B-D) or the low-current bunched mode with  $\text{Bi}^{3+}$  (Figs. 4A'-D'+8) yielded large area views ( $500 \times 500 \mu\text{m}^2$ ) with high secondary ion yields per primary ion pulse at high mass resolution ( $m/\Delta m = 3500$  at mass 41) and lateral resolution of 10 to 7  $\mu\text{m}$ . (2) For high-lateral resolution images (Figs. 6+9) the burst-align mode with  $\text{Bi}^+$  or  $\text{Bi}^{3+}$  gave ion maps of small tissue areas ( $<150 \times 150 \mu\text{m}^2$ ) at a lateral resolution better than 1  $\mu\text{m}$  but with lower secondary ion yields per primary ion pulse at nominal mass resolution. The tracer data from this measurement type were suitable only for potassium, where the mass interferences for  $^{39}\text{K}$  were negligible and for  $^{41}\text{K}$  below 20%.

## Processing of cryo-SIMS data

Images of the major isotopes of the analytes were computed from the recorded mass spectra as ion counts per pixel. A "Poisson correction" (Stephan et al., 1994) was used to correct where multiple events would have occurred within the detection interval. Based on the number of measurement cycles and the number of detected counts the probability of a missed count event was calculated and the number of counts per pixel corrected by adding the calculated number of missed counts. We denote the resulting value signal ( $S$ ), in counts per pixel.

In order to know how much of an element in each pixel actually originated from the tracer solution it is necessary to correct for the tracer isotope originally present in the plant tissue. We therefore calculated  $F_E$ , the fraction of element E originating from the tracer solution, from the abundance of the tracer isotope in the pixel ( $A_E$ ) in relation to the tracer isotope abundance of the nutrient solution ( $A_{nE}$ ), but in each case allowing for the natural abundance of the tracer isotope ( $A_{0E}$ ). Being a fraction,  $F_E$  is not affected by topography or the chemical matrix.



$$F_E := \frac{A_E - A_{0E}}{A_{nE} - A_{0E}} \quad (\text{equation 1})$$

The natural abundance of the tracer isotope  $A_{0E}$  was taken from the literature (Böhlke et al., 2005) and the tracer abundance was calculated from the SIMS signals as:

$$A_E := \left( \frac{S^t}{\sum_I S^I} \right)_E \quad (\text{equation 2})$$

where  $S^I$  is the pixel signal of each isotope  $I$  of the element, and  $I = t$  for the tracer isotope representing the element. For calculation of  $A_E$  a threshold was chosen for  $\sum S^I$  below which we set  $F_E = 0$  in order to mask noise. The chosen threshold was 1% of the image maximum for potassium and calcium, and 5% for magnesium. Images of  $F_E$  were then scaled from zero to 255 and displayed in the NIH “fire2” palette.

For individual tissues and tissue areas (Fig. 5B-D),  $A_E$  was calculated by first defining regions of interest (ROI) with the aid of the software IonImage (IONTOF, Münster) based on the anatomical information from the corresponding cryo-SEM images. For these regions, the sum of  $S^I$  over all pixels in the ROI was used for calculation of  $A_E$  (equation 2), and  $F_E$  calculated from equation 1.

### The exchangeable fraction of element in the tissues

After a steady state for isotopic exchange of an element (E) between the xylem sap and tissue is reached, the tracer of exchangeable (unbound) element will have equal abundance in each place, but the non-exchangeable material will remain at natural abundance. Thus if the xylem sap is all unbound, with abundance  $A_{xE}$ , but the exchangeable fraction of the element in the tissue is  $e_{tE}$ , due either to chemical or physical sequestration, then the tracer abundance for the tissue ( $A_{tE}$ ) is

$$A_{tE} = e_{tE} A_{xE} + (1 - e_{tE}) A_{0E} \quad (\text{equation 3})$$

and from equation 1,

$$e_{tE} = F_{tE} / F_{xE} \quad (\text{equation 4})$$

### Limits of detection for stable isotope tracers with cryo-SIMS

The detection limits for the stable isotope tracers depend on the precision of the isotopic abundance measurements. To determine this limitation for our instrumental setup we analyzed air dried spots of half-strength Hoagland solution with natural isotopic abundance on clean silicon substrate (Table I). Taking the error margins from Table I it can be seen that  $^{26}\text{Mg}$  can be detected if the sample abundance exceeds the natural abundance by about 2.4%,  $^{41}\text{K}$  tracer by 1.0% and  $^{44}\text{Ca}$  tracer by 0.2%. Of course detection sensitivity also depends on statistical variability where tracer counts are small, which is more likely for data from single pixels.

### Cryo-SEM

The surfaces of frozen-hydrated samples were imaged with a LEO Gemini VP 1550 scanning electron microscope (Zeiss, Oberkochen, Germany) with a cold field emission electron source. The instrument is equipped with a BAL-TEC cryo-stage and an airlock for the cryo-shuttle. The samples were imaged at an acceleration voltage of 1.8 keV at a stage temperature below  $-120^{\circ}\text{C}$  and a pressure of  $2 \times 10^{-3}$  Pa. The surface was etched by transiently raising the temperature of the sample stage to  $-90^{\circ}\text{C}$  while the extent of sublimation was monitored by continuous scanning of the sample surface. Sufficient etching typically required 2 to 5 minutes. SEM images were optimized for printing using limits and curve settings in Adobe Photoshop<sup>®</sup>.

### Overlays of cryo-SIMS images onto cryo-SEM images

SIMS image overlays over SEM images were prepared using Adobe Photoshop<sup>®</sup>. Areas in the SIMS images with very low ion counts or tracer fractions were colored transparent, thus revealing the SEM structure. The lower inclusion threshold for Mg and Ca isotope images (Figs. 3A+B and E+F) and for  $F_{\text{Mg}}$  and  $F_{\text{Ca}}$  images (Figs. 4B and D and 9B and D) was set to 5.8% of the full scale. The threshold for K isotope images (Fig. 3C and D) was set to 3.9% and for  $F_{\text{K}}$  (Figs. 4C and 9C) to 1.5% due to the very high signal ( $S'$ ) and low

background in K. Since expected standard deviations for Mg and Ca images were larger than the selected thresholds no loss of relevant information arose from this procedure.

### **Collection of xylem sap**

Epicotyl and first internode above the primary leaves were excised and cut into pieces ca. 5 cm long. These were placed upright in 15 ml centrifugation tubes on a PTFE sieve, the tubes closed and centrifuged for 5 minutes with 1560 g. The volume of the collected sap was determined by weighting.

### **Acknowledgments**

The authors are very grateful to Alexandra Ley for performing light microscopy and some of the minimally invasive pressure probe and tracer application experiments. Marion Roeb and Anne Dreißer helped with plant cultivation. Special thanks go to Hans-Peter Bochem and the Institute of Bio- and Nanosystems 2 at Forschungszentrum Jülich for the liberal use of their SEM facilities, and to Ulrich Zimmermann, Department of Biotechnology, University of Würzburg, for lending the xylem pressure probe setup to H.U.S.. Many thanks go to Siggi Jahnke and Peter Blümner for critical discussion on many aspects of the work.

## **References**

- Benkert R, Balling A, Zimmermann U** (1991) Direct measurement of the pressure and flow in the xylem vessels of *nicotiana-tabacum* and their dependence on flow resistance and transpiration rate *Bot Acta* **104**: 423-432
- Biddulph O, Markle J** (1944) Translocation of radiophosphorus in the phloem of the cotton plant. *Am J Bot* **31**: 65-70
- Black JR, Epstein E, Rains WD, Yin QZ, Casey WH** (2008) Magnesium-isotope Fractionation During Plant Growth. *Environ. Sci. Technol.* **42**: 7831-7836
- Böhlke JK, de Laeter JR, De Bièvre P, Hidaka H, Peiser HS, Rosman KJR, Taylor PDP** (2005) Isotopic compositions of the elements, 2001. *J Phys Chem Ref Data* **34**: 57-67
- Gilmer F, Schurr U** (2007) Dynamic and nutrient fluxes in the xylem. *In* B Sattelmacher, WJ Horst, eds, *The Apoplast of higher plants: Compartment of storage, transport, and reactions*. Springer, Dordrecht, pp 221-229
- Horst WJ, Kollmeier M, Schmohl N, Sivaguru M, Wang Y, Felle HH, Hedrich R, Schröder W, Staß A** (2007) Significance of the root apoplast for aluminium toxicity and resistance of maize. *In* B Sattelmacher, WJ Horst, eds, *The apoplast of higher plants: Compartment of storage, transport and reactions* Springer, Dordrecht, pp 49-66
- Jeschke WD, Atkins CA, Pate JS** (1985) Ion circulation via phloem and xylem between root and shoot of nodulated white lupin. *J Plant Physiol* **117**: 319-330
- Jeschke WD, Hartung W** (2000) Root-shoot interactions in mineral nutrition. *Plant and Soil* **226**: 57-69
- Jeschke WD, Pate JS** (1991) Modeling of the partitioning, assimilation and storage of nitrate within root and shoot organs of castor bean (*Ricinus-Communis L.*). *J Exp Bot* **42**: 1091-1103
- Karley AJ, White PJ** (2009) Moving cationic minerals to edible tissues: potassium, magnesium, calcium. *Current Opinion in Plant Biology* **12**: 291-298
- Koroleva OA, Davies A, Deeken R, Thorpe MR, Tomos AD, Hedrich R** (2000) Identification of a new glucosinolate-rich cell type in *Arabidopsis* flower stalk. *Plant Physiol* **124**: 599-608

- Kuhn AJ, Schroeder WH, Bauch J** (2000) The kinetics of calcium and magnesium entry into mycorrhizal spruce roots. *Planta* **210**: 488-496
- Leigh RA** (2001) Potassium homeostasis and membrane transport. *J Plant Nutr Soil Sc* **164**: 193-198
- Marschner H** (1995) Mineral nutrition of higher plants, Ed 2. Academic Press Limited, London
- Marschner H, Kirkby EA, Engels C** (1997) Importance of cycling and recycling of mineral nutrients within plants for growth and development. *Bot Acta* **110**: 265-273
- Metzner R, Schneider HU, Breuer U, Schroeder WH** (2008) Imaging nutrient distributions in plant tissue using time-of-flight secondary ion mass spectrometry and scanning electron microscopy. *Plant Physiol* **147**: 1774-1787
- Pate JS, Layzell DB, McNeil DL** (1979) Modeling the transport and utilization of carbon and nitrogen in a nodulated legume. *Plant Physiol* **63**: 730-737
- Rygel J, Pritchard J, Zhu JJ, Tomos AD, Zimmermann U** (1993) Transpiration Induces Radial Turgor Pressure-Gradients in Wheat and Maize Roots. *Plant Physiol* **103**: 493-500
- Schneider HU, Wegner LH, Haase A, Zimmermann U** (2007) Long-distance water transport under controlled transpirational conditions: Minimal-invasive investigations by means of pressure probes and NMR imaging. *In* B Sattelmacher, WJ Horst, eds, *The apoplast of higher plants: Compartment of storage, transport and reactions* Springer, Dordrecht, pp 251-264
- Siebrecht S, Herdel K, Schurr U, Tischner R** (2003) Nutrient translocation in the xylem of poplar - diurnal variations and spatial distribution along the shoot axis. *Planta* **217**: 783-793
- Stelzer R, Lehmann H, Kramer D, Luttge U** (1990) X-ray microprobe analyses of vacuoles of spruce needle mesophyll, endodermis and transfusion parenchyma cells at different seasons of the year. *Bot Acta* **103**: 415-423
- Stephan T, Zehnpfenning J, Benninghoven A** (1994) Correction of Dead-Time Effects in Time-Of-Flight Mass-Spectrometry. *J Vac Sci Technol A* **12**: 405-410
- Steudle E, Peterson CA** (1998) How does water get through roots? *J Exp Bot* **49**: 775-788
- Stout PR, Hoagland DR** (1939) Upward and lateral movement of salt in certain plants as indicated by radioactive isotopes of potassium, sodium, and phosphorus absorbed by roots. *Am J Bot* **26**: 320-324

- Thompson MV, Zwieniecki MA** (2006) The role of potassium in long distance transport in plants. *In* NM Holbrook, MA Zwieniecki, eds, *Vascular transport in plants*. Elsevier academic press, San Diego, pp 221-240
- van Bel AJE** (1974) Absorption of L-alpha-alanine and L-alpha-amino-iso-butyric acid during their movement through xylem vessels of tomato stem segments *Acta Bot. Neerl.* **23**: 305-313
- van Bel AJE** (1978) Free space of xylem translocation pathway of tomato stem. *J Exp Bot* **29**: 295-303
- van der Schoot C, van Bel AJE** (1990) Mapping membrane-potential differences and dye-coupling in internodal tissues of tomato (*Solanum-lycopersicon* L.). *Planta* **182**: 9-21
- van Ieperen W** (2007) Ion-mediated changes of xylem hydraulic resistance in planta: fact or fiction? *Trends Plant Sci* **12**: 137-142
- Wegner LH, Zimmermann U** (2009) Hydraulic conductance and K<sup>+</sup> transport into the xylem depend on radial volume flow, rather than on xylem pressure, in roots of intact, transpiring maize seedlings. *New Phytol* **181**: 361-373
- Wistuba N, Reich R, Wagner HJ, Zhu JJ, Schneider H, Bentrup FW, Haase A, Zimmermann U** (2000) Xylem flow and its driving forces in a tropical liana: concomitant flow-sensitive NMR imaging and pressure probe measurements. *Plant Biol.* **2**: 579-582
- Wolf O, Munns R, Tonnet ML, Jeschke WD** (1991) The role of the stem in the partitioning of Na<sup>+</sup> and K<sup>+</sup> in salt-treated barley. *J Exp Bot* **42**: 697-704
- Wolterbeek HT, Vanluijpen J, Debruin M** (1985) Actual escape area and lateral escape from the xylem of the alkali ions Na<sup>+</sup>, K<sup>+</sup>, Rb<sup>+</sup> and Cs<sup>+</sup> in tomato. *Physiol Plantarum* **65**: 467-475
- Zimmermann U, Rygol J, Balling A, Klock G, Metzler A, Haase A** (1992) Radial Turgor and Osmotic-Pressure Profiles in Intact and Excised Roots of *Aster-Tripolium* - Pressure Probe Measurements and Nuclear Magnetic-Resonance-Imaging Analysis. *Plant Physiol* **99**: 186-196

## Tables

**Table I: Isotopic composition of natural material and in the applied nutrient tracer solution.** Abundance of tracer isotopes ( $A_E$ ) for the elements of magnesium, potassium and calcium was calculated from SIMS signals (equation 2) of air-dried solution drops of natural isotopic composition, and tracer solution on silicon substrate (see equation 2; mean [%]  $\pm 2\sigma$ , n=3). Literature data (Böhlke et al 2005) for natural material are also shown to illustrate SIMS precision.

<b>Magnesium isotopes</b>	$^{24}\text{Mg}$	$^{25}\text{Mg}$	$^{26}\text{Mg}$
tabulated	79.0	10.0	11.0
natural	$79.1 \pm 2.4$	$9.6 \pm 1.4$	$12.8 \pm 2.4$
tracer	$2.0 \pm 0.2$	$1.0 \pm 0.2$	$97 \pm 0.2$
<b>Potassium isotopes</b>	$^{39}\text{K}$	$^{41}\text{K}$	
tabulated	93.3	6.7	
natural	$93.7 \pm 1.0$	$6.3 \pm 1.0$	
tracer type 1 experiments	$2.9 \pm 0.6$	$97.1 \pm 0.6$	
tracer type 2, 3, 4 experiments	$5.5 \pm 0.6$	$94.5 \pm 0.6$	
<b>Calcium isotopes</b>	$^{40}\text{Ca}$	$^{44}\text{Ca}$	
tabulated	96.9	2.1	
natural	$97.8 \pm 0.2$	$2.2 \pm 0.2$	
tracer	$3.2 \pm 2.6$	$96.7 \pm 2.6$	



**Table II: Environmental conditions for growth and during experiments.**

Tracer uptake rates were identical to transpiration rates in all experiments except type 3 where transpiration rate was  $0.1 \text{ ml min}^{-1}$ . In type 4 experiments, uptake rates began at  $0.2 \text{ ml min}^{-1}$  and were below  $0.05 \text{ ml min}^{-1}$  after 20min.

Experiment	Sampling time [min]	Application	Relative humidity [%]	Tracer uptake rate [ $\text{ml min}^{-1}$ ]
Type 1	20	cut-stem	34-36	0.2
Type 2	20	cut-stem	66-67	0.1
Type 3	20	microcapillary	50-61	0.001
Type 4	240	cut-stem	44-63	0.05

## Figures

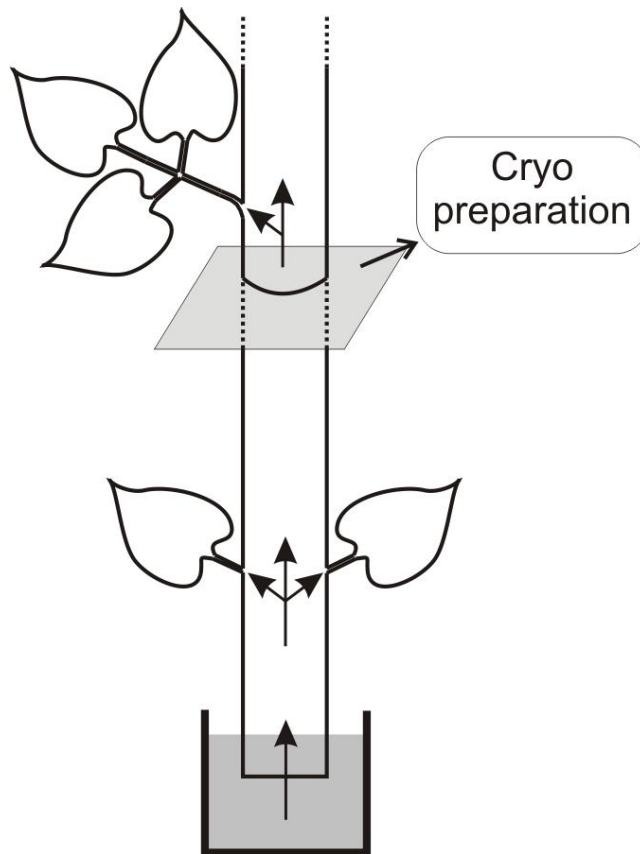


**Figure 1:** Method of administering nutrient tracer solution to a *Phaseolus vulgaris* (cv Fardenlosa) climbing bean. The stem was cut through under water directly above the soil and transferred to the tracer solution which entered the transpiration stream until a 4 cm portion of stem was cut from the internode above the primary leaves, about 25 cm from the cut. The portion was immediately shock frozen, and remained below  $-130^{\circ}\text{C}$  until all analysis was completed. The samples were fractured to produce cross-sectional surfaces that were cryo-planed and transferred to cryo-SIMS for isotopic analysis, and finally freeze-etched to show anatomical detail by cryo-SEM (see further details in Metzner et al., 2008).

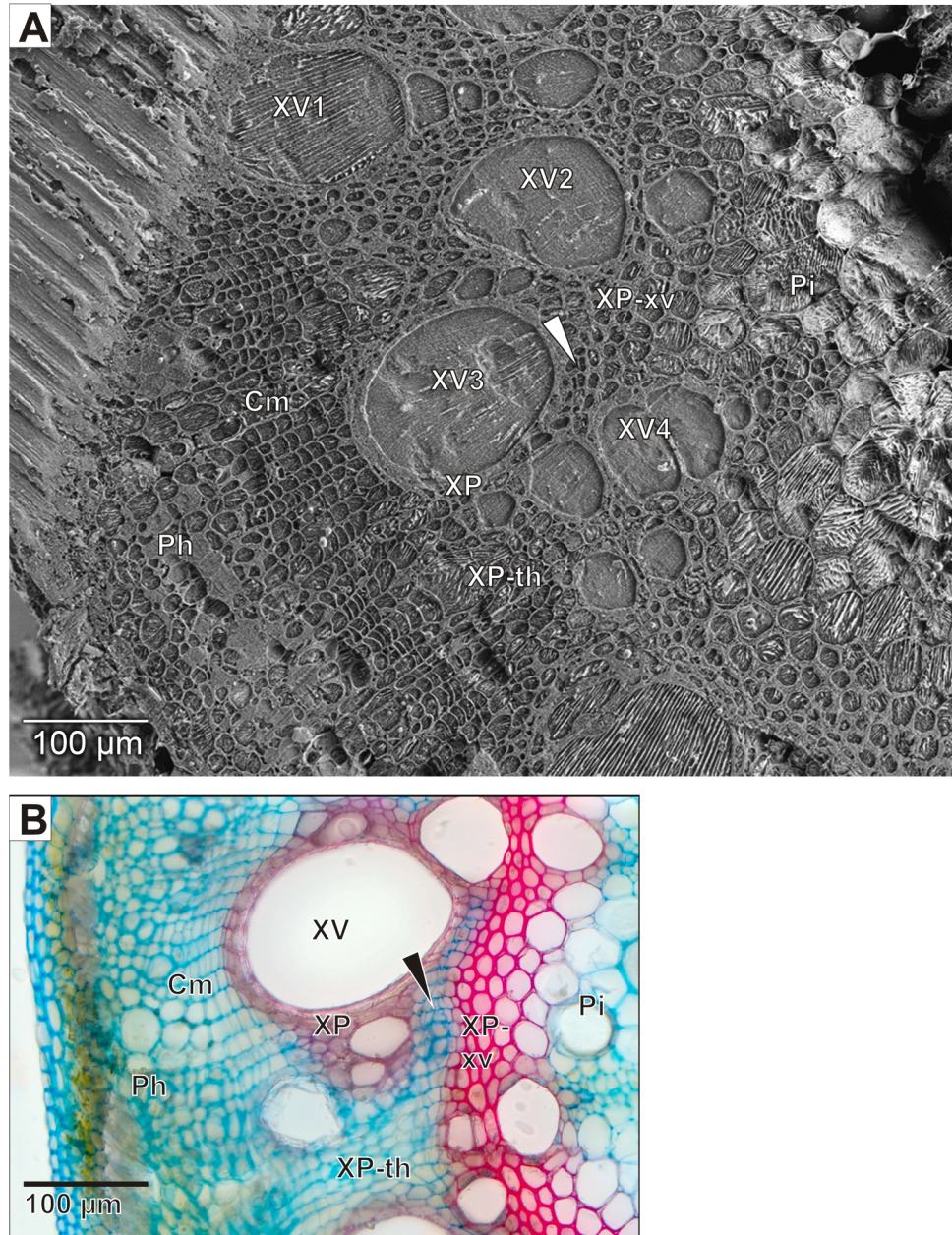


**Figure 2:** Cross-sectional anatomy of the stem tissue. A, Tissue structures revealed in Cryo-SEM by freeze-etching the surface after the sample has been analysis by cryo-SIMS. Xylem vessels (XV1-4), and two types of xylem parenchyma, are visible. Thick-walled xylem parenchyma is composed of two subtypes, the small and weakly vacuolated cells enclosing the vessels in an axial sheath (XP) and larger strongly vacuolated cells between the vessels (XP-xv), while thin-walled xylem parenchyma (XP-th) occurs between the cambium and the thick-walled xylem parenchyma. There are also islands of thin-walled xylem parenchyma (XP-is, arrowhead) within the thick-walled. Xylem is bordered towards the center of the stem by the pith (Pi), and beyond that there is airspace. Towards the stem

periphery is the cambium (Cm) and phloem (Ph). On the upper left is tissue and water that had not been cryo-planed. B, Light microscopic image of a hand section of a comparable tissue area. Double staining with astra-blue (cellulic cell walls stain blue) and safranin (lignified cell walls stain red).

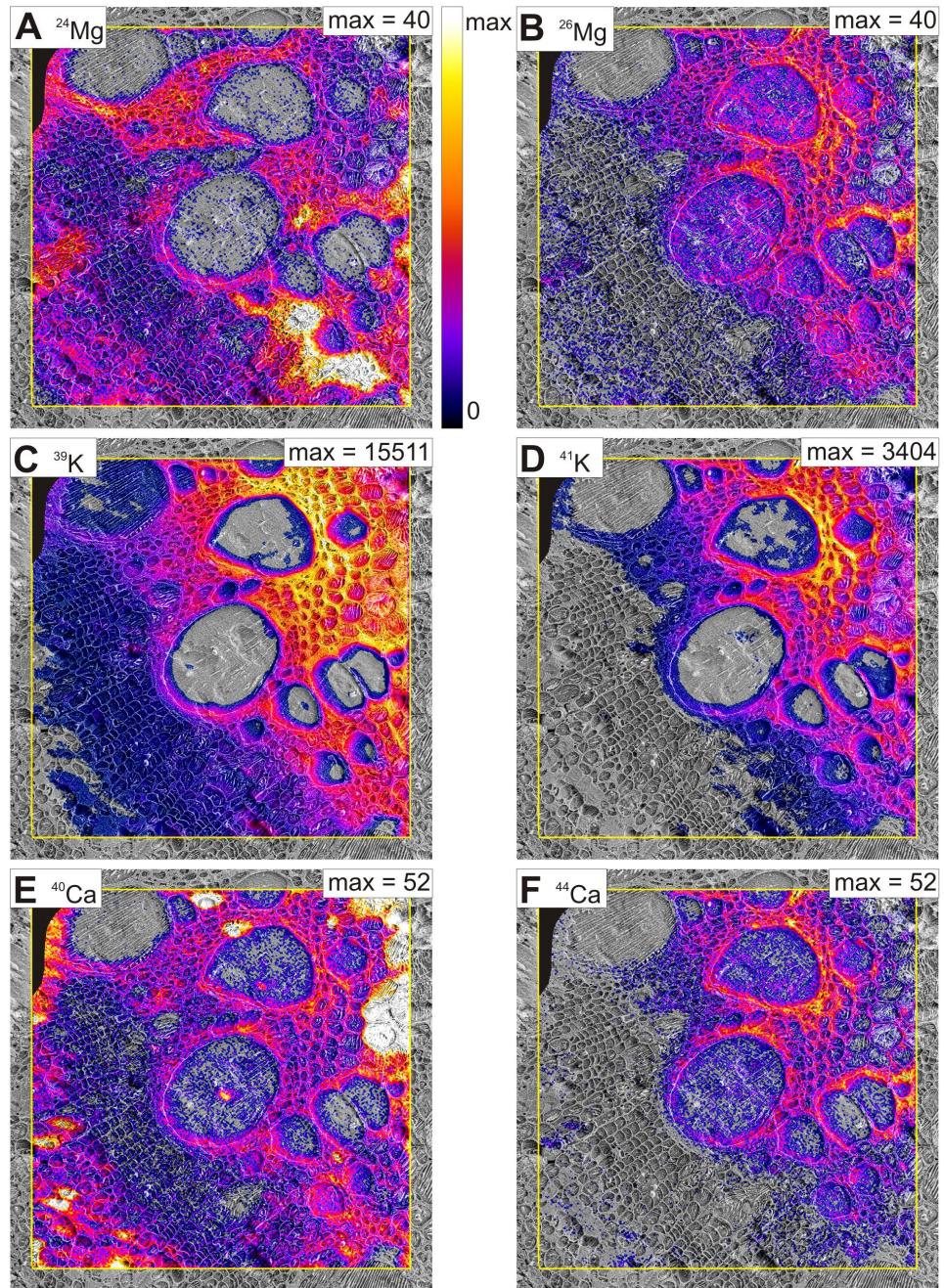


**Figure 3:** Cryo-SIMS mappings of major isotopes of magnesium, potassium and calcium.

The images show the major natural isotope (LHS) and major tracer isotope (RHS) in one sample taken 20 minutes after the stem was cut and tracer solution entered (see Fig. 1), laid over the relevant cryo-SEM image (Fig. 2A). All tracer isotopes were enriched to >95% isotopic abundance in the input solution, flow rate  $0.2 \text{ ml min}^{-1}$ . Scaling is from zero (counts per pixel). Scale maxima were selected to display detail, at the expense of saturation in white areas in the  $^{24}\text{Mg}$  and  $^{40}\text{Ca}$  images. Original maximum counts per pixel

were for A) 96 counts and for E) 434 counts. A threshold of 5.8% for images A+B and E+F and of 2.5% for C+D of the colorscale was set, below which pixels were set transparent. A small area in the upper left corner of the images is excluded, the surface had not been properly cryo-planed. Imaged region: 500 x 500  $\mu\text{m}$ ; resolution 256 x 256 pixels.

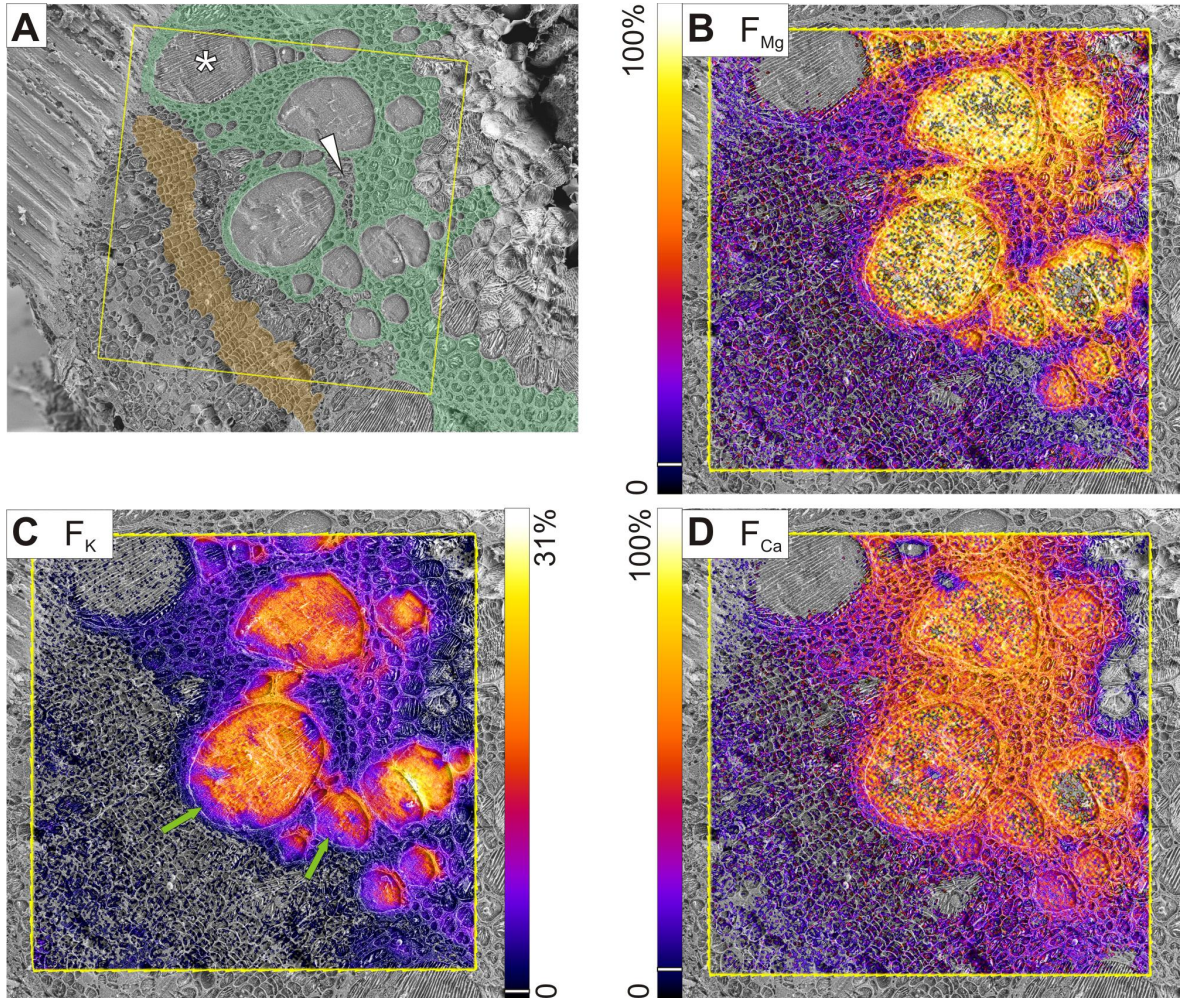


**Figure 4:** Typical stem structure and mappings of tracer fractions for magnesium, potassium and calcium. Samples were taken after 20 minutes of tracer solution flow. A, Cryo-SEM images with colour-coded overlay to help in the identification of tissue types: thick-walled xylem parenchyma (green), cambium (yellow). Asterisk indicates immature vessel and white arrowhead thin-walled xylem parenchyma within thick-walled parenchyma. B-D, Fractions of tracer ( $F_{Mg}$ ,  $F_K$ ,  $F_{Ca}$ ) are scaled from zero to the indicated maximum. For better visualization, pixels were set transparent where fractions fell below a threshold of the colorscale (indicated by white bars): for  $F_{Mg}$  in B 5%;  $F_K$  in C 1.5%;  $F_{Ca}$  in D 5%. Scanned cryo-SIMS area:  $500 \times 500 \mu\text{m}^2$ ; resolution:  $256 \times 256$  pixels. Images were overlaid on the corresponding cryo-SEM images.

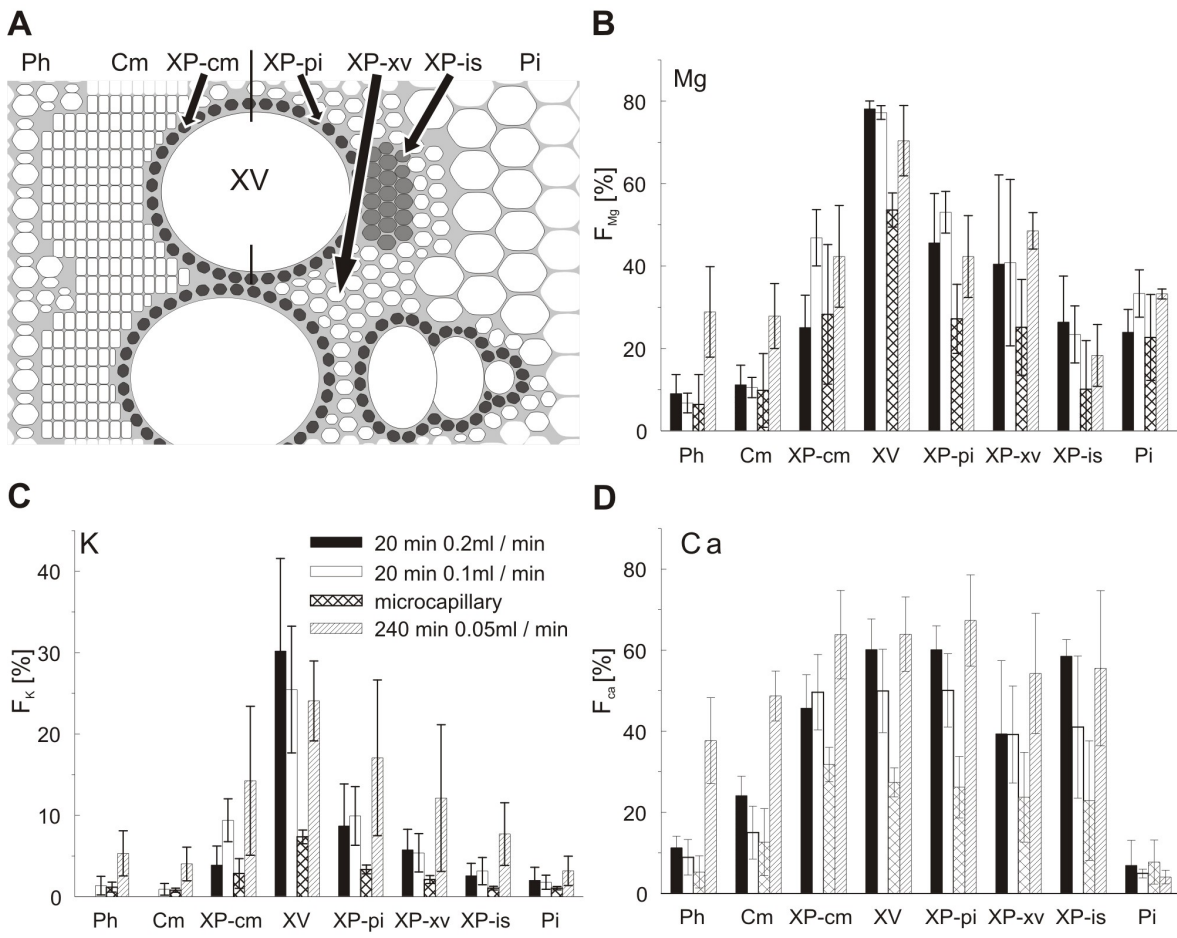


**Figure 5:** Fractions of tracer in various types of stem tissue.

A, Scheme of the ROI, specified according to anatomical criteria defined in Fig 2 with XP subdivided into a half ring facing the cambium (XP-cm) and a half ring facing the pith (XP-pi). B to D, fractions of magnesium, potassium and calcium tracer for the selected ROI, from three different experiments (error bars indicating one standard deviation). Black columns: 20 minutes cut-stem application, transpiration rate  $0.2 \text{ ml min}^{-1}$ . Fractions of potassium in the phloem and cambium were below detection limit. White columns: transpiration rate  $0.1 \text{ ml min}^{-1}$ . Cross hatched columns: microcapillary, 20 minutes application, transpiration rate  $0.1 \text{ ml min}^{-1}$ . Hatched columns: 240 minutes cut-stem application; transpiration rate  $0.05 \text{ ml min}^{-1}$ .



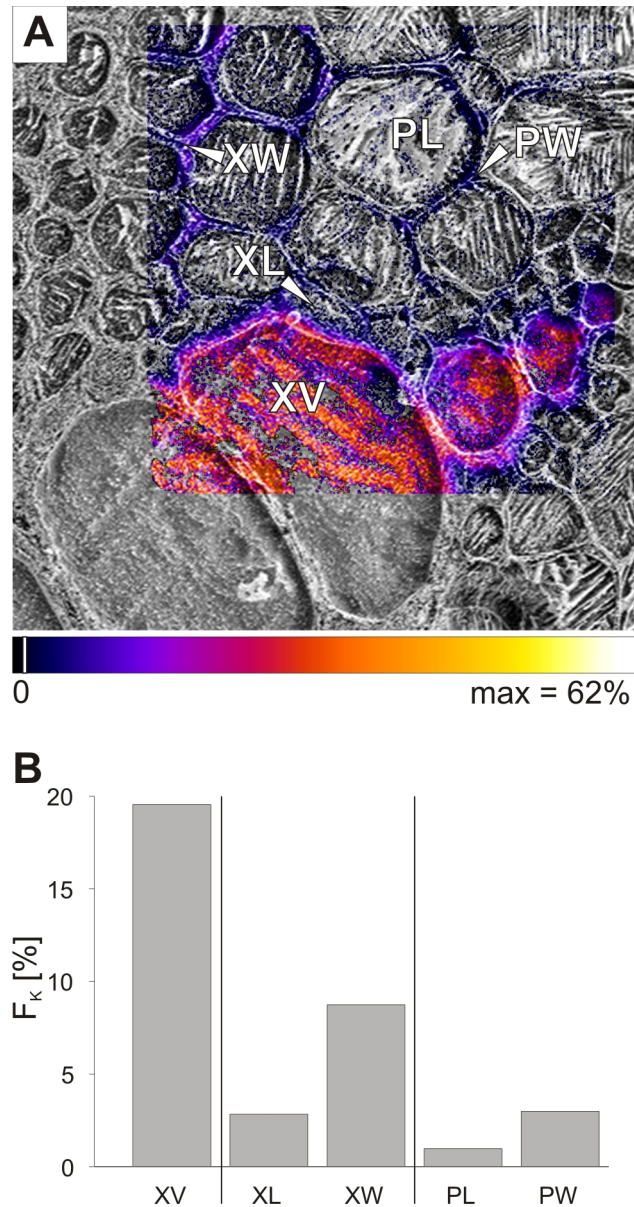


**Figure 6:** Potassium tracer fraction  $F_K$  measured at high lateral resolution, 20 min after start of tracer application. A, Potassium tracer fraction,  $F_K$ , imaged for a bundle of metaxylem vessels (right hand side in Fig. 4C), as overlaid on the corresponding cryo-SEM image. B, Bar chart of  $F_K$  representing the ROI for the lumina (XL) and walls (XW) of small thick-walled xylem parenchyma cells bordering the xylem vessels (XV).  $F_K$  was also calculated separately for the lumina (PL) and walls (PW) of the pith, as visible towards the upper right in A. Scanned cryo-SIMS area: 121 x 121  $\mu\text{m}$ ; resolution: 256 x 256 pixels. Pixels were set transparent where fractions fell below a threshold of 2% of the colorscale (indicated by white bar).

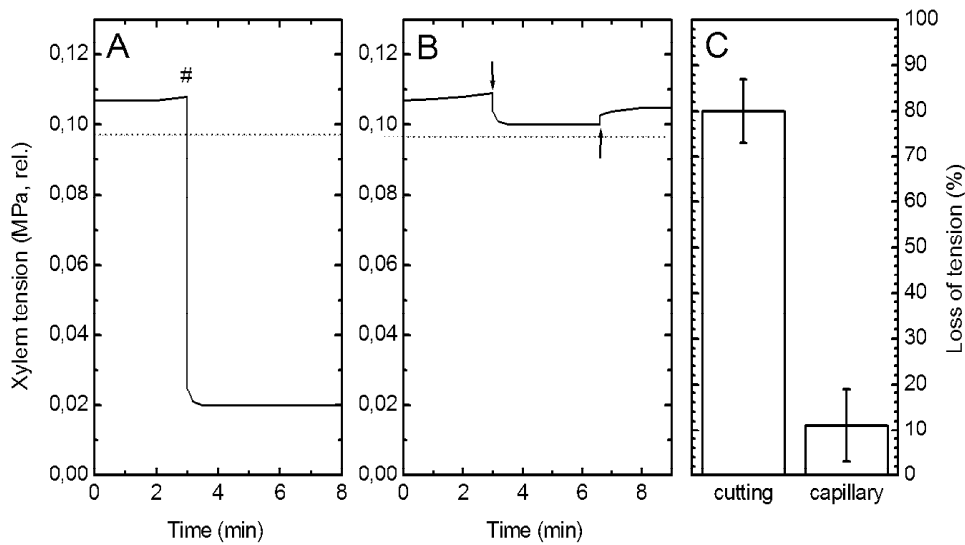


**Figure 7:** Xylem tension (relative to the atmosphere) during preparation for application of tracer solution, and during solution uptake. A, Application to the entire bean stem via the cut-stem and B, to one xylem vessel via a microcapillary. Tension was monitored by the minimally invasive xylem pressure probe technique. C, The percentage loss in tension with capillary feeding ( $n=4$ ) and via the cut-stem (mean  $\pm$  standard deviation,  $n=6$ ). Downward-directed arrow: Insertion of application microcapillary; upward-directed arrow: Withdrawal of this microcapillary; #: Cutting of stem under water. The horizontal dashed line in A and B marks the saturation water vapour pressure (0.0977 MPa).

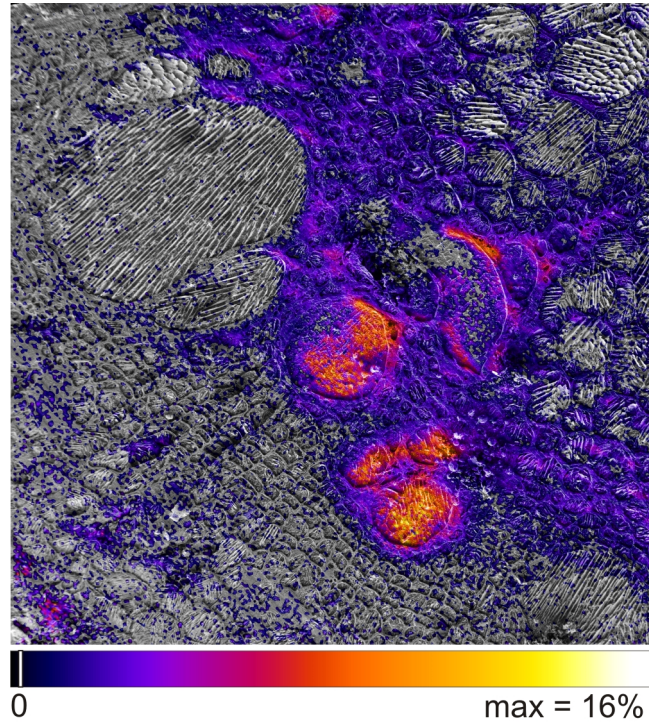


**Figure 8:** Typical distribution of K tracer fractions after tracer application via microcapillary for 20 minutes, overlaid onto the corresponding cryo-SEM image. Similar distribution was found in three out of three experiments; Cryo-SIMS area is 500 x 500  $\mu\text{m}$ ; resolution: 256 x 256 pixels.

Pixels were set transparent where fractions fell below a threshold of 1.5% of the colorscale (indicated by white bar).

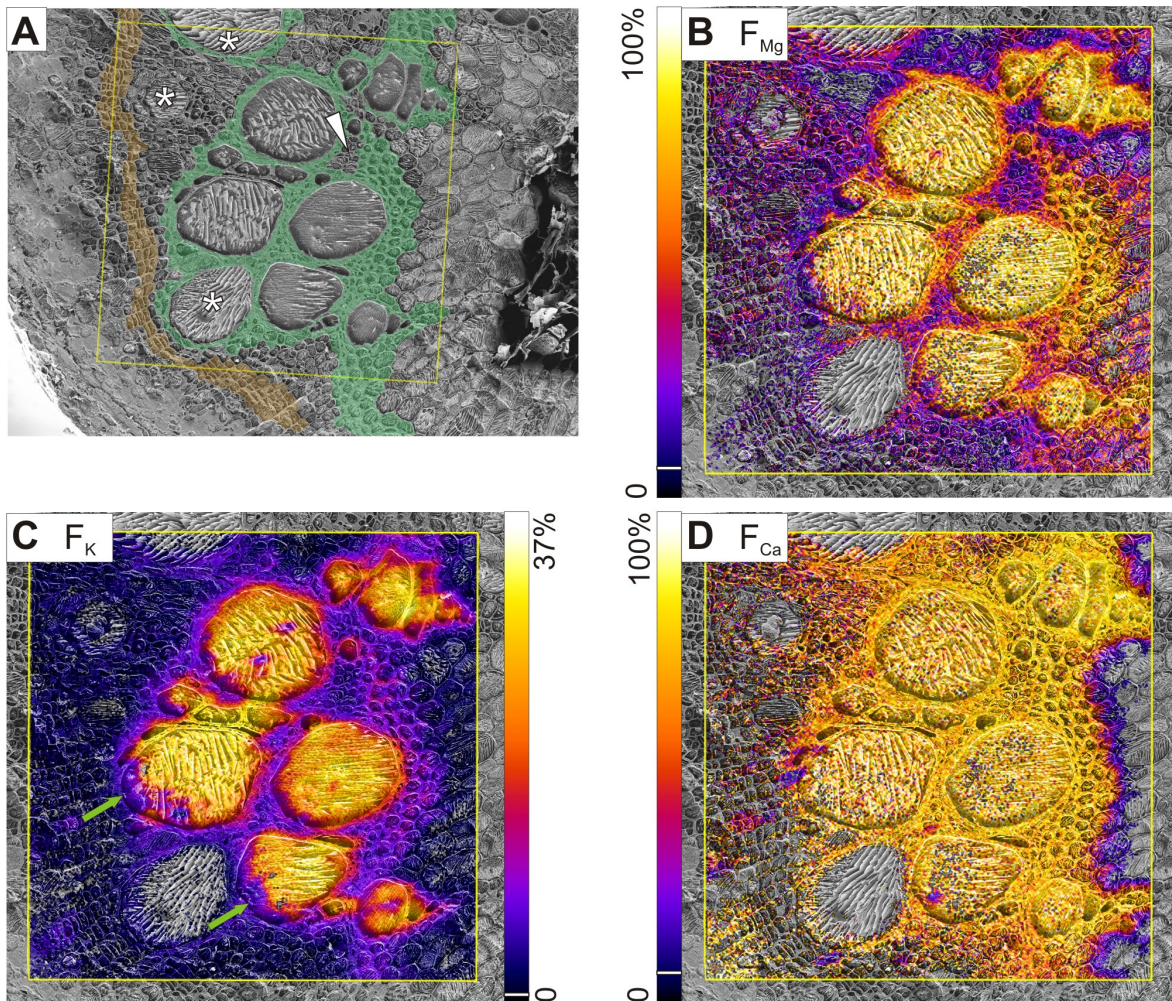


**Figure 9:** Stem structure and mappings of tracer fractions for magnesium, potassium and calcium. Samples were taken after 240 minutes of tracer solution flow. A, Cryo-SEM image with colour-coded overlay to help in the identification of tissue types: thick-walled xylem parenchyma (green), cambium (yellow). Asterisks indicate immature vessels and white arrowhead thin-walled xylem parenchyma within thick-walled parenchyma. B-D, Fractions of tracer are scaled from zero to the indicated maximum and overlaid on the corresponding cryo-SEM images. Pixels were set transparent where fractions fell below a threshold of the colorscale (indicated by white bars): for Mg in B 5%; K in C 1.5%; Ca in D 5%.

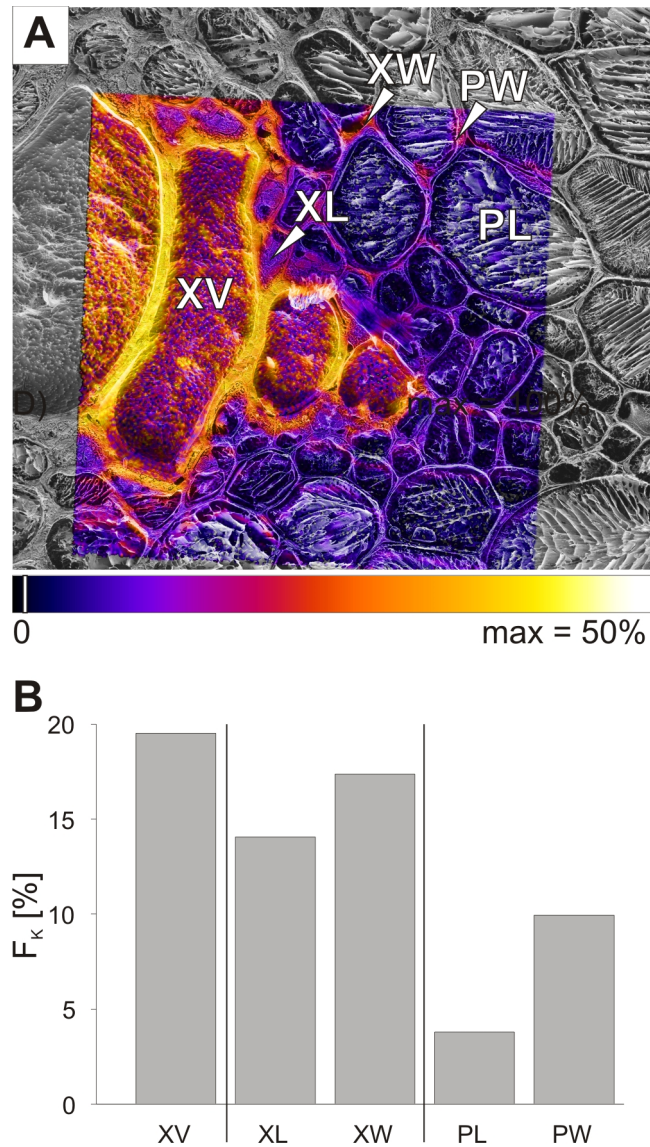


**Figure 10:** Potassium tracer fraction  $F_K$  at high lateral resolution, 240 min after start of tracer application. A, potassium tracer fraction,  $F_K$ , imaged for a bundle of metaxylem vessels (same as in upper right corner in Fig. 9C), as overlaid on the corresponding cryo-SEM image. B, Bar chart of  $F_K$  representing the ROI for the lumina (XL) and walls (XW) of small thick-walled xylem parenchyma cells bordering the xylem vessels (XV).  $F_K$  in the pith visible towards the upper and lower right for the lumina (PL) and walls (PW). Scanned cryo-SIMS area  $115 \times 115 \mu\text{m}^2$ ; resolution  $256 \times 256$  pixels; Pixels were set transparent where fractions fell below a threshold of 2% of the colorscale (indicated by white bar).

### 5.3 Third publication: Dynamics of water and nutrients in stems

Status: **Submitted** (October 6, 2009)

Metzner R, Thorpe MR, Breuer U, Blümmer P, Schurr U, Schroeder WH (sub 2009b)  
**Contrasting dynamics of water and mineral nutrients in stems shown by stable isotope tracers and cryo-SIMS.** *Plant, Cell & Environment* (*submitted*)

#### Own contribution

- Experimental design
- Experiments
- Sample preparation
- Cryo-SIMS analysis
- Data analysis and interpretation
- Preparation of manuscript

---

## **Contrasting dynamics of water and mineral nutrients in stems shown by stable isotope tracers and cryo-SIMS**

*Ralf Metzner<sup>1,2,\*</sup>, Michael R. Thorpe<sup>2</sup>, Uwe Breuer<sup>1</sup>, Peter Blümner<sup>2</sup>, Ulrich Schurr<sup>2</sup> and  
Walter H. Schroeder<sup>2</sup>*

<sup>1</sup>Central Division of Analytical Chemistry, <sup>2</sup>Phytosphere Institute (ICG-3),  
Forschungszentrum Jülich, Leo Brandt Straße, 52425 Jülich, Germany

Running title: Xylem transport dynamics of water and nutrients

Keywords: xylem, transport, mineral nutrients, potassium, calcium, magnesium, water, ToF-SIMS, frozen-hydrated, stable isotopes

\* corresponding author:

Address:

Phytosphere Institute (ICG 3)

Forschungszentrum Jülich

Leo Brandt Straße

52425 Jülich, Germany

Phone: +49 (0) 2461-612652

Fax: +49 (0) 2461-612492

Email: [r.metzner@fz-juelich.de](mailto:r.metzner@fz-juelich.de)

## Abstract

Lateral exchange between xylem and surrounding tissues help to de-couple root uptake of water and nutrients from their utilization in all parts of a plant. We studied some aspects of the dynamics of lateral interactions between xylem vessels and surrounding stem tissues, using cryo-secondary ion mass spectrometry (cryo-SIMS) to map stable isotope tracers for water ( $\text{H}_2^{18}\text{O}$ ), magnesium ( $^{26}\text{Mg}$ ), potassium ( $^{41}\text{K}$ ) and calcium ( $^{44}\text{Ca}$ ) delivered to the transpiration stream of bean shoots (*Phaseolus vulgaris* cv. Fardenlosa Shiny) via a cut stem. At various times after tracers entered at the cut, a stem sample, 25 cm upstream was shock-frozen, and analysed below  $-130^\circ\text{C}$ .

The entering water equilibrated within minutes across the entire cross-section, and in contrast the nutrient tracers showed a very heterogeneous distribution between stem tissues, even after 4 h. Dynamics of nutrients in the tissues revealed a fast and extensive exchange of nutrients in the xylem parenchyma, with for example calcium being completely replaced by tracer in less than 5 min. The pith also showed fast exchange with the xylem vessels but only minor replacement while cambium and phloem showed very slow exchange. Potassium tracer fractions in the vessels showed that sap concentration was up-regulated for many hours during its 30 s movement through the stem. Some of the potassium needed for this up-regulation may have been re-circulated from the phloem.



## Introduction

The coordinated distribution of water and nutrients via xylem and phloem throughout the shoot is one of the major functions of the stem of higher plants. The demand for mineral nutrients and water in the tissues varies during their development and on a much faster time-scale, xylem flow is highly variable, depending on the environmental conditions. So, to prevent nutrient excess where transpiration is high (e.g. in leaves) and deficiency where it is low (e.g. apices), the nutrient fluxes must be regulated on a wide range of scales in both time and space. Since the xylem transport pathways are inert, a regulation of the nutrient flux must involve the living tissues surrounding the vessels via retrieval, storage and release of nutrients, as in buffering of carbohydrate flux (Thorpe *et al.*, 2005), although ion exchange processes in the cell walls may also play a role. Most research on these regulatory processes has focussed on xylem loading in roots (de Boer & Volkov, 2003, Köhler & Raschke, 2007), on leaf unloading (Canny, 1995a), and on re-circulation via the phloem (Jeschke & Hartung, 2000, Marschner, Kirkby & Engels, 1997), although stem tissues are likely to be important to supply nutrients to low-transpiring tissues e.g. by transfers from xylem to phloem (Dasilva & Shelp, 1990, McNeil, 1980, van Bel, 1990) or from xylem to xylem (Atkins, 1999). Further, the dynamic aspects of all these processes are clearly important in the context of environmental variability, but have gained rather little attention, yet.

This role of the stem tissues in nutrient regulation is difficult to study due to the high tensions in the conducting xylem vessels, their inaccessibility, and the likelihood of damage during any access. Microbeam techniques offer the spatial resolution and the possibility to image whole tissue areas and show vessel-tissue interactions, but sample preparation is critical, especially for diffusible species. The best method to preserve the distribution of analytes in the original sample is shock-freezing and analysis of frozen-hydrated sample (recently reviewed by McCully, Canny & Huang, 2009). Electron microprobes such as energy-dispersive x-ray analysis (EDXA) lack the sensitivity to detect most mineral nutrients at physiological concentrations in plant tissues (Enns, McCully & Canny, 1998, Rowan, McCully & Canny, 2000), but secondary ion mass spectrometry (SIMS) does have the required sensitivity (Metzner *et al.*, 2008), and in addition allows stable isotope tracers to be used. These tracers are preferable, in comparison with dyes and chemical analogues, as they have identical transport characteristics, even at highly selective barriers such as cellular membranes. Similarly, water potential equilibration

across a horizontal stem has been a byword of plant water relations, but there are few data to show equilibration within tissues.

The principles of SIMS and its application to frozen-hydrated plant tissues have been described elsewhere (Metzner *et al.*, 2008). A focussed, pulsed primary ion beam is scanned across a sample surface to sputter and ionize material, and these secondary ions are analyzed by a mass spectrometer. In a time-of-flight instrument, as used in this study, a complete mass spectrum for each pixel is recorded, so that several tracers can be used simultaneously. In stable isotope tracer experiments, nutrients fed to the organism can be deduced by their isotopic signature. Integrity of samples after preparation and analysis, as well as structural information for assigning tracers to tissues, can be shown by scanning electron microscopy of the frozen samples (cryo-SEM).

In this study we analyzed frozen-hydrated samples by cryo-SIMS in a multi-tracer approach to investigate the dynamic interaction of magnesium, potassium, calcium and water between xylem vessels and surrounding tissues in the stem of climbing bean. Stable isotope tracers can show ion dynamics in biological systems (e.g. Kuhn, Schroeder & Bauch, 2000, Schroeder & Fain, 1984), and here nutrient tracers ( $^{26}\text{Mg}$ ,  $^{41}\text{K}$  and  $^{44}\text{Ca}$ ) were applied to the transpiration stream of cut shoots at low physiological concentrations, together with water tracer for different periods of time, producing a series of snapshots of the tracer distribution in the stem. Heavy water ( $\text{D}_2\text{O} = {}^2\text{H}_2\text{O}$ ) has been used for MRI flow imaging in plants (Gussoni *et al.*, 2001, Link & Seelig, 1990) and in studies of transpiration (Meinzer *et al.*, 2006), but  $\text{H}_2^{18}\text{O}$ , with physical properties close to  $\text{H}_2\text{O}$ , has been used in ecophysiological and paleoclimatic studies (Barbour, 2007) is more suitable for SIMS detection (as discussed below). Nevertheless, because heavy water is not chemically identical to  $\text{H}_2\text{O}$ , we checked its suitability for tracing water.

Here we investigated lateral water and nutrient exchange dynamics, and xylem nutrient regulation in bean shoots by following tracer dynamics within a shoot cross-section in a time sequence after a step change in the transpiration stream's composition.

## Materials and Methods

### Plant material

Plants of climbing bean (*Phaseolus vulgaris* L. cv. Fardenlosa Shiny) were grown from seed in 1.7 l pots with standard soil substrate (ED 73, Einheitserde, Fröndenber, Germany) in a chamber with 12 h / 12 h light / dark cycle, illumination of  $300 \mu\text{mol m}^{-2} \text{s}^{-1}$  (PAR) by fluorescent lamps (15 × 36-W Fluora, Osram, Munich, Germany), temperatures between 19 °C and 22 °C, relative humidity between 55 and 70%, and automatic watering twice a day. During experiments plants, approximately four weeks old with at least three mature trifoliolate leaves, experienced the same conditions.

### Tracers and their application

Tracers were delivered to the shoot by first cutting the stem under tap water directly above the soil, and then rapidly transferring the cut end into a tracer solution, which was taken up by the transpiration stream until stem samples were excised after 5, 10, 20 or 240 min. The transpiration rate of uncut control plants was determined by weight loss, with their pots wrapped in plastic foil.

A tracer solution consisting of 2.5 mM each of  $^{26}\text{MgCl}_2$ ,  $^{41}\text{KCl}$ ,  $^{44}\text{CaCl}_2$ ,  $\text{NaNO}_3$  was applied, and for water tracing it had 50 %  $\text{H}_2^{18}\text{O}$  and 50 % deionised water for 5, 10 and 20 min experiments. In one 20 min experiment,  $\text{D}_2\text{O}$  (enriched to 99.9 % D, according to manufacturer, in comparison to the tabulated natural abundance of 0.02 %: Böhlke *et al.*, 2005) replaced the deionised water, giving 49.8% isotopic abundance for  $\text{D}_2\text{O}$ . For the 240 minutes experiments no water tracer was used.  $^{26}\text{MgCl}_2$  and  $^{44}\text{CaCl}_2$  were purchased from Medgenix (Düsseldorf, Germany),  $^{41}\text{KCl}$  and  $\text{H}_2^{18}\text{O}$  from Isoflex (Moscow, Russia),  $\text{D}_2\text{O}$  from ENSI, Argentina and  $\text{NaNO}_3$  from Sigma-Aldrich (Steinheim, Germany).

### Sampling of frozen-hydrated tissue

Frozen-hydrated tissue samples from the bean shoots were prepared as described in detail elsewhere (Metzner *et al.*, 2008). In short, ca. 4-cm-long samples from the first internode above the primary leaves were excised, rapidly mounted in copper rivets, and shock-frozen by plunging into melting propane (-189 °C) less than 30 s after excision. Throughout all subsequent preparation and measurement steps the ambient temperature was kept below -130 °C. Frozen samples were trimmed and their cross-sectional surfaces planed under vacuum, prior to analyses, with the aid of a cryo-microtome (MED 020/GBE with BU

012092-T and VCT-100, BAL-TEC, Witten, Germany), and subsequently transferred via the VCT-100 cryo-shuttle through airlock systems to the cryo- SIMS and cryo-SEM.

## Cryo-SIMS measurements

Isotopes were imaging in the surface of frozen-hydrated samples using a ToF-SIMS IV mass spectrometer (IONTOF, Münster, Germany), with an airlock system and cryostage (described fully in Metzner *et al.*, 2008). A complete secondary-ion mass spectrum was recorded for each pulse and pixel. Two types of image were acquired during the 6-8 h measurement necessary for each sample: (1) Overview images ( $500 \times 500 \mu\text{m}^2$  e.g. Figs. 2A, B and 3D-L), with mass resolution  $m/\Delta m$  of 3500 at mass 41 and lateral resolution of ca.  $7 \mu\text{m}$ . (2) High-spatial resolution images ( $<150 \times 150 \mu\text{m}^2$  e.g. Fig. 5B and C) at a spatial resolution better than  $1 \mu\text{m}$ , but at nominal mass resolution. These latter images were suitable only for potassium (mass interferences  $<20\%$  for  $^{41}\text{K}^+$  signal and negligible for  $^{39}\text{K}^+$ ), and for water (mass interferences for  $\text{H}_3\text{O}^+$  and  $\text{H}_3^{18}\text{O}^+$   $<1.5\%$ ). For imaging of the molecules taken to reflect water, it is possible that the ions detected as  $\text{H}_3\text{O}^+$  were made up out of atoms originating from larger molecules, such as cellulose, rather than ions from the ice. Nevertheless, this contribution from molecular fragments is probably negligible, firstly because the significantly stronger binding forces in such molecules would inhibit the production of ionised fragments compared to the production from ice, and secondly because water is usually by far the dominant material.

Images were computed from the recorded mass spectra as ion counts per pixel in a selected mass window. A “Poisson correction” (Stephan, Zehnpfenning & Benninghoven, 1994) was applied because multiple events could have occurred within the detection interval, the resulting value was denoted as “signal” ( $S$ ), in counts per pixel.

The signal  $S$  is related to the local concentration of the analyte, but the immediate atomic vicinity of the atoms or molecules of the analyte, the so called matrix can strongly affect signal generation (Vickerman & Briggs, 2001), and biological tissues have a particularly inhomogeneous matrix. The local topography of the sample surface also affects the signal. These two factors of matrix and topography could cause the signal to vary strongly with position to an unknown amount without any variation in isotope concentration. The topography problem can be reduced by cryo-planing the sample surface (Metzner *et al.*, 2008). However the abundance  $A_E$  of the tracer isotope of nutrient element

or water molecule  $E$  is a faithful measure, since the influence of the local matrix and topography on signal generation is the same for all isotopes and cancels in equation 1:

$$A_E := \left( \frac{S^t}{\sum_I S^I} \right)_E \quad (\text{equation 1})$$

where  $S^I$  is the pixel signal from each isotope  $I$  of the element, and  $I = t$  for the tracer isotope representing the element. In cases  $A_E$  was calculated for specific regions of interest (ROI: Fig. 4B-E), as defined with software IonImage (IONTOF, Münster, Germany) using anatomical information from the cryo-SEM,  $S^t$  and  $S^I$  was calculated on an ROI, not pixel basis.

Although the applied solution was highly enriched in the stable tracer isotopes, it did contain the other isotopes, and some tracer isotopes were originally present in the plant tissue. Therefore  $F_E$  was calculated, the fraction of element or molecule  $E$  originating from the tracer solution, on the basis of the abundance of the tracer isotope in the pixel ( $A_E$ ), in relation to the tracer isotope abundance of the nutrient solution ( $A_{nE}$ ), but in each case corrected by the natural abundance of the tracer isotope ( $A_{0E}$  from Böhlke *et al.*, 2005):

$$F_E := \frac{A_E - A_{0E}}{A_{nE} - A_{0E}} \quad (\text{equation 2})$$

A threshold for  $\sum S^I$  was chosen, below which  $F_E$  was set to zero in order to mask noise. The chosen threshold per pixel was 1 % of the image maximum.

## Correlating two cryo-SIMS images

For comparing signal distributions in two images, we plotted for each pixel at coordinates  $x, y$  signal ( $S$ ) of picture 1 at the abscissa and of picture 2 at the ordinate. In this plot, the 65,000 points ( $256 \times 256$  pixels) could not be resolved and so they are illustrated in a greyscale image. Identical pictures would give a straight line of slope 1 and their similarity can be quantified by linear regression and correlation analysis.

## Inferring concentration from isotope dilution

The isotopic abundance ( $A_X$ ) of the tracers in a vessel sampled some 25 cm from the cut where tracer solution entered was always lower than that in the applied nutrient tracer solution ( $A_N$ ). If the reduction was caused by radial inflow, from the adjacent tissues, of element with a different isotopic abundance ( $A_T$ ), then the element's concentration ( $c_X$ ) in the sampled vessel can be calculated from the input concentration ( $c_N$ ), using a standard method for elemental analysis from mass spectrometry, "isotope dilution". The unknown sample is spiked by an aliquot with a different isotopic abundance of the analyte (Ingram & Hayden, 1954) and the analyte is quantified by determining the shift in isotopic abundance. The method depends on the fact that if samples with mass  $c_N$ ,  $c_T$ , are mixed to give mass  $c_X (=c_N+c_T)$ , and if they have isotopic abundances for one isotope  $A_N$ ,  $A_X$  and  $A_T$  in the corresponding samples, then mass conservation requires that

$$c_X = c_N \frac{(A_N - A_T)}{(A_X - A_T)} \quad (\text{equation 3})$$

Thus the sap concentration can be calculated from eq (3), provided there is no change in volume. For a derivation of equation 3 see supplementary material.

### Exchangeable fraction of element

In the steady state for isotopic exchange of an element ( $E$ ) between the xylem vessels and a region of the tissue for the unbound element in that region the element's isotopic abundance will be equal to its abundance in the applied solution, whereas non-exchangeable element will remain at natural abundance. Thus if element  $E$  in xylem sap has abundance  $A_{xE}$ , but in the tissue there is some chemical or physical sequestration and the exchangeable fraction of element is  $e_{tE}$ , then the tracer abundance for the entire tissue ( $A_{tE}$ ) is

$$A_{tE} = e_{tE} A_{xE} + (1 - e_{tE}) A_{0E} \quad (\text{equation 4})$$

and from equation 2,

$$e_{tE} = F_{tE} / F_{xE} \quad (\text{equation 5})$$

### Limits of detection for stable isotope tracers with cryo-SIMS

The detection limits for stable isotope tracers depend on the precision and standard deviation of the isotopic abundance measurements. To determine this limitation for our instrumental setup we analyzed frozen hydrated drops of water and air dried spots of half-strength Hoagland solution with natural isotopic abundance on clean silicon substrate (Table I). Taking the standard deviation from Table I it can be seen that H<sub>2</sub><sup>18</sup>O tracer can be detected if the sample abundance exceeds the natural abundance by about 0.02%, <sup>26</sup>Mg tracer by 2.4 %, <sup>41</sup>K tracer by 1.0 % and <sup>44</sup>Ca tracer by 0.2 %. Detection sensitivity depends primarily on the statistical variability where tracer counts are small, especially for single pixels.

### **Cryo-SEM**

The surfaces of frozen-hydrated samples were imaged with a LEO Gemini VP 1550 scanning electron microscope (Zeiss, Oberkochen, Germany) with a cold field emission electron source (full details in Metzner *et al.*, 2008). After SIMS analysis, the sample surface was freeze-etched before imaging, to show the structure by transiently warming the sample stage to -90°C. SEM images were optimized for printing using levels and curves settings in Adobe Photoshop.

### **Collection and analysis of xylem sap**

Whole internodes were excised and cut into pieces ca. 5 cm long. Each of these was placed in a 15ml plastic centrifugation tube upright on a PTFE sieve positioned 1cm above the end of the tube, and centrifuged for 5 min at 1560 g. Sap collected below the sieve was weighed, and analyzed for cations by ion chromatography on an ICS-3000 (Dionex, Germering, Germany) equipped with conductivity- and subsequent UV-detector AD 25 and an IonPac CG16/CS16 chromatography column at 40°C.

## Results

We studied the dynamics of both nutrient and water movement in the xylem vessels, and their spreading into surrounding tissues, using stable isotope tracers for water ( $\text{H}_2^{18}\text{O}$ ), magnesium ( $^{26}\text{Mg}$ ), potassium ( $^{41}\text{K}$ ) and calcium ( $^{44}\text{Ca}$ ). In some experiments, heavy water ( $\text{D}_2\text{O}$ ) was used as well as the  $\text{H}_2^{18}\text{O}$ , to test the suitability of heavy water as a tracer at this spatial scale. After continuous uptake of tracer solution via the cut stem for 5, 10, 20 or 240 min, samples were excised from the first internode above the primary leaves, immediately shock frozen, and maintained below  $-130^\circ\text{C}$  until all analyses were complete. The tissue structure was well preserved as shown in the freeze-etched samples (Fig. 1). At this magnification the tissues used for this report showed no sign of damage due to ice crystal growth or stresses from differential contraction.

The uptake rate,  $0.1 \text{ ml min}^{-1}$ , resembled the transpiration rate of uncut control plants. To estimate the volume of xylem vessels in the 25 cm of stem between application and sampling site xylem sap from control plants was gathered by centrifugation. This gave a volume of  $46.1 \mu\text{l} \pm 18.8 \mu\text{l}$  ( $n=7$ ), so on average the sap would have been replaced 2.2 times per minute if all solution speeds were the same.

### SIMS signals for both water tracers showed virtually identical images

The major secondary ion used to map water with cryo-SIMS was  $\text{H}_3\text{O}^+$  and to map the  $^{18}\text{O}$  containing water tracer,  $\text{H}_3^{18}\text{O}^+$  was used. The images of water,  $\text{H}_3\text{O}^+$  (Fig. 2A), and of tracer,  $\text{H}_3^{18}\text{O}^+$  (Fig. 2B), appeared to be identical, apart from a numerical factor in the signal: clearly tracer had moved throughout the tissue at this sampling time (20 min). This similarity of water and  $\text{H}_2^{18}\text{O}$  distribution (Fig. 2A and B) was quantified in a scatter plot for the correlation of the intensities of each image (Fig. 2C). The correlation,  $r = 0.98$ , confirmed that the spatial distribution of water and  $\text{H}_2^{18}\text{O}$ -tracer were indeed almost identical. Where  $\text{D}_2\text{O}$  was supplied as well, the scatter plot (Fig. 2D) showed more scatter and a slightly reduced correlation of water and  $\text{H}_2^{18}\text{O}$  ( $r = 0.96$ ). The distribution of  $\text{D}_2\text{O}$  was also highly correlated to water in this double labelling experiment ( $r = 0.98$ : Fig. 2E).



## Water and nutrients show contrasting distributions and dynamics

The fractions  $F$  for each element which derived from the applied tracer solution for samples taken after 5, 10 or 20 min of tracer application (Fig. 3D-L) differed between stem tissues. Magnesium images were very similar to potassium and are therefore not shown in figure 3, but the replicated data for all three nutrients are summarized in figure 4.

Within 5 min, all tracers had arrived at the sampling site (Fig. 3D, G, J) and started to spread into surrounding tissues, but water and nutrients showed completely different dynamics. The fraction of water from the tracer solution was uniform throughout the cross-section at all times (Fig. 3D-E and 4B), except for slightly smaller fractions within the thick walled xylem parenchyma (Fig. 5B). This water fraction was uniform throughout the cross-section and increasing continuously, but reached only 60% after 20 min (Fig. 4B), when there had already been a 44 fold replacement of xylem sap. In contrast to the uniform distribution of the water tracer fraction, nutrients showed large differences between tissues. There was a difference between xylem vessels and the surrounding thick-walled xylem parenchyma, and differences again between them and cambium, phloem and pith (Fig. 3G-L). At 5 min, the sheath enclosing the conducting xylem vessels was the only tissue area with notable tracer fractions (Fig. 3G, J). At 10 and 20 min, this region of high tracer fraction had spread to the bulk of the thick-walled xylem parenchyma for potassium and calcium (see Fig. 3H, I, K, L). Tracer fractions in the cambium and phloem, as well as in the pith, remained low at all times.

Calculated nutrient tracer fractions for areas selected from anatomical criteria (Fig. 4) were always highest for the xylem vessel lumina where, unlike water, the fractions did not increase with time, but reached maxima at 10 min (Fig. 4C-E). From these maxima, fractions declined to lower levels at 20 min, and were similar at 240 min (Figs. 4C-E). Despite similar dynamics, magnitudes were quite different for different elements. At the 10 min peak, for example, magnesium, potassium and calcium were 88, 41 and 72 %, and the values at 20 min were with 77, 26 and 50 % not significantly different from those at 240 min (71, 24 and 64 %: Fig. 4C-E). Comparing fractions in the xylem vessels and the xylem parenchyma, calcium was equal at most times, but both potassium and magnesium showed strong differences. Calcium tracer fractions were equal at 5 min in the sub-regions within the xylem parenchyma forming the axial sheath around the xylem vessels (XP-pi and XP-cm; Fig. 4E) and the vessels themselves. In the bulk of the xylem parenchyma situated between the xylem vessels (XP-xv), fractions tended to be lower until 10 min, but

increased continuously, approaching the values in the sheath after 20 min, whereas in the sheath itself it followed the dynamics of the xylem sap closely. The only exception was at 10 min, when the values in the xylem vessels were largest, and lower in the axial sheath. Fractions of both potassium and magnesium were always much lower in the xylem parenchyma than in the vessel lumina, although the elements showed different kinetics. For example, the potassium fraction  $F_K$  in the xylem parenchyma reached a stable situation at 5 min. Fractions of magnesium, in contrast, reached stable values after 10 min (XP-pi) to 20 min (XP-cm and XP-xv). Potassium fractions in all xylem parenchyma, XP, were below half of the vessel values, while magnesium reached more than two-thirds of the fractions in the vessels.

In the pith, tracer fractions for K and Ca were small (at around 2% and 5% respectively: Fig. 5D and E) and changed very little after 5 min, while magnesium was also stable after 20 min but the fraction was much higher (ca. 33 %).

In both cambium and phloem, nutrients dynamics were quite different from other tissues, with all nutrient fractions increasing steadily (somewhat like the water tracer). Fractions of all nutrient tracers were very small after 5 to 20 min ( $F_{Mg} < 10\%$ ,  $F_{Ca} < 15\%$  and  $F_K < 2.5\%$ ) but after 240 min they were much larger with  $F_{Ca}$  in the cambium almost equal to the neighbouring XP-cm.

## **Distribution of water and potassium at subcellular spatial resolution**

Tracer distribution at a higher spatial resolution, better than  $1\mu\text{m}$ , in selected metaxylem bundles (e.g. 20 min sample, Fig. 3), allowed cell wall and symplast to be distinguished for potassium (with an uncertainty due to mass interferences of 20%: Metzner *et al.*, 2008) and water tracer ( $\text{H}_3^{18}\text{O}$ , uncertainty 1.5 % of signal). Calcium and magnesium data had unacceptable mass interferences to be useful. For the water tracer fraction (Fig. 5B), the lumina of all cells had similar values, including the vessels themselves, but values were obviously lower in the (lignified) walls of the thick-walled xylem parenchyma. In contrast, the potassium tracer fraction in the cell lumina (Fig. 5C) was much higher for the vessels than for other cells; and in each cell, the lumina values were lower than for the wall, even for those vessels, to which tracer solution had been supplied at the stem excision.

## Quantification of xylem vessel content

At the sampling site isotope tracer fractions of nutrients in the xylem vessels at the sampling site were always well below 100% (Fig. 4), suggesting that nutrient ions—at their natural isotopic abundance—were continually entering vessels from surrounding tissue, hence up-regulating nutrient concentrations, and reducing abundance. Indeed, centrifugation-extracted xylem sap from plants perfused for 20 min with nutrient solution had potassium concentrations that were much higher than the applied solution, calcium was also higher, while magnesium was a little lower and close to concentrations found in the sap of control plants (uncut; Table II). It is likely that the high potassium concentration in the centrifugation-extracted sap was partly caused by contamination from the cuts. In one case where stable isotope tracers were applied, and the extracted sap concentration was similar to the other extract samples, the isotopic abundance for potassium,  $A_K = 12.8\%$  was much lower than the abundances typically found in the xylem vessel lumina of frozen hydrated samples (29.3% after 20 min of tracer application), suggesting contamination of the extracted sap by potassium with natural isotopic abundance ( $A_K = 6.7\%$ ).

Concentrations calculated from isotopic abundances in the vessels at the sampling site after 20 min tracer application (equation 3), were higher than the applied solution (Table II). Compared to the measured concentrations, the estimates for both Mg and Ca were a little higher, whereas potassium at  $9.8 \text{ mmol l}^{-1}$  was significantly below the measured value  $16.5 \text{ mmol l}^{-1}$  (Table II).

For comparison of nutrient pools we estimated the total amount of potassium in the perfused part of the stem, assuming that 90 % of the stem volume consisted of symplast, with a concentration of about  $100 \text{ mmol l}^{-1}$  (Leigh, 2001), giving a total potassium content of 0.08 mmoles.

## Discussion

New spatial information about the transport dynamics of water and several nutrients in the stem of bean was obtained by using stable isotope tracers and the newly established cryo-SIMS methodology (Metzner et al. 2008). Nutrient solution was applied to cut bean stems, thereby generating a sudden step in the composition of the transpiration stream, allowing us to observe the consequent responses in nutrients and water in the stem after 5 to 240 min of solution uptake. In the nutrient solution, potassium concentration was a factor of eight lower than in natural sap, calcium was lower by a factor of 1.5, and magnesium near the natural level (Table II). In this solution all three nutrient cations, and the water itself, were replaced by enriched stable isotopes of naturally low abundance, so that their location in the cryo-samples could be detected (Fig. 2A, B). Since we could not assume that SIMS images were quantitative, due to heterogeneity in the chemical environment where secondary ions are sputtered from the sample (Metzner *et al.*, 2008), our interpretation of tracer movement was based largely on  $F_E$ , the fraction of atoms of element  $E$  originating from the applied tracer solution (see Methods, equation 2). Thus  $F$  depends on both new and original material; a high value of  $F$  can be either due to high concentrations of tracer, or low concentrations of the native element.

The tracer fractions  $F_E$  in xylem content were measured some 25 cm from the application site, and therefore depend on interactions of the transpiration stream with surrounding tissues all along the stem between application and sampling sites. Without any such exchange,  $F_E$  in the vessels would quickly reach 100 %. Within stem tissues, the value of  $F_E$  depends (1) on the value in the xylem vessels, since this was the source for radial spreading, but also (2) on the exchange process between the vessels and tissues, and (3) the fraction of exchangeable material in the tissue. Tracer solution was continuously supplied to the transpiration stream; therefore  $F_E$  in the vessels can be considered to be a stable source for radial spreading once the original sap was continuously replaced by the tracer solution in the xylem conduits. The time until equilibrium is reached for a specific tissue depends on the exchange rate with the vessels and on the amount of natural element present in the tissue, since slow exchange and large amounts of natural material will extend the time to reach equilibrium. At equilibrium (when  $F_E$  values are steady with time) the value of  $F_E$  at any site depends on the fraction of material that can exchange with material in xylem vessels. In this equilibrium state the exchangeable (unbound) fraction of material in the tissue and the source (i.e. xylem vessels) will have equal isotopic abundance. Non-

exchangeable material remains at natural abundance. Therefore we calculated the exchangeable fraction in each tissue ( $e_E$ ), using the tracer fraction in the vessels and the fractions in the tissue (equation 5). The size of the exchangeable fraction can be limited by physical isolation (e.g. enclosed in vacuoles) or by chemical binding of the element in the tissue (e.g. to pectins in cells walls). Before equilibrium,  $e_E$  gives the currently exchanged fraction of the element. Apart from characterizing the dynamics of nutrient and water movement in the vessels and tissues, we also took the opportunity to compare the properties of  $^2\text{H}$  (D, deuterium) and  $^{18}\text{O}$  labelled water.

### **$\text{D}_2\text{O}$ and $\text{H}_2^{18}\text{O}$ are both good tracers for water**

High concentrations of  $\text{D}_2\text{O}$  (>25%) affect plant membrane ultrastructure (Waber, 1984) and hence membrane transport (Sacchi & Cocucci, 1992, Waber, 1984). Nevertheless, our data using medium  $\text{D}_2\text{O}$  enrichment (>40 %) showed that both  $\text{H}_2^{18}\text{O}$  and  $\text{D}_2\text{O}$  are suitable as tracers for water in plant tissues, neither showing a significant difference from water (Fig. 2C and E). The substitution of  $^{18}\text{O}$  for  $^{16}\text{O}$  is a minor perturbation to the molecule (Hart *et al.*, 2005), and so  $\text{H}_2^{18}\text{O}$  should be a good tracer for water. Indeed, ordinary water and  $^{18}\text{O}$ -enriched water images (Fig. 2A and B), were very closely correlated ( $r = 0.98$ ; Fig. 2C), demonstrating the similarity of labelled and unlabelled water movement. This similarity also suggests a high permeability for radial water movement of all tissues. Additionally, if  $\text{D}_2\text{O}$  were to have affected water transport, then the relationship between  $\text{H}_2^{18}\text{O}$  and  $\text{H}_2\text{O}$  should have been affected by the presence of  $\text{D}_2\text{O}$ . This relationship was hardly affected (compare Fig. 2 C and D), displaying a similar correlation ( $r = 0.96$ ) in the presence of  $\text{D}_2\text{O}$ . We conclude that the influence of  $\text{D}_2\text{O}$  on water permeability is negligible, for the amount we used (40 – 50 %), certainly in comparison with the enormous variations in permeability for the nutrient tracers. Furthermore, the distribution of  $\text{D}_2\text{O}$  also showed a close correlation with  $\text{H}_2\text{O}$  ( $r = 0.98$ ; Fig. 2E), demonstrating that dilute  $\text{D}_2\text{O}$  is also a good and inexpensive tracer for water. Isotope effects are well known to occur, in diffusion, evaporation, exchange with organic molecules and enzymatically catalyzed reactions, and they are informative for ecophysiological and paleoclimatic studies (Barbour, 2007), but they are negligible at the sensitivity of our measurements. We conclude therefore that  $\text{H}_2^{18}\text{O}$  and  $\text{D}_2\text{O}$  are equally acceptable as tracers for water within the limits of the temporal and spatial resolution in our experiments. Nevertheless, it is not advisable to use  $\text{D}_2\text{O}$  as a tracer for water in cryo-SIMS measurements when other isotope

tracers are also of interest, due to the large number of combinations of H and D in water clusters  $(\text{H}_2\text{O})_n\text{H}^+$  that dominate the mass spectrum of secondary ions, with high probability of a mass near another tracer. It is therefore preferable to use  $\text{H}_2^{18}\text{O}$  and avoid such interfering peaks in the mass spectrum.

### **Radial water equilibrium is very fast in the stem**

Fast and unhindered radial exchange of water throughout the cross section of the bean stem was shown by our data: the fraction of water originating from the tracer solution ( $F_{\text{H}_3\text{O}}$ ), was similar in all tissues to that in the conducting vessels, even at the first sampling time of 5 min (Fig. 4B). The fraction of exchangeable water in the stem tissues ( $e_{\text{H}_3\text{O}}$ ) was therefore 100% (see equation 5). An exception was xylem parenchyma where the  $\text{H}_3^{18}\text{O}$  fraction was 10 % to 15 % lower than in other tissues, even after 20 min (Fig. 3E and F), despite the proximity to vessels. High spatial resolution images of this region showed that the lower tracer fraction occurred only in cell walls of the thick-walled xylem parenchyma (Fig. 5B). This finding suggests that less water from the vessels penetrated this dense material, and followed a cell-to-cell pathway, similar to that in leaves (Ye, Holbrook & Zwieniecki, 2008) and some roots (Bramley *et al.*, 2009).

Lateral water movement through tissues has been studied in roots (Steudle & Peterson, 1998), leaves (Canny, 1995b, Fricke, 2000, Maurel *et al.*, 2008), and in studies of water storage in tree stems (Gartner, 1995). The movement can be in cell walls (apoplastic), within the cytoplasm and plasmodesmata (symplastic) and from cell to cell via crossing of the plasmamembrane (transcellular). Each of these pathways has its different permeabilities and mechanisms of regulation (Steudle & Peterson, 1998; Wegner & Zimmermann, 2009). Concerning the apoplast, permeability is generally considered to be high, giving rapid radial equilibration of plant water potential (Nobel, 1999) except where there are barriers in specialized tissue such as the root endodermis (Steudle, 1997), and our data certainly support this view for the stem, showing no sign of an isolated compartment. Since labelling was almost uniform, including cell walls (Figs. 3D-F and 5B), we conclude that the diffusivity of water was high everywhere, and the different pathways were indistinguishable in our system, other than, possibly, in the xylem parenchyma. Such equilibration is normally taken for granted in formulations of plant water relations (Nobel, 1999, Steudle, 1989), and is obvious in MRI where diffusivity appears to be high (Gussoni *et al.*, 2001, Van der Weerd *et al.*, 2002). We could image

water tracer with a spatial resolution that could distinguish water movement in the symplast and vacuoles of plasma-rich cells (Fig. 5B) (unlikely with other techniques: Steudle *et al.*, 1998), demonstrating that this equilibration occurs on a finer scale than has been observed previously.

The slow increase of water label in the xylem vessels (Fig. 4B) is an expected consequence of rapid radial equilibration of tracer (seen in stem sections) between the sites of tracer entry and sampling. Other measurements using isotopic tracers led to the same conclusion (e.g. Meinzer *et al.*, 2006, Ohya *et al.*, 2008). Fast radial equilibration of water was even observed in species like sugarcane (Bull, Gayler & Glasziou, 1972) where solute diffusion is restricted (Walsh, Sky & Brown, 2005). Of course, this has to be recognized if tracers are used to measure water flow in plants (Link *et al.*, 1990, Waring & Roberts, 1979), either by duration long enough to guarantee for a steady state, or by suitable analysis of the transient state.

## Regulation of xylem nutrients

The nutrient concentrations in the tracer solution were lower than in the xylem sap of control plants, and we found good evidence for regulation of the solution as it passed through the vessels. We quantified these effects of the stem on the composition of xylem sap from the change in tracer fractions at the sampling site, during passage of the xylem vessels. An influx of nutrients with a lower isotopic abundance than the tracer solution would lead to a reduction in tracer fractions at the sampling level. All nutrient tracer fractions were below 100 % in all our experiments, even after 4 h. Three lines of evidence suggested that these lowered fractions are mainly the result of release of nutrients from intracellular storage:

- 1) Although diffusive exchange with the apoplast (i.e. xylem vessel walls and stem tissues) would have lowered nutrient fractions initially, the dynamics of fractions in the xylem vessels could not have come from diffusive exchange alone. Since the tracer solution was supplied continuously, isotopic abundances of the apoplastic nutrients would converge towards that of the tracer solution, and the tracer fractions in xylem vessels at the sampling site would converge towards 100 % with time. In contrast, all nutrient tracer fractions initially rose to maxima at about 10 min, but then over the next 10 min declined to lower levels, that persisted over at least 4 h (Fig. 4C-E). This persisting low tracer fractions show that there was a continuing and steady influx of unlabelled nutrients for at

least 4 h. A constant influx can only be explained by a controlled and continuous release from intracellular storage that began after a delay of about 10 min. The initial increase to the maxima at 10 min, occurred in the same timescale as the response in the water tracer, suggesting that both were caused by diffusive exchange. The 10 min time delay would be a combination of the transit time for ions to move from regions of stem storage into xylem vessels, and the response time for inducing a change in release processes. Such a response time is reasonable for post-translational adjustments in enzyme activity.

2) Continuing flux cannot be provided without release from symplastic sources. The isotopic dilution of tracer during movement of the transpiration stream was most dramatic for potassium, with a vessel tracer fraction  $F_K$  of only 25%, implying that there was an increase of potassium concentration, from the  $2.5 \text{ mmol l}^{-1}$  of the input solution to  $9.8 \text{ mmol l}^{-1}$  at the sampling site (Table II). If the sources of the influx were labelled to the extent observed in the xylem parenchyma the inferred concentration is higher,  $15.0 \text{ mmol l}^{-1}$ . The lateral nutrient input necessary for the upregulation of concentration, from  $2.5 \text{ mmol l}^{-1}$  to  $9.8 \text{ mmol l}^{-1}$  during 20 min, was a considerable fraction of stem potassium and during 240 min the amount of potassium entering the sap (0.09 mmoles) was similar to the total content of the perfused stem (0.08 mmoles), mostly symplastic and therefore under metabolic control. Thus if intracellular potassium homeostasis occurred (Leigh, 2001), most potassium delivered to the xylem must have been replaced by phloem transport from distal regions of the shoot, i.e. by nutrient cycling.

3) Sap extracted from plants supplied with nutrient solution showed an increase in potassium concentration. Sap, extracted after 20 min application of solution showed a concentration even larger than the above estimates (Table II:  $16.5 \text{ mmol l}^{-1}$ ). The discrepancy from  $9.8 \text{ mmol l}^{-1}$  calculated from isotope dilution was probably due to symplastic contamination. Such contamination was implicated in a 20 min replicate that was analysed by cryo-SIMS, because the extracted sap had a very low isotopic abundance ( $A_{41K}$  of 12.8% compared to the 29.3% for the xylem vessel lumina after 20 min: Fig. 4D). This difference in abundances suggests that the extracted sap was contaminated by an equal amount of potassium to that entering before the extraction, but even the uncontaminated concentration would still be significantly higher than the input solution (Table II).

Release of potassium is likely to be mediated by potassium channels, such as the Shaker-type channels in root xylem parenchyma thought to be responsible for the loading of potassium into root xylem (Maathuis, 2007, Wegner & De Boer, 1997).



When Gilmer and Schurr (2007) perfused xylem of an *isolated* length of *Ricinus* (i.e. with no phloem connections from a shoot), there was little up-regulation with input solutions containing potassium below  $7 \text{ mmol l}^{-1}$ , consistent with the need for a potassium supply from good phloem connections if up-regulation of xylem potassium is to be possible. Interestingly, if their input concentration was above  $7 \text{ mmol l}^{-1}$ , there was down-regulation, which need not be hampered by lack of phloem connections if the stem tissues could sequester the excess potassium. The need for phloem connections in regulating xylem characteristics was also shown where phloem-borne potassium was found to regulate xylem conductivity in branches of maple (Zwieniecki *et al.*, 2004).

In comparison with potassium in the vessels, magnesium had a much higher peak in tracer fraction, of almost undiluted tracer (90 %), declining a little to a steady value of about 70%. Calcium also rose initially to high levels of around 70% and did not decline significantly from those values. The smaller change for magnesium and calcium in the transpiration stream during its passage through the stem corresponds to the more moderate treatment (Ca concentration was changed to 0.7 of its natural value, Mg to 1.7) than for potassium (0.1). The tracer fraction of both magnesium ( $F_{\text{Mg}}$ , 77 %) and calcium ( $F_{\text{Ca}}$ , 50 %) implied some up-regulation of the input solution, but the measured concentration were not significantly different from the applied solution for magnesium and only slightly higher for calcium (Table II). This observation of fractions remaining below 100 % but without apparent change from the concentration of the input solution may reflect isotopic exchange of magnesium and calcium with the surrounding tissues during passage of the xylem vessels. If for calcium there was influx of natural nutrient from stem tissues it must have been from unlabelled tissues, since concentrations calculated for an influx from labelled xylem parenchyma are highly unrealistic (Table II). Nevertheless the decline in tracer fractions and the steady fractions after 20 minutes point to the stem symplast as the source for unlabelled nutrient. Contamination of the sampled sap was significant for potassium (as discussed above), but may not have been so significant for magnesium and calcium, due both to their lower intracellular concentration and to stronger binding. In conclusion an up-regulation of the nutrient concentration in the xylem vessels by the stem tissues, possibly as a part of a nutrient homeostasis, appears very likely (at least for potassium) and emphasizes the importance of an interaction between transpiration stream and stem tissues for regulating nutrient fluxes within the shoot. Although data for a wider

range of treatments is needed to confirm that this observed increase in xylem concentration was indeed an example for regulation, these initial results are consistent with regulation.

### **Stem tissues for nutrient exchange and storage**

Nutrient fractions in the stem tissues reflect the integral of all exchange up to the time of sampling, whereas the xylem vessel content shows the results of exchange during about 30 s only, the average time for sap in the stem to be replaced. Consequently nutrient fractions in the tissues will be much less variable than in the vessels, unless all exchanges are extremely fast, such as we saw for water. The dynamics of the nutrient tracers in different tissues depend on the rates and amounts of nutrients for storage, and so the tracer dynamics can indicate likely storage properties for the different tissues.

The axial sheath of xylem parenchyma around the vessels reached a steady state quite quickly (Mg, K, Ca within 10, 5, 5 min). The apoplast would not contain enough material to give the very high exchangeable fractions we saw for these elements (66 %, 39 %, 94 % rising to 100 % at 20 min), since their location is mostly intracellular (i.e. Mg and K) or at least not purely apoplastic (i.e. Ca; Marschner, 1995). Therefore we must conclude that much of the symplastic pool of these nutrients in the axial sheath was exchangeable.

The exchange of more than half of the tissue magnesium within 10 min was surprising, since free cytosolic magnesium has a low concentration ( $0.4 \text{ mmol l}^{-1}$ ; (Yazaki *et al.*, 1988). Large amounts are bound to ATP, and it is high in the xylem parenchyma (van Bel, 1990), and so this bound magnesium is apparently quite mobile.

For potassium the high mobility was less surprising, since it is largely in an ionic form in all regions (Marschner, 1995). Equilibration was reached for the bulk of the xylem parenchyma just as quickly as in the axial sheath (Fig. 4C-E), suggesting that the whole xylem parenchyma may have been engaged in the regulation of axial nutrient flow with a response time of minutes.

Exchange of calcium between vessels and xylem parenchyma was even more intense than for potassium, with its fractions closely following the dynamics of the xylem vessels (Fig. 4E). This implies that all calcium in the xylem parenchyma was exchanged against tracer calcium within less than 5 min, rather like water, except at 10 min when fractions in the vessels increased so fast that fractions in the tissues were not equilibrated. This very fast and complete exchange is remarkable, since calcium in the cell walls would

be limited by their high binding capacity (Marschner, 1995), and calcium in the cell lumina is mainly sequestered in the vacuole and organelles, or chemically bound (White, Banfield & Diaz, 1992). In explanation, perhaps the trauma such as a turgor shock associated with cutting the stem may have caused opening of calcium channels (well known to respond to trauma; White *et al.*, 1992) to give a high turnover between apoplastic and symplastic pools.

Nutrients in the pith, despite its distance from the vessels, showed similarly fast equilibration times to the axial sheath (K and Ca: 5 min; Table III). Magnesium took longer to reach equilibrium (10 min), but the exchangeable fractions were much larger than for potassium and calcium. The short times indicate a fast exchange of all these elements with the xylem vessels. Magnesium showed a much larger exchangeable fractions (43 % compared to 8 - 9 % for Ca and K), but the high fraction probably reflects a larger amounts of potassium and calcium in the pith cells (as reported by Metzner *et al.*, 2009) All three nutrients exchanged between xylem vessels and pith quite rapidly, making it a possible tissue to play a role in fast (minutes) regulation of axial nutrient flux.

The phloem and cambium, in contrast to xylem parenchyma and pith, showed no tracer in a steady state within 20 min of tracer application. But the large fractions exchanged by 240 min (ranging from 16 % - 76 %: Table III) showed that significant fractions of these nutrients were exchangeable. The observation that exchangeable fractions prior to 20 min were low (0.7 % - 8 %) shows that exchange with the xylem vessels was slow, and not that large fractions were immobile.

## Conclusions

Characterization of the dynamics of the exchange of water, magnesium, potassium and calcium between the transpiration stream and stem tissues and their role for nutrient flux in the xylem of a climbing bean was enabled by stable isotope tracer detection with cryo-SIMS protocols. These allowed investigation of diffusible tracers at the cell and tissue level, revealing for water unrestricted radial exchange, down to the subcellular level, with the possible exception of the lignified cell walls of the xylem parenchyma where less labelling occurred. Deuterium and  $^{18}\text{O}$  labelled water were shown to be equally applicable for tracing water in plant tissues, but for cryo-SIMS studies involving multi element multi isotope tracers  $\text{H}_2^{18}\text{O}$  is more favourable.

Radial nutrient exchange with the xylem vessels and the stem was more restricted with different exchange characteristics for each tissue, but there was still some fast exchange especially with the xylem parenchyma and the pith. For the phloem and cambium exchange was much slower. In the xylem parenchyma, all three nutrients showed exchange of large fractions with tracer from the xylem vessels (calcium 100%) revealing a high mobility in the apoplast, but also a fast exchange of the nutrients in the symplast. Fast exchange even of the bound intracellular calcium and magnesium indicates the dynamic status even of nutrients like calcium (e.g. pectates) and magnesium (e.g. Mg-ATP) traditionally viewed as low mobility cations. These intense interactions point to an important role of the stem xylem parenchyma in a fast regulation of nutrient flux in the xylem vessels.

Such regulation in the xylem vessels was demonstrated by isotopic dilution, indicating an up-regulation of potassium concentration in the more dilute input solution, supporting any proposed mechanism of nutrient homeostasis in the xylem vessels. In the light of these findings we suggest that future work should focus on the xylem vessels and tissues as a composite transport system, as it has been suggested for the root, since the intense and fast exchange indicates the potential for strong interactions that are likely to be important for nutrient distribution in the plant.

## Acknowledgements

The authors are very grateful to Alexandra Ley for performing light microscopy on bean stem cross-sections. We thank Hans-Peter Boehm and the Institute of Bio- and Nanosystems 2 for the liberal use of their SEM facilities. Special support came from

Marion Roeb and Beate Uhlig for plant cultivation. Andreas Aversch and the ICG workshop team contributed by general technical assistance. Special thanks for stimulating discussions on this manuscript go to Sigggi Jahnke, Gregor Huber, Carel Windt, Heike Schneider and Hanno Scharr.

## References

- Atkins C. (1999) *Biochemical aspects of assimilate transfers along the phloem path: N-solutes in lupins*. Paper presented at the International Conference on Assimilate Transport and Partitioning (ICATP 99), Newcastle, Australia.
- Barbour M.M. (2007) Stable oxygen isotope composition of plant tissue: a review. *Functional Plant Biology*, **34**, 83-94.
- Böhlke J.K., de Laeter J.R., De Bièvre P., Hidaka H., Peiser H.S., Rosman K.J.R. & Taylor P.D.P. (2005) Isotopic compositions of the elements, 2001. *Journal of Physical and Chemical Reference Data*, **34**, 57-67.
- Bramley H., Turner N.C., Turner D.W. & Tyerman S.D. (2009) Roles of Morphology, Anatomy, and Aquaporins in Determining Contrasting Hydraulic Behavior of Roots. *Plant Physiology*, **150**, 348-364.
- Bull T.A., Gayler K.R. & Glasziou K.T. (1972) Lateral movement of water and sugar across xylem in sugarcane stalks. *Plant Physiology*, **49**, 1007-1011.
- Canny M.J. (1995a) Apoplastic water and solute movement - New rules for an old space. *Annual Review of Plant Physiology and Plant Molecular Biology*, **46**, 215-236.
- Canny M.J. (1995b) Potassium Cycling in Helianthus - Ions of the Xylem Sap and Secondary Vessel Formation. *Philosophical Transactions of the Royal Society of London Series B-Biological Sciences*, **348**, 457-469.
- Dasilva M.C. & Shelp B.J. (1990) XYLEM-TO-PHLOEM TRANSFER OF ORGANIC NITROGEN IN YOUNG SOYBEAN PLANTS. *Plant Physiology*, **92**, 797-801.
- de Boer A.H. & Volkov V. (2003) Logistics of water and salt transport through the plant: structure and functioning of the xylem. *Plant Cell and Environment*, **26**, 87-101.
- Enns L.C., McCully M.E. & Canny M.J. (1998) Solute concentrations in xylem sap along vessels of maize primary roots at high root pressure. *Journal of Experimental Botany*, **49**, 1539-1544.
- Fricke W. (2000) Water movement between epidermal cells of barley leaves - a symplastic connection? *Plant Cell and Environment*, **23**, 991-997.
- Gartner B.L., ed (1995) *Plant stems: Physiology and functional anatomy* (illustrated ed.). Academic Press.
- Gilmer F. & Schurr U. (2007) Dynamic and nutrient fluxes in the xylem. In: *The Apoplast of higher plants: Compartment of storage, transport, and reactions* (eds B. Sattelmacher & W.J. Horst), pp. 221-229. Springer, Dordrecht.

- Gussoni M., Greco F., Vezzoli A., Osuga T. & Zetta L. (2001) Magnetic resonance imaging of molecular transport in living morning glory stems. *Magnetic Resonance Imaging*, **19**, 1311-1322.
- Hart R.T., Benmore C.J., Neufeind J., Kohara S., Tomberli B. & Egelstaff P.A. (2005) Temperature dependence of isotopic quantum effects in water. *Physical Review Letters*, **94**, 4.
- Ingram M.G. & Hayden R.J. (1954) *Handbook on Mass Spectrometry*. NRC-USA.
- Jeschke W.D. & Hartung W. (2000) Root-shoot interactions in mineral nutrition. *Plant and Soil*, **226**, 57-69.
- Köhler B. & Raschke K. (2007) Loading of ions into the xylem of the root. In: *The Apoplast of higher plants: Compartment of storage, transport and reactions* (eds B. Sattelmacher & W.J. Horst), pp. 181-200. Springer, Dordrecht.
- Kuhn A.J., Schroeder W.H. & Bauch J. (2000) The kinetics of calcium and magnesium entry into mycorrhizal spruce roots. *Planta*, **210**, 488-496.
- Leigh R.A. (2001) Potassium homeostasis and membrane transport. *Journal of Plant Nutrition and Soil Science-Zeitschrift für Pflanzenernährung und Bodenkunde*, **164**, 193-198.
- Link J. & Seelig J. (1990) COMPARISON OF DEUTERIUM NMR IMAGING METHODS AND APPLICATION TO PLANTS. *Journal of Magnetic Resonance*, **89**, 310-330.
- Maathuis F.J.M. (2007) Monovalent cation transporters; establishing a link between bioinformatics and physiology. *Plant and Soil*, **301**, 1-15.
- Marschner H. (1995) *Mineral nutrition of higher plants*. (2 ed.). Academic Press Limited, London.
- Marschner H., Kirkby E.A. & Engels C. (1997) Importance of cycling and recycling of mineral nutrients within plants for growth and development. *Botanica Acta*, **110**, 265-273.
- Maurel C., Verdoucq L., Luu D.T. & Santoni V. (2008) Plant aquaporins: Membrane channels with multiple integrated functions. *Annual Review of Plant Biology*, **59**, 595-624.
- McCully M.E., Canny M.J. & Huang C.X. (2009) Cryo-scanning electron microscopy (CSEM) in the advancement of functional plant biology. Morphological and anatomical applications. *Functional Plant Biology*, **36**, 97-124.

- McNeil D.L. (1980) THE ROLE OF THE STEM IN PHLOEM LOADING OF MINERALS IN LUPINUS-ALBUS L CV ULTRA. *Annals of Botany*, **45**, 329-338.
- Meinzer F.C., Brooks J.R., Domec J.C., Gartner B.L., Warren J.M., Woodruff D.R., Bible K. & Shaw D.C. (2006) Dynamics of water transport and storage in conifers studied with deuterium and heat tracing techniques. *Plant Cell and Environment*, **29**, 105-114.
- Metzner R., Schneider H.U., Breuer U. & Schroeder W.H. (2008) Imaging nutrient distributions in plant tissue using time-of-flight secondary ion mass spectrometry and scanning electron microscopy. *Plant Physiology*, **147**, 1774-1787.
- Metzner R., Schneider H.U., Breuer U., Thorpe M.R., Schurr U. & Schroeder W.H. (2009) Tracing cationic nutrients from xylem into stem tissue of *Phaseolus vulgaris* by stable isotope tracers and cryo-secondary ion mass spectrometry. **in preparation**.
- Nobel P.S. (1999) *Physicochemical and environmental plant physiology*. (2, illustrated ed.). Academic Press.
- Ohya T., Tanoi K., Hamada Y., Okabe H., Rai H., Hojo J., Suzuki K. & Nakanishi T.M. (2008) An analysis of long-distance water transport in the soybean stem using (H<sub>2</sub>O)-O-15. *Plant and Cell Physiology*, **49**, 718-729.
- Rowan A., McCully M.E. & Canny M.J. (2000) The origin of the exudate from cut maize roots. *Plant Physiology and Biochemistry*, **38**, 957-967.
- Sacchi G.A. & Cocucci M. (1992) EFFECTS OF DEUTERIUM-OXIDE ON GROWTH, PROTON EXTRUSION, POTASSIUM INFLUX, AND INVITRO PLASMA-MEMBRANE ACTIVITIES IN MAIZE ROOT SEGMENTS. *Plant Physiology*, **100**, 1962-1967.
- Schroeder W.H. & Fain G.L. (1984) Light-Dependent Calcium Release from Photoreceptors Measured by Laser Micro-Mass Analysis. *Nature*, **309**, 268-270.
- Stephan T., Zehnpfenning J. & Benninghoven A. (1994) Correction of Dead-Time Effects in Time-Of-Flight Mass-Spectrometry. *Journal of Vacuum Science & Technology A*, **12**, 405-410.
- Stedle E. (1989) WATER-FLOW IN PLANTS AND ITS COUPLING TO OTHER PROCESSES - AN OVERVIEW. *Methods in Enzymology*, **174**, 183-225.
- Stedle E. (1997) Water transport across plant tissue: Role of water channels. *Biology of the cell*, **89**, 259-273.



- Steudle E. & Peterson C.A. (1998) How does water get through roots? *Journal of Experimental Botany*, **49**, 775-788.
- Thorpe M.R., Minchin P.E.H., Gould N. & McQueen J. (2005) The stem apoplast: A potential communication channel in plant growth regulation. In: *Vascular transport in plants* (eds N.M. Holbrook & M.A. Zwieniecki), pp. 201 - 220. Elsevier Academic press, San Diego.
- van Bel A.J.E. (1990) Xylem-phloem exchange via the rays - the undervalued route of transport. *Journal of Experimental Botany*, **41**, 631-644.
- Van der Weerd L., Claessens M., Efde C. & Van As H. (2002) Nuclear magnetic resonance imaging of membrane permeability changes in plants during osmotic stress. *Plant Cell and Environment*, **25**, 1539-1549.
- Vickerman J.C. & Briggs D. (2001) *ToF-SIMS Surface Analysis by Mass Spectrometry*. IM Publication and Surface Spectra Limited
- Waber J. (1984) EFFECT OF HEAVY-WATER (99+PERCENT-D2O) ON BEET ROOT PERMEABILITY. *Environmental and Experimental Botany*, **24**, 253-257.
- Walsh K.B., Sky R.C. & Brown S.M. (2005) The anatomy of the pathway of sucrose unloading within the sugarcane stalk. *Functional Plant Biology*, **32**, 367-374.
- Wegner L.H. & De Boer A.H. (1997) Properties of two outward-rectifying channels in root xylem parenchyma cells suggest a role in K<sup>+</sup> homeostasis and long-distance signaling. *Plant Physiology*, **115**, 1707-1719.
- White P.J., Banfield J. & Diaz M. (1992) UNIDIRECTIONAL CA<sup>2+</sup> FLUXES IN ROOTS OF RYE (SECALE-CEREALE L) - A COMPARISON OF EXCISED ROOTS WITH ROOTS OF INTACT PLANTS. *Journal of Experimental Botany*, **43**, 1061-1074.
- Yazaki Y., Asukagawa N., Ishikawa Y., Ohta E. & Sakata M. (1988) ESTIMATION OF CYTOPLASMIC FREE MG-2+ LEVELS AND PHOSPHORYLATION POTENTIALS IN MUNG BEAN ROOT-TIPS BY INVIVO P-31 NMR-SPECTROSCOPY. *Plant and Cell Physiology*, **29**, 919-924.
- Ye Q., Holbrook N.M. & Zwieniecki M.A. (2008) Cell-to-cell pathway dominates xylem-epidermis hydraulic connection in *Tradescantia fluminensis* (Vell. Conc.) leaves. *Planta*, **227**, 1311-1319.

Zwieniecki M.A., Melcher P.J., Feild T.S. & Holbrook N.M. (2004) A potential role for xylem-phloem interactions in the hydraulic architecture of trees: effects of phloem girdling on xylem hydraulic conductance. *Tree Physiology*, **24**, 911-917.

## Tables

**Table I:** Isotopic abundance,  $A_E$ , of both natural material and the applied nutrient tracer solution. Literature data for major isotopes of natural material (tabulated: Böhlke *et al.*, 2005) are shown to illustrate SIMS precision. The abundance of oxygen, magnesium, potassium and calcium isotopes was calculated from SIMS signals from both solutions with natural isotopic abundance and from the enriched tracer solution (equation 1). For oxygen, the samples were frozen-hydrated drops on copper substrate; for magnesium, potassium and calcium the samples were air-dried solution drops on silicon substrate (mean [%]  $\pm$  2 standard deviations, n=3).

<b>Oxygen</b>	<b>16O</b>	<b>18O</b>	
natural	99.8 $\pm$ 0.02 (H <sub>3</sub> O <sup>+</sup> )	0.2 $\pm$ 0.02 (H <sub>3</sub> <sup>18</sup> O <sup>+</sup> )	
tracer	60.8 $\pm$ 5.4 (H <sub>3</sub> O <sup>+</sup> )	39.2 $\pm$ 5.4 (H <sub>3</sub> <sup>18</sup> O <sup>+</sup> )	
tabulated	99.8	0.2	
<b>Magnesium</b>	<b>24Mg</b>	<b>25Mg</b>	<b>26Mg</b>
natural	79.1 $\pm$ 2.4	9.6 $\pm$ 1.4	12.8 $\pm$ 2.4
tracer	2.0 $\pm$ 0.2	1.0 $\pm$ 0.2	97 $\pm$ 0.2
tabulated	79.0	10.0	11.0
<b>Potassium</b>	<b>39K</b>	<b>41K</b>	
natural	93.7 $\pm$ 1.0	6.3 $\pm$ 1.0	
tracer	5.5 $\pm$ 0.6	94.5 $\pm$ 0.6	
tabulated	93.3	6.7	
<b>Calcium</b>	<b>40Ca</b>	<b>44Ca</b>	
natural	97.8 $\pm$ 0.2	2.2 $\pm$ 0.2	
tracer	3.2 $\pm$ 2.6	96.7 $\pm$ 2.6	
tabulated	96.9	2.1	

**Table II:** Nutrient concentrations in xylem vessels ( $\text{mmol l}^{-1} \pm \text{sd}$ ). Samples from undisturbed plants, and after 20 min nutrient solution application to the cut stem (experimental plants), were extracted by centrifugation of stem sections and analysed by ion chromatography. \*Computed from the tracer isotopic abundance at the sampling site (equation 3), mean abundances  $\pm$  standard deviation ( $n=3$ ) listed in brackets. Row 4 assuming radial influx of nutrients with natural isotopic abundance and row 5 assuming influx labelled similar to the xylem parenchyma axial sheath at the sampling site, which is the maximal labelling of all tissues.

	<b>Mg</b>	<b>K</b>	<b>Ca</b>
Uncut plants (n=12)	1.5 $\pm$ 0.5	20.4 $\pm$ 5.7	3.4 $\pm$ 0.8
Applied nutrient solution	2.5	2.5	2.5
Experimental plants, measured (n=4)	2.9 $\pm$ 0.4	16.5 $\pm$ 1.8	4.0 $\pm$ 0.2
*Computed for natural abundance influx (isotopic abundance)	3.3 (77 % $\pm$ 1 %)	9.8 (29 % $\pm$ 7 %)	5.0 (50 % $\pm$ 10 %)
*Computed for maximal abundance detected influx	4.1	15.0	254.5

**Table III:** For each tissue and nutrient this table lists the equilibration time, the equilibrium tracer fraction  $F_{EQ}$ , and the exchangeable fraction  $e_E$  (equation 5). The equilibrium time is defined as the first sampling time when the tracer fraction reached value ( $F_{EQ}$ ) that did not change any more. XP-cm and XP-xv are not listed separately, since they did not show significant differences from XP-pi. For the phloem and cambium where this equilibrium was never reached, the exchanged fractions at 240 minutes are given, they are the minimum values.  $F_E$  is tabulated as the mean  $\pm$  standard deviation (n=3), except \*Mg (XP-Pi) is mean  $\pm$  difference (n=2).

Tissue	Shortened form	Nutrient	Equilibration time [min]	$F_{EQ}$ [%]	$e_E$ [%]
Xylem Vessels	XV	Mg	20	77.2 $\pm$ 1.7	-
		K	20	25.5 $\pm$ 7.8	-
		Ca	20	49.9 $\pm$ 10.3	-
Xylem Parenchyma - pith side	XP-Pi	Mg*	10	51.2 $\pm$ 4.0	66
		K	5	9.9 $\pm$ 3.6	39
		Ca	5	23.6 $\pm$ 17.9	94
Pith	Pi	Mg	20	33.3 $\pm$ 5.7	43
		K	5	2.3 $\pm$ 2.0	9
		Ca	5	4.9 $\pm$ 1.1	8
Cambium	Cm	Mg	>20	>27.9 $\pm$ 7.9	>36
		K	>20	>4.0 $\pm$ 2.1	>16
		Ca	>20	>48.7 $\pm$ 6.1	>76
Phloem	Ph	Mg	>20	>28.8 $\pm$ 11.0	>37
		K	>20	>5.3 $\pm$ 2.8	>21
		Ca	>20	>37.7 $\pm$ 10.6	>59

## Figure legends

**Figure 1:** Anatomy of bean stem tissues in the transverse plane. Tissue structure was revealed in cryo-SEM by removal of a minute amount of surface water (freeze-etching) after cryo-SIMS analysis. Four large xylem vessels are visible (XV1-4) with associated smaller vessels embedded in two types of xylem parenchyma. Xylem parenchyma mainly shows two different cell types, the small and lowly vacuolated cells forming a one or two cell layer thick axial sheath around the vessels (XP-pi: sheath-half facing the pith; XP-cm: sheath-half facing the cambium) and the larger highly vacuolated cells between the xylem vessels (XP-xv). All these cells were thick-walled, but between the thick-walled parenchyma and the cambium, where cells were differentiating there are thin-walled xylem parenchyma cells. Histological staining of fresh hand-sections for light microscopy showed that thick-walled parenchyma is lignified while thin-walled is not (data not shown). Neighbouring the xylem, towards the stem periphery are the cambium (Cm) and phloem (Ph) and, towards the centre, the pith (Pi). In the upper right corner is the hollow centre. No rays were visible in this sample, nor in any other sample.

**Figure 2:** Correlation between the distribution of water and the two water tracers ( $\text{H}_2^{18}\text{O}$  and  $\text{D}_2\text{O}$ ). Cryo-SIMS images show the signal of the most intense water-related secondary ion ( $\text{S}^{\text{H}30}$ ; A) and the water tracer  $\text{H}_2^{18}\text{O}$  ( $\text{S}^{\text{H}3180}$ ; B). Both images were obtained after 20 minutes of a nutrient tracer solution entering the transpiration stream containing  $\text{H}_2^{18}\text{O}$  via the cut stem 25 cm below (upstream from) the imaged site. Enrichment of  $\text{H}_2^{18}\text{O}$  was 43 % in the applied solution; flow rate was  $0.1 \text{ ml min}^{-1}$ . Images are scaled from zero (counts per pixel) to maximum as indicated in the colourbar next to each image and displayed in the NIH “fire2” palette. Area imaged is  $500 \times 500 \mu\text{m}^2$  at  $256 \times 256$  pixels. To compare signal distributions correlation- or scatterplots of each pixel in two different images were generated. Therefore, the signal of a certain pixel in picture 1 is plotted at the abscissa versus the signal of the corresponding pixel in picture 2 at the ordinate. Due to this representation the number of points in the scatter plot is very high therefore they are illustrated in a greyscale image with highest density equals white. Hence, such a correlation diagram would give a straight line of slope 1 for identical pictures. Therefore, similarity can be checked by linear regression and correlation analysis. The regression coefficient ( $r$ ) can be used as a measure of the similarity of the two images. C) Scatterplot

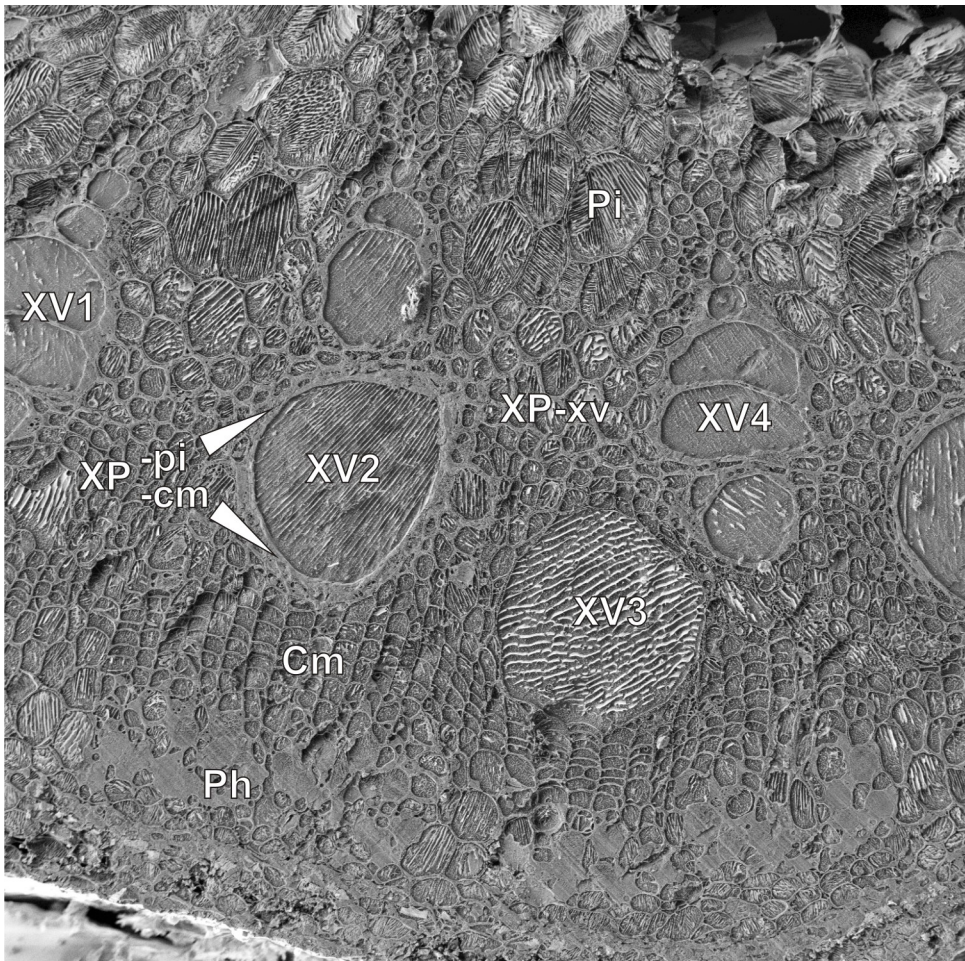
comparing  $\text{H}_2^{18}\text{O}$  with  $\text{H}_2\text{O}$  from A and B. Another experiment where both  $\text{H}_2^{18}\text{O}$  and  $\text{D}_2\text{O}$  were applied gave scatterplots (D) for water against  $\text{H}_2^{18}\text{O}$  and (E) for water against  $\text{D}_2\text{O}$ .

**Figure 3:** Tissue structure of the bean stem, and corresponding fractions of water (tracer:  $\text{H}_2^{18}\text{O}$ ), potassium and calcium originating from the tracer solution (see equation 2). A-C: cryo-SEM-images to help identify the tissue, with thick-walled xylem parenchyma highlighted green. Fractions of tracer ( $F_{\text{H}_3\text{O}}$ , D-F;  $F_{\text{K}}$ , G-I and  $F_{\text{Ca}}$ , J-L) after 5, 10 and 20 minutes of tracer flow into the cut shoot are scaled from zero to the indicated maximum. Scanned area is  $500 \times 500 \mu\text{m}^2$  with  $256 \times 256$  pixel resolution.

**Figure 4:** Fractions of tracer in various types of stem tissue. (A), Scheme of the regions of interest (ROI), specified according to anatomical criteria defined in Figure 1. (B-E) Mean fractions of water (tracer:  $\text{H}_2^{18}\text{O}$ ), magnesium, potassium and calcium originating from the tracer solution for the specified ROI. Note that the vessel fractions (enclosed within boxes) reflect radial exchange during passage of sap through the stem, whereas tissue fractions reflect all processes after tracer application began. The data are from three different experiments, with error bars indicating one standard deviation, except that there were two 10 min samples, shown as mean  $\pm$  difference. There was no water tracer in the 240 min experiments.

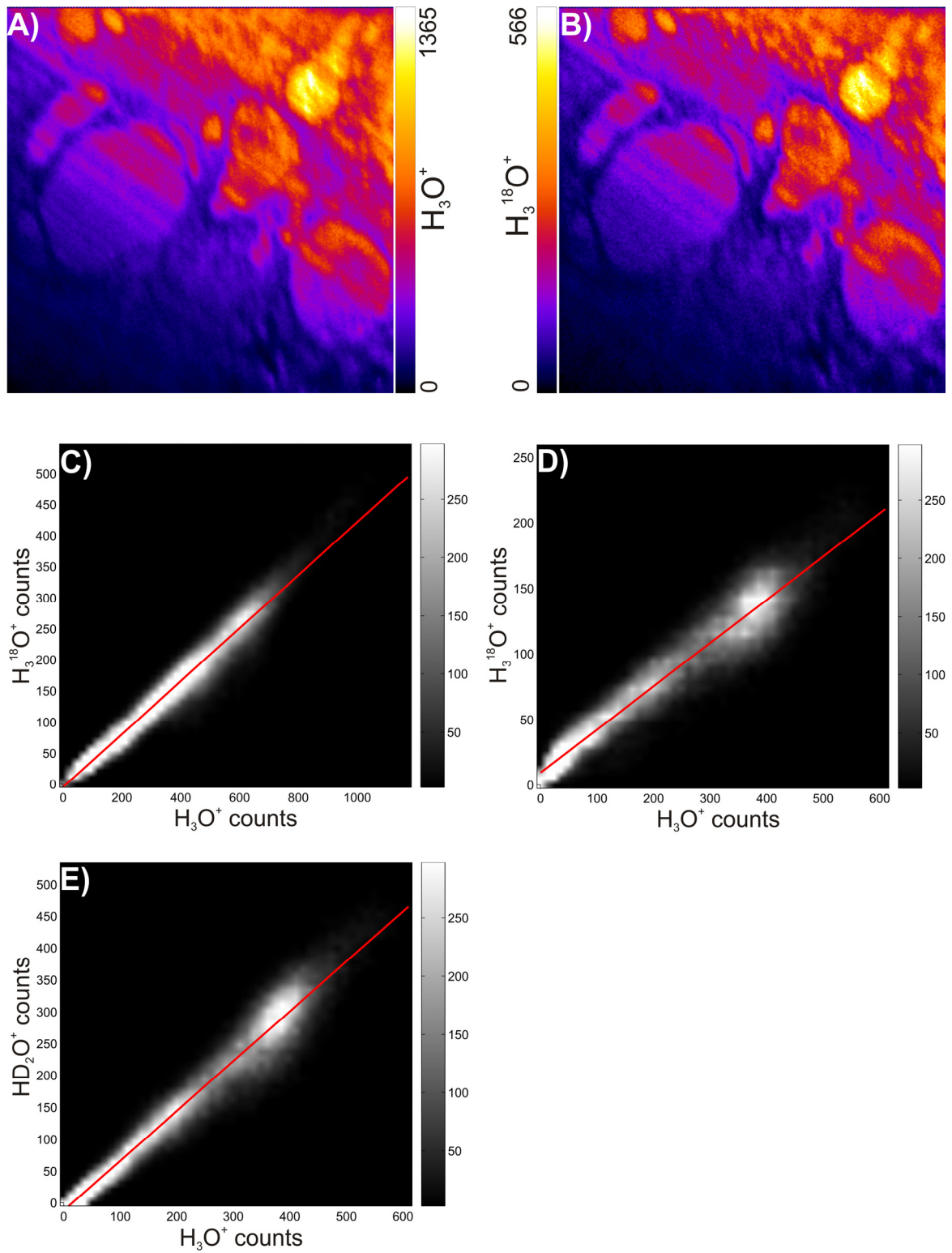
**Figure 5:** Subcellular spatial resolution images of tissue structure and fractions of water and potassium originating from the tracer. The area is the metaxylem region in the upper right corner of Figure 3C, F and I. (A) The cryo-SEM image shows the small cells of the xylem parenchyma sheath enclosing the vessels in the centre, next to them the larger cells of the XP-xv and the neighbouring large, thin-walled pith cells (Pi). The yellow frame indicates area analyzed by cryo-SIMS, and arrowheads indicate some cells of the xylem parenchyma sheath that were rich in cytoplasm. Fractions of water (B) and potassium tracer (C) were scaled from zero to indicated maximum. The cryo-SIMS image area is  $150 \times 150 \mu\text{m}^2$  with a resolution of  $256 \times 256$  pixel. For abbreviations of tissues see Figure 1.

## Figures



**Figure 1**



**Figure 2**

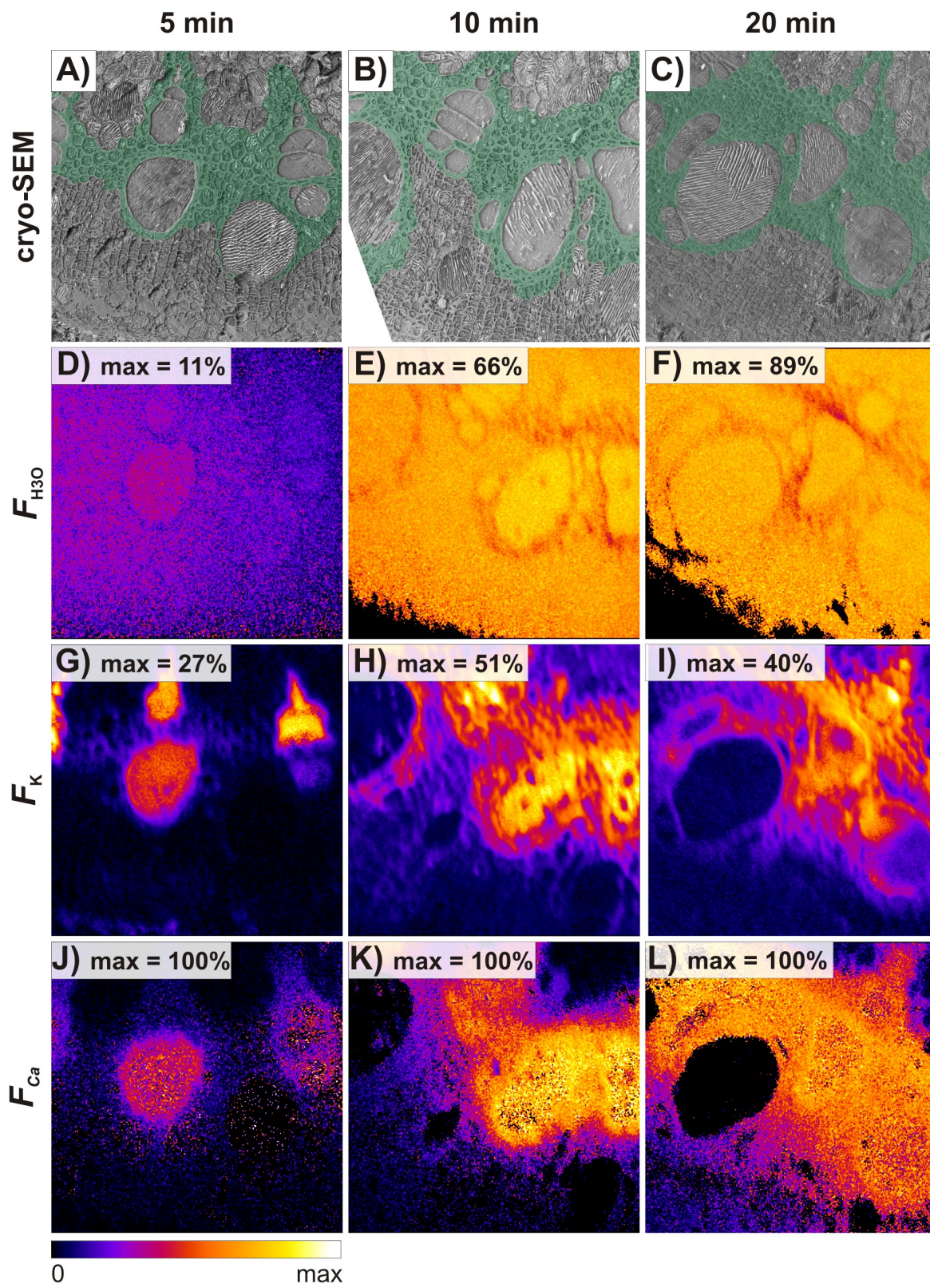
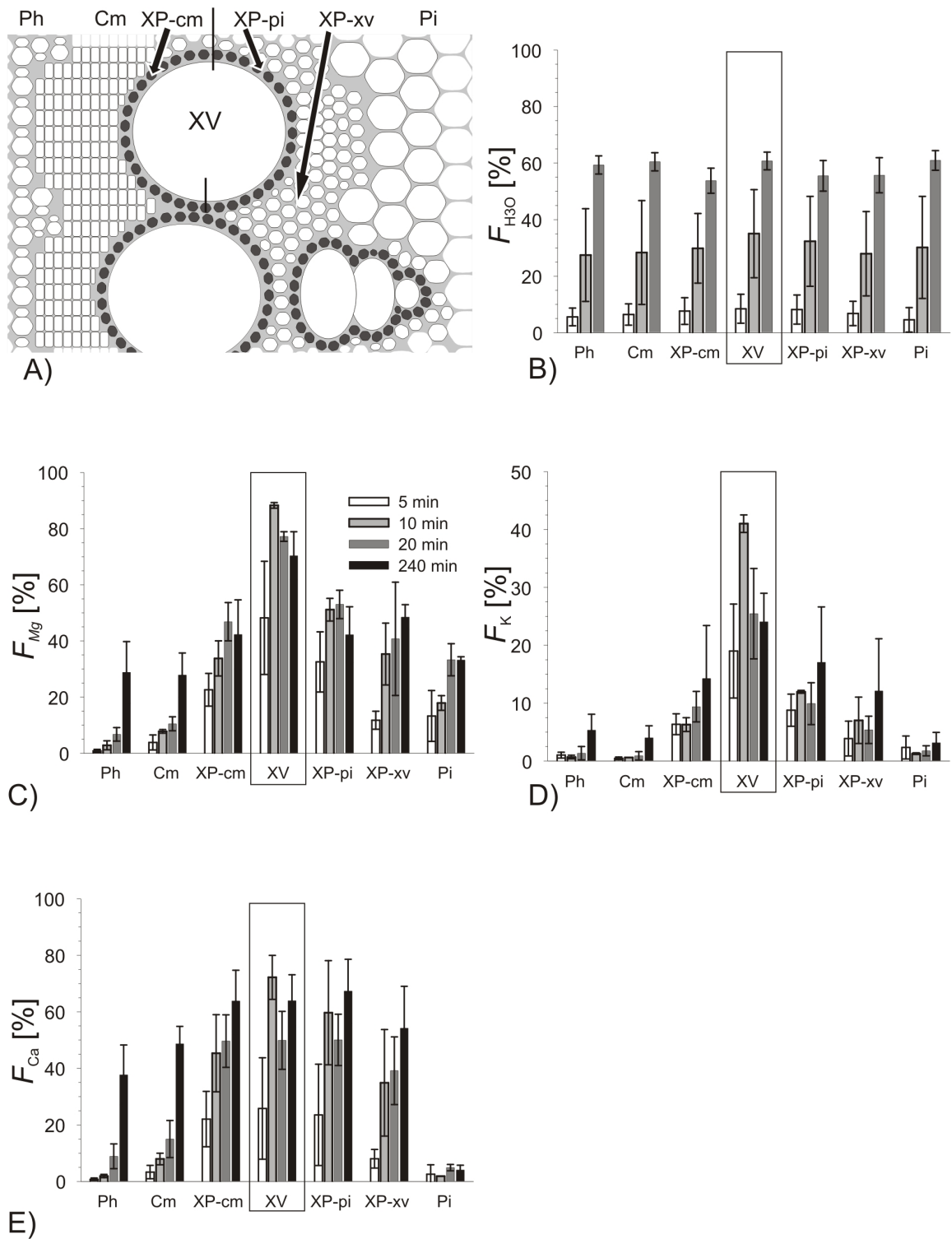
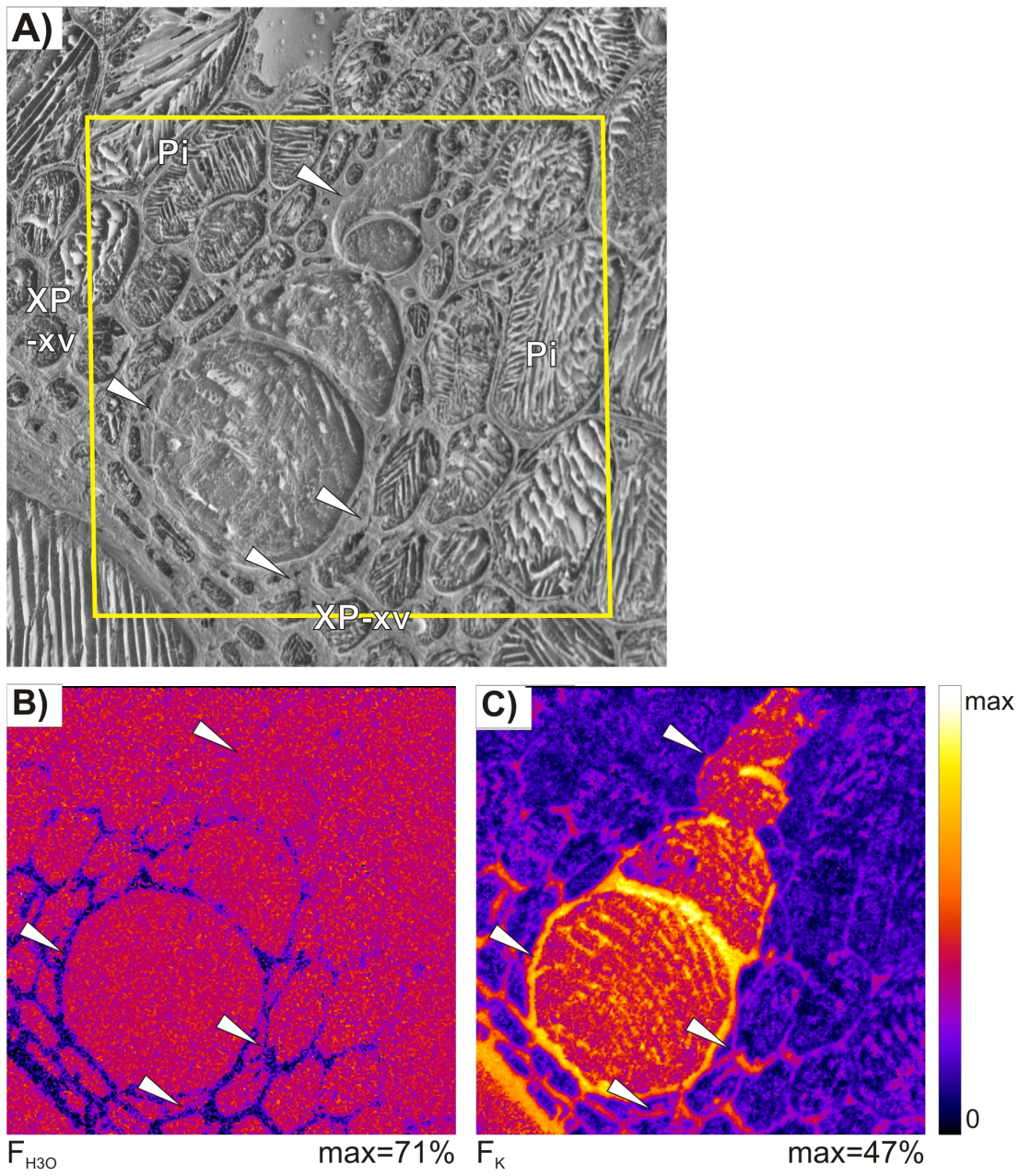


Figure 3



**Figure 4**

**Figure 5**

## Supporting information

### Derivation of equation (3)

The isotopic dilution of an initial amount of tracer (here  $^{41}\text{K}$  enriched solution for example) by added potassium with a different isotopic abundance is treated in the following way.

A known volume flow rate,  $J_N$  (nutrient solution taken up), with total potassium concentration,  $c_N$  and isotope fraction,  $A_N$ , is combined with an unknown (but very small compared to the transpiration stream) volume flow rate,  $J_T$  (radial influx from the stem tissues), with isotope fraction,  $A_T$ . For the sake of clarity this combined mix of **N** and **T** is named **X** (xylem vessel content at sampling site), of which only the isotope fraction,  $A_X$ , is known. The objective is to find an expression for the total concentration,  $c_X$  of a tracer nutrient exemplified here by potassium.

**Definitions** (with  $i = \text{N, X and T}$  for the input solution, xylem vessel content and tissue-derived nutrient):

$c_i$  = concentrations at input and output

$m_i^{41}, m_i^{39}, S$  = mass flow rates of the minor and major isotopes, and of the total element

$J_i$  = volume flow rates

Known:  $c_N, A_N, A_X, A_T, J_N$ . Unknown  $c_X, J_X, J_T$

The total potassium flow rate is defined as:

$$S_i = m_i^{41} + m_i^{39} = C_i J_i \quad (\text{A1})$$

If the isotope  $^{41}\text{K}$  abundance for each compartment is given by

$$A_i = \frac{m_i^{41}}{m_i^{41} + m_i^{39}} \quad (\text{A2})$$

then

$$S_i = \frac{m_i^{41}}{A_i} = \frac{m_i^{39}}{(1 - A_i)} \quad (\text{A3})$$

Starting point of the calculation are the following equations for mass and volume conservation:

$$m_X^{39} = m_N^{39} + m_T^{39} \quad \text{and} \quad m_X^{41} = m_N^{41} + m_T^{41} \quad (\text{A5})$$

$$J_X = J_N + J_T \quad (\text{A4})$$

Therefore from A5, using A3 to substitute for  $m_i^{41}$  and  $m_i^{39}$ , the two mass equations become

$$S_X A_X = S_N A_N + S_T A_T \quad (\text{A6})$$

$$S_X (1 - A_X) = S_N (1 - A_N) + S_T (1 - A_T) \quad (\text{A7})$$

Substituting the solution for  $S_3$  from A6 in A7, and solving for  $S_2$ ,

$$S_X = S_N \frac{A_N - A_T}{A_X - A_T} \quad (\text{A8})$$

The concentration at level 2 is thus

$$c_X = c_N \frac{J_N (A_N - A_T)}{(J_N + J_T)(A_X - A_T)} \quad (\text{A9})$$

Usually radial influx to the xylem vessels in stems is much smaller in volume compared to the transpiration stream due to a lack of water sources in the tissues or even negligible if the flux is mediated by ion channels. Hence  $J_T \ll J_N$  and equation (A9) can be simplified to

---

$$c_X = c_N \frac{A_N - A_T}{A_X - A_T} \quad (\text{A10})$$

This is given as equation 3 in materials and methods

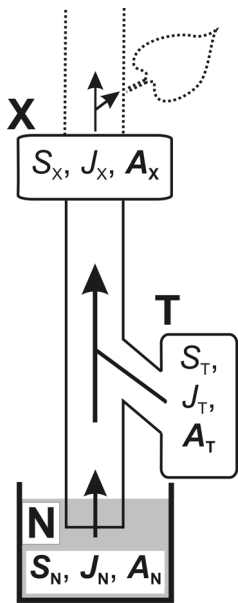


**Figure S1:** Schematic diagram for the calculation of the concentration in the xylem vessel content at the sampling site (X) from the nutrient solution taken up by the transpiration stream (N) and the radial input of nutrient from the stem tissues (T).  $S$  mass flow of the total element,  $J$  volume flow rate and  $A$  isotopic abundance of the tracer isotope. Known variables are expressed in bold letters.



---

## 6 Acknowledgements

This dissertation would not have been possible without the support of many people, who I would like to thank in this place:

- Prof. Dr Ulrich Schurr for giving me the opportunity to work on an interesting and challenging topic in plant physiology and constant support during critical stages of the dissertation
- Dr. Stephan Küppers and Dr. Uwe Breuer for financial support during the first part of my PhD project, access to the SIMS-instrument, for patient introduction into the secrets of SIMS and for critical and stimulating discussions on data interpretation
- Dr. Walter Schröder for supervision of the biological part of this dissertation, introduction into cryo preparation and performing the superb cryo-SEM imaging
- PD Dr. Heike Schneider for supervision of the biological part of this dissertation, performing the pressure probe measurements, and together with Alexandra Ley developing a technique to apply tracers minimally invasive to the xylem
- Dr. Michael Thorpe for endless patience and help during the preparation of the last two manuscripts and many critical and stimulating discussions about transport
- Dr. Peter Blümner, Dr. Marion Menzel, Dr. Siggi Jahnke, Dr. Gregor Huber, Dr. Carel Windt, Dr. Hanno Scharr, Dr. Kerstin Füllner and Jonas Bühler for help with software, mathematical and physical problems but first of all for constant encouragement and support in the most critical times during my thesis. This helped me more than I can say with few words
- Andreas Aversch for aid with software, computers and for help with many other problems I encountered during this project
- Beate Uhlig, Marion Roeb and the team of the ICG-Workshop for plant cultivation and construction of new equipment for the cryo-preparation
- Andrea Stärk and Dr. Astrid Besmehn for technical help in many problems concerning use of the ToF-SIMS and its software
- Dr. Sven Kayser and the IONTOF company for improving the cryostage of the ToF-SIMS instrument used in this project
- And last but not least all the other people whose support has given me the strength to meet the challenges of the last years, first of all Inga, Iris, Imke, Guido, Lotte, Markus, Claudia and many others.



---

## Curriculum vitae

Ralf Metzner

\* 25.04.1977, Hanau, Germany

Nationality: German

### Professional life

---

03/2005 – present	<b>Doctoral studies / Scientific Assistant</b> Institute of Chemistry and Dynamics of the Geosphere 3: Phytosphere and central division of analytical chemistry, Forschungszentrum Jülich GmbH, Jülich, Germany
05/2002 – 02/2005	<b>Student Research Assistant</b> Institute of Plant Ecology, Justus Liebig University, Gießen, Germany
1996 – 1997	<b>Alternative Service</b> Praunheimer Werkstätten, Frankfurt, Germany (Workshop for handicapped people)

### Studies

---

21/10/2004	<b>Diploma</b> Institute of Plant Ecology, Justus Liebig University, Gießen, Germany
10/1997 – 02/2005	<b>Student (biology)</b> Justus-Liebig-University, Giessen

### School

---

19/06/1996	<b>Abitur</b>
1993 – 1996	<b>Grammar School</b> Albert-Einstein-Gymnasium, Maintal, Germany
1987 - 1993	<b>Comprehensive school</b> Dietrich-Bonhoeffer-Schule, Maintal, Germany
1983 – 1987	<b>Elementary School</b> Werner-von-Siemens-Schule, Maintal, Germany

